Thermoelectric Materials, Phenomena, and Applications: A Bird's Eye View

Terry M. Tritt and M.A. Subramanian, Guest Editors

Abstract

High-efficiency thermoelectric (TE) materials are important for power-generation devices that are designed to convert waste heat into electrical energy. They can also be used in solid-state refrigeration devices. The conversion of waste heat into electrical energy may play an important role in our current challenge to develop alternative energy technologies to reduce our dependence on fossil fuels and reduce greenhouse gas emissions.

An overview of various TE phenomena and materials is provided in this issue of *MRS Bulletin.* Several of the current applications and key parameters are defined and discussed. Novel applications of TE materials include biothermal batteries to power heart pacemakers, enhanced performance of optoelectronics coupled with solid-state TE cooling, and power generation for deep-space probes via radioisotope TE generators. A number of different systems of potential TE materials are currently under investigation by various research groups around the world, and many of these materials are reviewed in the articles in this issue. These range from thin-film superlattice materials to large single-crystal or polycrystalline bulk materials, and from semiconductors and semimetals to ceramic oxides. The phonon-glass/electron-crystal approach to new TE materials is presented, along with the role of solid-state crystal chemistry. Research criteria for developing new materials are highlighted.

Keywords: *energy, thermal conductivity, thermoelectricity.*

Introduction

Thermoelectric Phenomena: Background and Applications

Over the past decade, there has been heightened interest in the field of thermoelectrics, driven by the need for more efficient materials for electronic refrigeration and power generation.[1,2] Some of the research efforts focus on minimizing the lattice thermal conductivity, while other efforts focus on materials that exhibit large power factors. Proposed industrial and military applications of thermoelectric (TE) materials are generating increased activity in this field by demanding higher-performance high-temperature TE materials than those that are currently in use. The demand for alternative energy technologies to reduce our dependence on fossil fuels leads to important regimes of research, including that of high-temperature energy harvesting via the direct recovery of waste heat and its conversion into useful electrical energy. Thus, the development of higher-performance TE materials is becoming ever more important. Power-generation applications are currently being investigated by the automotive industry as a means to develop electrical power from waste engine heat from the radiator and exhaust systems for use in next-generation vehicles. In addition, TE refrigeration applications include seat coolers for comfort and electronic component cooling. Of course, the deep-space applications of NASA's Voyager and Cassini missions using radioisotope thermoelectric generators (RTGs) are well established (see Reference 3 and the article by Yang and Caillat in this issue). A key factor in developing these technologies is the development of higher-performance TE materials, either completely new materials or through more ingenious materials engineering of existing materials.

Thermoelectric refrigeration is an environmentally "green" method of small-scale, localized cooling in computers, infrared detectors, electronics, and optoelectronics as well as many other applications. However, most of the electronics and optoelectronics technologies typically require only small-scale or localized spot cooling of small components that do not impose a large heat load. If significant economical cooling can be achieved, the resulting "cold computing" could produce speed gains of 30–200% in some computer processors based on complementary metal oxide semiconductor (CMOS) technology. Cooling of the processors is perceived by many to be the fundamental limit to electronic system performance.[4] Thus, the potential payoff for the development of low-temperature TE refrigeration devices is great, and the requirement for compounds with properties optimized over wide temperature ranges has led to a much expanded interest in new TE materials. Recent utilization of Peltier coolers (see next section) for the refrigeration of biological specimens and samples is an emerging TE application.

The development and potential of bulk materials for TE applications is an active area of research. High-temperature bulk materials such as skutterudites, clathrates, half-Heusler alloys, and complex chalcogenides are being investigated (see the article by Nolas et al. in this issue). These materials possess complex crystal structures and exhibit properties that are favorable for potential thermoelectric materials. For example, skutterudites and clathrates are cage-like materials that have voids in which "rattler" atoms are inserted to significantly lower the thermal conductivity due to the rattling atoms' ability to scatter phonons. Recently, ceramic oxide materials have also shown potential as high-

temperature TE materials (see Koumoto et al. in this issue). The potential of nanomaterials and their role in TE research are an emerging area of interest (see Rao et al. in this issue). Bulk material applications are demanding new breakthroughs in both materials and device engineering (see Yang and Caillat in this issue). The role of thin-film properties, applications, and recent results is also very important (see Böttner et al. in this issue). A more complete overview of state-of-the-art materials, a theoretical and experimental discussion of the basic principles, and an overview of some of the recent developments and materials are given in texts by Tritt[2] and Nolas.[5]

Seebeck and Peltier Effects

A discussion of thermoelectric effects and devices should start with one of the most fundamental TE phenomena, the Seebeck effect, or thermopower.[6–8] In the early 1800s, Seebeck observed that when two dissimilar materials are joined together and the junctions are held at different temperatures (T and $T + \Delta T$), a voltage difference (ΔV) develops that is proportional to the temperature difference (ΔT).[6] The ratio of the voltage developed to the temperature gradient ($\Delta V/\Delta T$) is related to an intrinsic property of the materials called the Seebeck coefficient, α. The Seebeck coefficient is very low for metals (only a few μV/K) and much larger for semiconductors (typically a few hundred μV/K).[9] A related effect—the Peltier effect—was discovered a few years later by Peltier,[10] who observed that when an electrical current is passed through the junction of two dissimilar materials, heat is either absorbed or rejected at the junction, depending on the direction of the current. This effect is due largely to the difference in Fermi energies of the two materials. These two effects are related to each other, as shown in the definition of the Peltier coefficient, $\Pi = \alpha T$. The rate at which the Peltier heat is liberated or rejected at the junction (Q_P) is given by $Q_P = \alpha I T$, where I is the current through the junction and T is the temperature in kelvin. There are also a number of thermomagnetic effects such as the Hall, Ettingshausen, and Nernst effects that are beyond the scope of this article. The reader is referred to the text by Nolas et al.[5] for a discussion of these effects.

Definition and Description of the Figure of Merit and Thermoelectric Performance

The potential of a material for TE applications is determined in large part by a measure of the material's figure of merit, ZT:*

$$ZT = \frac{\alpha^2 \sigma T}{\kappa} = \frac{\alpha^2 T}{\rho \kappa}, \qquad (1)$$

where α is the Seebeck coefficient, σ is the electrical conductivity, ρ is the electrical resistivity, and κ is the total thermal conductivity ($\kappa = \kappa_L + \kappa_E$, the lattice and electronic contributions, respectively). The power factor, $\alpha^2 \sigma T$ (or $\alpha^2 T/\rho$), is typically optimized in narrow-gap semiconducting materials as a function of carrier concentration (typically $\sim 10^{19}$ carriers/cm^3), through doping, to give the largest ZT.[9] High-mobility carriers are most desirable, in order to have the highest electrical conductivity for a given carrier concentration. The ZT for a single material is somewhat meaningless, since an array of TE couples is utilized in a device or module.

There are two materials in the TE couple, which is shown in Figure 1, an n-type and a p-type. Ignoring parasitic contributions that reduce the device performance, such as contact resistance and radiation effects, the resulting figure of merit for the couple (based solely on the TE materials) is given by

$$ZT = \frac{(\alpha_p - \alpha_n)^2 T}{[(\rho_n \kappa_n)^{1/2} + (\rho_p \kappa_p)^{1/2}]^2}. \qquad (2)$$

The coefficient of performance ϕ (refrigeration mode) and the efficiency η (power-generation mode) of the TE couple are directly related to the figure of merit shown in Equation 3 for the efficiency. The efficiency (η) of the TE couple is given by the power input to the load (W) over the net heat flow rate (Q_H), where Q_H is positive for heat flow from the source to the sink:

$$\eta = \frac{W}{Q_H}$$
$$= \frac{T_H - T_C}{T_H} \left[\frac{(1 + ZT_M)^{1/2} - 1}{(1 + ZT_M)^{1/2} + (T_C/T_H)} \right], \qquad (3)$$

where T_H is the hot-side temperature, T_C is the cold-side temperature, and T_M is the average temperature. Thus, one can see

---

*The expressions for figure of merit, Z and ZT, are used interchangeably in the field of thermoelectrics. Z is the figure of merit with units of 1/K (1/T), and ZT is the dimensionless (unitless) figure of merit. Both must specify the temperature at which the quoted value was obtained.

that η is proportional to $(1 + ZT_M)^{1/2}$ and that the efficiency would approach the Carnot efficiency if ZT were to approach infinity.

Thermoelectric Modules: Devices

The Peltier effect is the basis for many modern-day TE refrigeration devices, and the Seebeck effect is the basis for TE power-generation devices. The versatility of TE materials is illustrated in Figure 1, which shows a TE couple composed of an n-type (negative thermopower and electron carriers) and a p-type (positive thermopower and hole carriers) semiconductor material connected through metallic electrical contact pads. Both refrigeration and power generation may be accomplished using the same module, as shown in Figure 1. A TE module or device is built up of an array of these couples, arranged electrically in series and thermally in parallel. Thermoelectric energy conversion utilizes the Seebeck effect, wherein a temperature gradient is imposed across the device, resulting in a voltage that can be used to drive a current through a load resistance or device. This is the direct conversion of heat into electricity. Conversely, the Peltier heat generated when an electric current is passed through a TE material provides a temperature gradient, with heat being absorbed on the cold side, transferred through (or pumped by) the TE materials, and rejected at the sink, thus providing a refrigeration capability. The advantages of TE solid-state energy conversion are compactness, quietness (no moving parts), and localized heating or cooling. In addition, energy in the form of waste heat (0% efficiency) that would normally be lost may be converted into useful electrical energy ($\geq$7–8% efficiency) using a TE power-generation device.

The best TE materials currently used in devices have $ZT \approx 1$. This value has been a practical upper limit for more than 30 years, yet there are no theoretical or thermodynamic reasons for $ZT \approx 1$ as an upper barrier. As seen from Equation 1, ZT may be increased by decreasing κ_L or by increasing either α or σ. However, σ is tied to the electronic thermal conductivity, κ_E, through the Wiedemann–Franz relationship, and the ratio is essentially constant at a given temperature.

Some of the goals of current research efforts are to find new materials that either raise the current efficiency of TE devices (i.e., increase ZT) or have the capability of operating in new and broader temperature regimes, especially at lower temperatures ($T < 250$ K) and higher temperatures ($T > 400$ K). Over the past 30 years,
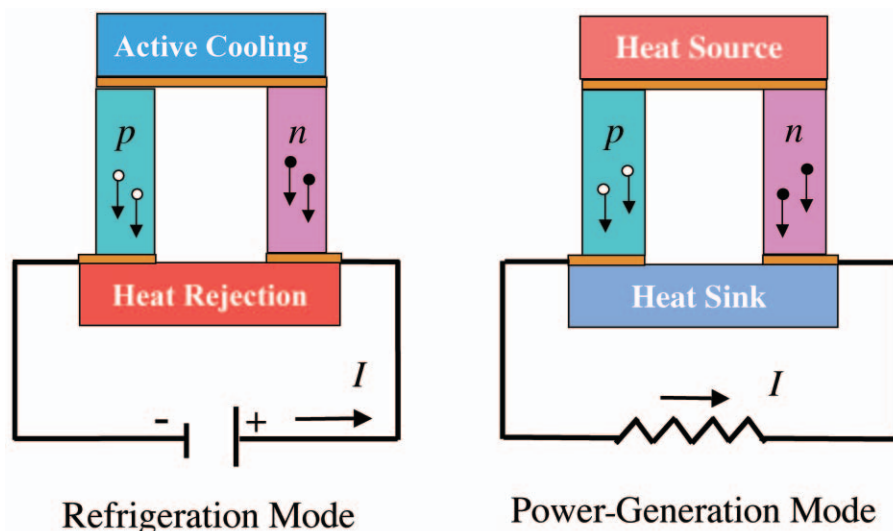
Figure 1. Diagram of a Peltier thermoelectric couple made of an n-type and a p-type thermoelectric material. Refrigeration or power-generation modes are possible, depending on the configuration. I is current.

alloys based on the Bi_2Te_3 system $[(Bi_{1-x}Sb_x)_2(Te_{1-x}Se_x)_3]$ and the $Si_{1-y}Ge_y$ system have been extensively studied and optimized for their use as TE materials to perform in a variety of solid-state TE refrigeration and power-generation applications.[11,12] These traditional TE materials have undergone extensive investigation, and there appears to be little room for future improvement in the common bulk structures. However, recent results on nanostructures of traditional TE materials have shown a promising new direction for these materials. In addition, entirely new classes of compounds will have to be investigated. Figure 2 shows ZT as a function of temperature for the Bi_2Te_3 and $Si_{1-y}Ge_y$ materials as well as many of the more recent bulk materials that have been developed over the last decade. The ZT of more exotic structures such as superlattices and quantum dot structures are not shown here but are addressed in the article by Böttner et al. in this issue.

Transport Properties

The thermopower, or Seebeck coefficient, can be thought of as the heat per carrier over temperature or, more simply, the entropy per carrier, $\alpha \approx C/q$, where C is the specific heat and q is the charge of the carrier.[7] For the case of a classical gas, each particle has an energy of $3/2(k_BT)$, where k_B is the Boltzmann constant. The thermopower is thus approximately k_B/e, where e is the charge of the electron. For metals, the heat per carrier is essentially a product of the electronic specific heat and the temperature divided by the number of

carriers (N), that is, $\alpha \approx C_{el}T/N$, and then α is approximately

$$\alpha \approx \frac{C_{el}}{q} \approx \left(\frac{k_B}{e}\right)\frac{k_BT}{E_F}, \qquad (4)$$

where E_F is the Fermi energy (related to the chemical potential of the material).

The Fermi energy is basically the energy such that at $T \approx 0$, all the states above this energy are vacant and all the states below are occupied. The quantity $k_B/e \approx 87\ \mu V/K$ is a constant that represents the thermopower of a classical electron gas. Metals have thermopower values of much less than 87 μV/K (on the order of 1–10 μV/K) and decrease with decreasing temperature, that is, $E_F \gg k_BT$.

In a semiconductor, a charged particle must first be excited across an energy gap E_g. In this case, the thermopower is approximated by

$$\alpha \approx \frac{C_{el}}{q} \approx \left(\frac{k_B}{e}\right)\frac{E_g}{k_BT}. \qquad (5)$$

Thus, the thermopower is larger than the characteristic value of 87 μV/K and increases with decreasing temperature. Semiconductors can exhibit either electron conduction (negative thermopower) or hole conduction (positive thermopower). The thermopower for different carrier types is given by a weighted average of their electrical conductivity values (σ_n and σ_p):

$$\alpha \approx \frac{(\alpha_n\sigma_n + \alpha_p\sigma_p)}{(\sigma_n + \sigma_p)}. \qquad (6)$$

It is necessary to dope the semiconductors with either donor or acceptor states to
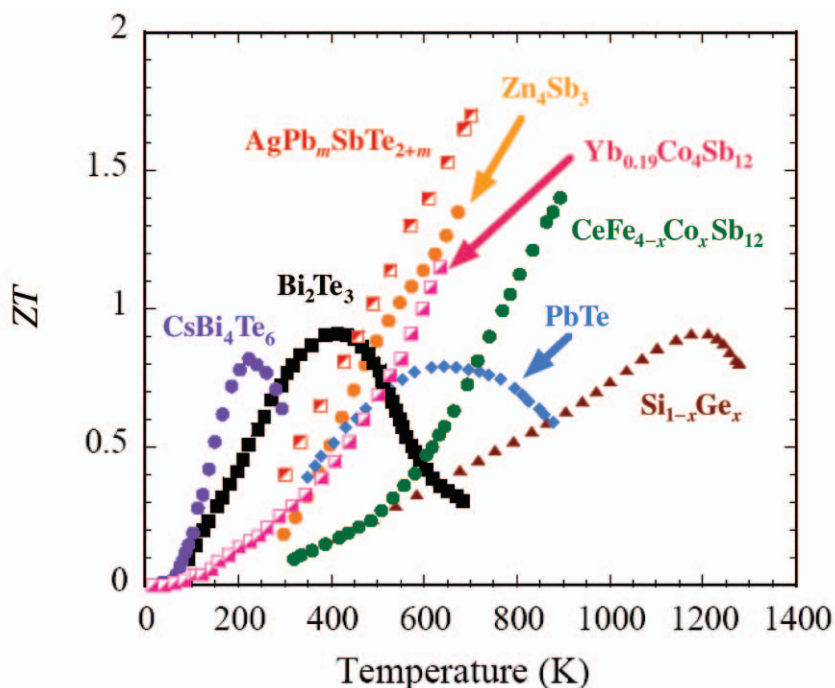

Figure 2. Figure of merit ZT shown as a function of temperature for several bulk thermoelectric materials.

allow extrinsic conduction of the appropriate carrier type, electrons or holes, respectively. It is apparent that the total thermopower will be lower than that of either of the individual contributions, unless the direct bandgap is large enough—typically on the order of $10(k_BT)$—to effectively minimize minority carrier contributions. Typical thermopower values required for good TE performance are on the order of 150–250 μV/K or greater.

For high-temperature applications, it is important to minimize the contribution of minority carriers in order to maintain a high thermopower. In addition, the thermal stability of the materials is an essential aspect. Atomic diffusion within the materials and interdiffusion of contacts can seriously deteriorate the properties of a given material at high temperatures. Aspects of this are discussed elsewhere.[2,5] These materials and devices are expected to operate at elevated temperatures for long periods of time without deterioration of their properties or performance. The effects of diffusion and thermal annealing are important to thoroughly investigate and understand in any set of potential TE materials over the expected operating temperature range of the materials.

The description of electrical conductivity for metals and semiconductors has been covered extensively in many texts on solid-state physics, and the reader is referred there.[13] There are a significant number of carriers and states available for conduction in metals, typically $n \approx 10^{22}$ carriers/cm^3. The electrical conductivity is then very large for metals, on the order of $10^6(\Omega$ cm$)^{-1}$. Again, for semiconductors, the carriers must be thermally excited across a gap for conduction to occur, as shown from the activated behavior that is derived for the temperature-dependence of the electrical conductivity [$\sigma \approx \sigma_0\exp(-E_g/k_BT)$]. There are two primary ways to achieve a high conductivity in a semiconductor, either by having a very small gap to excite across (E_g/k_BT) or by having very high-mobility carriers, as discussed later. Typical values of the electrical conductivity for a good TE material are on the order of about $10^3(\Omega$ cm$)^{-1}$.

The thermal conductivity κ is related to the transfer of heat through a material, either by the electrons or by quantized vibrations of the lattice, called phonons, such that $\kappa = \kappa_L + \kappa_E$, as mentioned earlier. The electrical conductivity and the thermal conductivity are interrelated, in that σ is tied to κ_E through the Wiedemann–Franz relationship: $\kappa_E = L_0\sigma T$, where the Lorentz number $L_0 = 2.45 \times 10^{-8}$ W $\Omega/$K^2 [or $L_0 = 2.45 \times 10^{-8}$(V^2/K^2)]. The lattice thermal conductivity is discussed later

in this article, in the section on minimum thermal conductivity. Typical thermal conductivity values for a good TE material are $\kappa < 2$ W m^{-1} K^{-1}, and typically, $\kappa_L \approx \kappa_E$.

Investigating New Thermoelectric Materials

The "Phonon-Glass/Electron-Crystal" Approach

Slack has described the chemical characteristics of candidates for a good TE material.[14] He states that the candidates should be narrow-bandgap semiconductors with high-mobility carriers. Mahan has also described the characteristics of good TE materials,[15,16] agreeing with Slack that the candidate material is typically a narrow-bandgap semiconductor [$E_g \approx 10(k_BT)$, or 0.25 eV at 300 K]. Also, the mobility of the carriers must remain high ($\mu \approx 2000$ cm^2/V s), while the lattice thermal conductivity must be minimized. In semiconductors, the Seebeck coefficient and electrical conductivity (both in the numerator of ZT) are strong functions of the doping level and chemical composition. These quantities must therefore be optimized for good TE performance. The thermal conductivity of complex materials can often be modified by chemical substitutions, and the lattice thermal conductivity needs to be as low as possible. Understanding these various effects and selecting optimization strategies can be an exceedingly difficult problem, because in complex materials there are often many possible degrees of freedom. Slack suggested that the best TE material would behave as a "phonon-glass/electron-crystal" (PGEC); that is, it would have the electrical properties of a crystalline material and the thermal properties of an amorphous or glass-like material. Materials engineering and the crystal chemistry approach to good TE materials are discussed later.

Minimum Thermal Conductivity

In many areas of research related to new TE materials, attempts are being made to reduce the lattice part of the thermal conductivity to essentially its minimum value, that is, where a minimum lattice thermal conductivity is achieved (when all the phonons have a mean free path essentially equal to the interatomic spacing of the constituent atoms). This is being attempted by scattering phonons in different frequency ranges using a variety of methods such as mass fluctuation scattering (a mixed crystal, in ternary and quaternary compounds), "rattling" scattering, grain-boundary scattering (due to the size of the grains), and interface scattering in thin films or multilayer systems.

The lattice thermal conductivity is given by $\kappa_L \approx (1/3)(v_sCL_{ph})$, where v_s is the velocity of sound, C is the heat capacity, and L_{ph} is the mean free path of the phonons. At high temperatures ($T > \sim300$ K), the sound velocity and the heat capacity are essentially temperature-independent in typical materials. Therefore, the magnitude and the temperature-dependence of κ_L are basically determined by the mean free path of the phonons. Slack defined the minimum thermal conductivity (κ_{min}) as the thermal conductivity when the mean free path is essentially limited by the interatomic distance between the atoms within the crystal.[17] Typical analysis of κ_{min} results in values of $\kappa_{min} \approx 0.25$–0.5 W m^{-1} K^{-1}.[14,17]

Minimum Thermopower

There are certain practical limits for each of the parameters used to calculate ZT. These practical limits must be possible in order to achieve a material viable for thermoelectric applications. For example, in Bi$_2$Te$_3$, in order to achieve a $ZT \approx 1$ at $T = 320$ K, $\sigma \approx 1$ mΩ cm, $\alpha \approx 225$ μV/K, and $\kappa \approx 1.5$ W m^{-1} K^{-1}. We have already discussed the ZT "barrier," which in effect is given by minimizing the thermal conductivity. It is practical to investigate materials where the electronic and lattice terms are comparable, on the order of 0.75–1 W m^{-1} K^{-1}. Let us look at the *hypothetical* situation of a material in which the lattice thermal conductivity is zero ($\kappa_L = 0$). We will also assume the scattering in this system is elastic and that the Wiedemann–Franz relationship, slightly rearranged [$\kappa_E/\sigma = L_0T$], is well behaved in this material. Then we can rewrite Equation 1 as

$$ZT = \alpha^2T/\rho\kappa_E = \alpha^2/L_0. \tag{7}$$

Therefore, for a material to be a viable TE material, it must possess a minimum thermopower that is directly related to the value of ZT and L_0. Given this description, in order to achieve a certain value of ZT, the material would require that $\alpha = (L_0)^{0.5} = 157$ μV/K for $ZT = 1$, and $\alpha = (2L_0)^{0.5} = 225$ μV/K for $ZT = 2$. Of course, any "real" material will possess a finite κ_L, and these values for the thermopower will have to be higher to achieve the projected values of ZT.

Solid-State Crystal Chemistry Approaches to Advanced Thermoelectric Materials

Thermoelectrics has always been a materials design problem involving intricate tuning of structure–property relationships in complex solids through principles of solid-state chemistry and physics. The dis-

cussion thus far indicates that new materials must be able to eventually achieve certain minimum values of important parameters in order to be considered as a potential TE material. It does not matter if a material has a $\kappa_L \approx \kappa_{min}$; if it cannot be "tuned" or doped in order to attain a minimum thermopower (150 µV/K), it will not be able to achieve $ZT \approx 1$.

Classical Approach: Bulk Binary Semiconductors

Within the framework of simple electronic band structure of solids, in general, metals are poor TE materials. Hence, most of the early TE work put much emphasis on semiconductors.[18] As stated earlier, in order to have a maximum ratio of electrical to thermal conductivity, the material should have a low carrier concentration, on the order of 10^{18}–10^{19} cm^3, with very high mobilities. Crystal structure and bonding strongly influence the mobility. Materials with diamond or zinc-blende structures with a high degree of covalent bonding frequently have high mobilities (e.g., Si, Ge, InSb), but also exhibit high thermal conductivity values. On the other hand, low lattice thermal conductivities are found in conjunction with low Debye temperatures and high anharmonic lattice vibrations. These conditions are best satisfied by highly covalent intermetallic compounds and alloys of the heavy elements such as Pb, Hg, Bi, Tl, or Sb, and S, Se, or Te. Once a material system has been selected with a favorable electrical-to-thermal conductivity ratio, one optimizes the composition to further enhance the ZT by doping the material to maximize the density of states at the Fermi level and achieve a high Seebeck coefficient.

The most studied TE material, Bi_2Te_3, crystallizes in a layer structure (Figure 3) with rhombohedral–hexagonal symmetry with space group $R\overline{3}m$ (D^5_{3d}). The hexagonal unit cell dimensions at room temperature are $a = 3.8$ Å and $c = 30.5$ Å. The layers stacked along the c-axis are

··· Te–Bi–Te–Bi–Te ··· Te–Bi–Te–Bi–Te ···.

The Bi and Te layers are held together by strong covalent bonds, whereas the bonding between adjacent Te layers is of the van der Waals type. This weak binding between the Te layers accounts for the ease of cleavage along the plane perpendicular to the c-axis and the anisotropic thermal and electrical transport properties of Bi_2Te_3. For example, the thermal conductivity along the plane perpendicular to the c-axis (1.5 W m^{-1} K^{-1}) is nearly twice that of the value along the c-axis direction (0.7 W
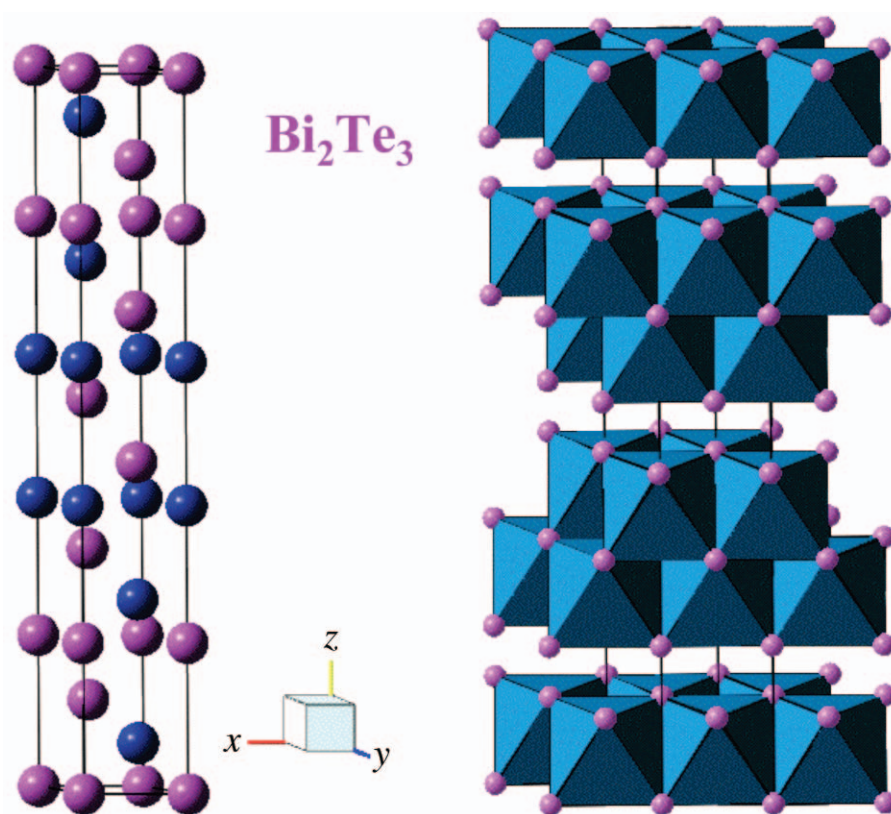

Figure 3. Crystal structure of the state-of-the-art thermoelectric material, Bi_2Te_3. The blue atoms are Bi and the pink atoms are Te.

m^{-1} K^{-1}). When grown from a melt or by zone refining, the Bi_2Te_3 crystals are always nonstoichiometric and show p-type behavior. On the other hand, n-type materials could be grown from the melt containing excess Te, iodine, or bromine. The thermal conductivity values of both p- and n-type Bi_2Te_3 are ~1.9 W m^{-1} K^{-1}, giving a ZT of about 0.6 near room temperature. Ioffe[9] suggested that alloying could further reduce the lattice thermal conductivity of Bi_2Te_3 through the scattering of short-wavelength acoustic phonons. The optimum compositions for thermoelectric cooling devices are normally $Bi_2Te_{2.7}Se_{0.3}$ (n-type) and $Bi_{0.5}Sb_{1.5}Te_3$ (p-type) with $ZT \approx 1$ near room temperature.

In contrast to Bi_2Te_3, PbTe crystallizes in a cubic NaCl-type crystal structure, and the TE properties are isotropic. Both p-type and n-type thermoelements can be produced by doping of acceptors (e.g., Na_2Te or K_2Te) or donors (PbI_2, $PbBr_2$, or Ge_2Te_3). In analogy with the Bi_2Te_3, the solid-solution compositions (e.g., PbTe-SnTe) have been made to lower the lattice thermal conductivity.[19] The ZT value of PbTe solid solutions is low near room temperature but rises to $ZT \approx 0.7$ at 700 K,

making PbTe a prime candidate for power generation in that temperature range. It is possible to achieve ZT in excess of unity at 700 K in structurally related solid-solution compositions, $AgSbTe_2$ (80%)-GeTe(20%), known as TAGS (alloys containing Te, Ag, Ge, Sb). However, due to high-temperature stability issues, these compositions are not currently favored in TE devices.

Neither Si nor Ge is a good TE material, as the lattice thermal conductivity is very large (150 W m^{-1} K^{-1} for Si and 63 W m^{-1} K^{-1} for Ge). The lattice thermal conductivity can be substantially reduced by alloy formation between the two elements. The best alloy composition is $Si_{0.7}Ge_{0.3}$; its thermal conductivity is about 10 W m^{-1} K^{-1}, and the reduction relative to Si and Ge is apparently due to the increased phonon–phonon and phonon–electron scattering.[19] Remarkably, such a large reduction does not unduly reduce the carrier mobility, and $ZT \approx 0.6$–0.7 could be realized at elevated temperatures. Due to their exceptional stability at high temperatures (~1200 K), these alloys are of interest to NASA for use in RTGs in deep-space probes.

Modern Solid-State Chemistry Design Concepts for High-ZT Materials

Complex Inorganic Structures. Most of the earlier investigations mentioned so far focused on binary intermetallic semiconductor systems. Recent approaches to high-performance bulk TE materials focus on ternary and quaternary chalcogenides containing heavy atoms with low-dimensional or isotropic complex structures to take advantage of the large carrier effective masses and low lattice thermal conductivity associated with such systems.[20] Along these lines, $CsBi_4Te_6$ possessing the layered structure has been identified as a material showing a ZT of 0.8 at 225 K, which is 40% greater than that of the $Bi_{2-x}Sb_xTe_{3-y}Se_y$ alloys.[21] Other potential low-temperature TE materials currently under investigation are low-dimensional semiconducting or semimetallic doped layered pentatellurides ($ZrTe_5$ and $HfTe_5$).[22] These compounds have a structure similar to Bi_2Te_3, with van der Waals gaps between the individual layers. Although doped pentatellurides exhibit very high power factors (exceeding the optimally doped Bi_2Te_3 solid solutions) in the low-temperature range (<250 K), their thermal conductivity is relatively high ($\sim$4–8 W m^{-1} K^{-1}), and the materials need to be compositionally tuned further to make them useful as thermoelectrics.

Recently, cubic quaternary compounds with a complex formula $Ag_nPb_mM_nTe_{m+2n}$ (M = Sb, Bi), crystallizing in the PbTe structure, have been reported.[23] The composition $AgPb_{10}SbTe_{12}$ shows an exceptionally high ZT value (>2) at elevated temperature (shown in Figure 2). This is due to the very low total thermal conductivity of the bulk material, possibly arising from compositional modulations (seen as "nanodots") similar to the one found in superlattices. If this is verified, it provides an additional "knob" to turn to achieve high ZT in bulk materials. Another group of materials under investigation are half-Heusler alloys, with the general formula MNiSn (M = Zr, Hf, Ti). A complex composition of the type $Zr_{0.5}Hf_{0.5}Ni_{0.5}Pd_{0.5}Sn_{0.99}Sb_{0.01}$ shows a ZT of 0.7 at $T \approx 800$ K, highlighting the intricate balance in structure, composition, and property relationships in these compounds.[24] The β-Zn_4Sb_3 system has been reinvestigated for TE power-generation applications at the Jet Propulsion Laboratory.[25]

Crystal Structures with "Rattlers." The method of lowering the lattice thermal conductivity through mixed-crystal or solid-solution formation does not always produce enough phonon scattering to lower the lattice thermal conductivity to κ_{min}. Slack's concept of a "phonon-glass/electron-crystal," described earlier, avoids this limitation. The concept of κ_{min} is successfully verified in crystal structures with large empty cages or voids where atoms can be partially or completely filled in such a way that they "rattle," resulting in the scattering of the acoustic phonons. This approach especially works well in highly covalent semiconductor materials based on clathrates (Si, Ge, or Sn) and void structures formed by heavy elements of low electronegativity differences (e.g., $CoSb_3$-based skutterudites). Some doped skutterudites show exceptionally high ZT values at elevated temperatures ($ZT \approx 1.5$ at 600–800 K). The structure–property relationships of these materials are discussed in the article by Nolas et al. in this issue.

Oxide Thermoelectrics. There are numerous oxides with metal atoms in their common oxidation states that are stable at elevated temperatures and show electrical properties ranging from insulating to superconducting. Nevertheless, oxides have received very little attention for TE applications. This is due to their strong ionic character, with narrow conduction bandwidths arising from weak orbital overlap, leading to localized electrons with low carrier mobilities. This situation changed with the unexpected discovery of good TE properties in a strongly correlated layered oxide, $NaCo_2O_4$.[26] This oxide attains $ZT \approx 0.7$–0.8 at 1000 K. Inspired by the striking TE performance of $NaCo_2O_4$, most of the current studies are focused on Co-based layered oxides, such as $Ca_3Co_4O_9$ and $Bi_2Sr_3Co_2O_y$, crystallizing in "misfit" (lattice-mismatched) layered structures.[26] Among the n-type oxides, Al-doped ZnO ($Al_{0.02}Zn_{0.98}O$) shows reasonably good TE performance ($ZT \approx 0.3$ at 1000 K).[27]

Rare-Earth Intermetallics with High Power Factors. As mentioned earlier, metallic compounds are not suitable for TE applications. The exceptions to this rule are intermetallic compounds containing rare-earth elements (e.g., Ce and Yb), with localized magnetic moments where the Seebeck coefficient can approach $\sim$100 μV/K with metal-like conductivities.[28,29] In these compounds, the $4f$ levels lie near the Fermi energy and form narrow non-parabolic bands, resulting in a large density of states at the Fermi level and large Seebeck coefficient values. The highest Seebeck values are found in cubic $YbAl_3$ (n-type) and $CePd_3$ (p-type). $YbAl_3$ shows a very high power factor (120–180 μW/cm K^2, or 3.6–5.4 W m^{-1} K^{-1}) at room temperature (300 K), which is nearly 4–5 times larger than that observed in optimized Bi_2Te_3-based thermoelectrics.[30] Unfortunately, the large thermal conductivity (15–22 W m^{-1} K^{-1}) lowers the ZT to about 0.2 at room temperature. Recently, the lattice thermal conductivity of this system has been lowered by doping Mn in the interstitial positions, resulting in the increase of ZT to about 0.4 at room temperature.[31] As mentioned earlier, $ZT = 1$ requires a minimum Seebeck coefficient value of 156 μV/K. The correlated metal with the highest Seebeck coefficient is $CePd_3$, which has a maximum of 125 μV/K at 140 K.[29] Future investigations should focus on increasing the Seebeck coefficients of these materials above $\sim$150 μV/K through compositional and structural tuning.

Engineered Crystal Lattices. The approaches in bulk materials research rely heavily on the thermodynamic stability of the phases at a given condition, whereas thin-film deposition can yield metastable "designer" phases with unique properties. Quantum well systems (0D, 1D, and 2D) take advantage of their low-dimensional character through physical confinements in quantum dots, nanowires, and thin-film structures to enhance the electronic properties of a given material.[32] In addition, nanostructured semiconductor materials could scatter mid- to long-wavelength phonons and thereby reduce the lattice thermal conductivity to κ_{min}.

Researchers at the Research Triangle Institute (RTI) have demonstrated a significant enhancement in ZT through the construction of Bi_2Te_3/Sb_2Te_3 superlattices.[33] These materials exhibited $ZT \approx 2.4$ at $T \approx 330$ K. The enhancement is attributed to creating a "nanoengineered" material that is efficient in thermal insulation while remaining a good electrical conductor. The thermal insulation arises from a complex localized behavior for phonons, while the electron transmission is facilitated by optimal choice of band offsets in these semiconductor heterostructures. Also, there have been reports on PbTe/PbTeSe quantum dot structures that yield $ZT \approx 1.3$–1.6.[34] These materials have been grown as thick films that are then "floated off" the substrate to yield freestanding films, which were measured to yield these results. The enhancement in ZT in the superlattice materials appears to be more from a reduction in the lattice thermal conductivity than an increase in power factor.

Summary

Currently, there are no theoretical or thermodynamic limits to the possible

values of ZT. Given the current need for alternative energy technologies and materials to replace the shrinking supply of fossil fuels, the effort is becoming more urgent. Energy-related research will grow rapidly over the next few years, and higher-performance thermoelectric materials and devices are direly needed. Slack estimated that an optimized phonon-glass/electron-crystal material could possibly exhibit values of $ZT \approx 4$.[14] This gives encouragement that such materials may be possible and could address many of our energy-related problems. Thus, a systematic search and subsequent thorough investigation may eventually yield these much-needed materials for the next generation of TE devices.

Although many strategies are being employed in hopes of identifying novel TE materials, the PGEC approach appears to be the best, as will become apparent in the following articles. One has to decide whether "holey" semiconductors (materials with cages, such as skutterudites or clathrates) or "unholey" semiconductors (such as SiGe or PbTe) are the best to pursue, and which tuning parameters are available to improve these materials.[35] To date, none of the new materials has displaced the current state-of-the-art materials (Bi_2Te_3, PbTe, or SiGe) in a commercial TE device. These materials have held that distinction for more than 30 years.

However, given the many materials yet to be investigated, there is certainly much more work ahead and promise for developing higher-efficiency thermoelectric materials and devices. While the results are very exciting, thin films may be most appropriate for small-scale electronic and optoelectronics applications where small heat loads or low levels of power generation are more appropriate. To address large-scale refrigeration (home refrigerators) or power-generation (automotive or industrial) requirements, higher-performance bulk materials will have to be developed.

Certainly, theoretical guidance, in terms of band structure calculations and modeling, will be essential to identifying the most promising TE materials. In addition, rapid yet accurate characterization of materials and verification of results are also essential in order to effectively advance this field of research. A multidisciplinary approach will be required to develop higher-efficiency thermoelectric materials and devices. The techniques used to develop "designer materials" needed for thermoelectrics will most likely prove important in other areas of materials research as well.

References

1. The reader is referred to the many MRS Symposium Proceedings volumes on the topic of thermoelectric materials and energy-conversion technologies: *Thermoelectric Materials—New Directions and Approaches* (Mater. Res. Soc. Symp. Proc. **478**, 1997); *Thermoelectric Materials 1998—The Next Generation Materials for Small-Scale Refrigeration and Power Generation Applications* (Mater. Res. Soc. Symp. Proc. **545**, 1999); *Thermoelectric Materials 2000—The Next Generation Materials for Small-Scale Refrigeration and Power Generation Applications* (Mater. Res. Soc. Symp. Proc. **626**, 2001); *Thermoelectric Materials 2001—Research and Applications* (Mater. Res. Soc. Symp. Proc. **691**, 2002); *Thermoelectric Materials 2003—Research and Applications* (Mater. Res. Soc. Symp. Proc. **793**, 2004); and *Materials and Technologies for Direct Thermal-to-Electric Energy Conversion* (Mater. Res. Soc. Symp. Proc. **886**, 2006) in press.
2. T.M. Tritt, ed., "Recent Trends in Thermoelectric Materials Research," *Semiconductors and Semimetals*, Vols. 69–71, treatise editors, R.K. Willardson and E. Weber (Academic Press, New York, 2000).
3. Jet Propulsion Laboratory Thermoelectric Science and Engineering Web site, http://www.its.caltech.edu/~jsnyder/thermoelectrics/ (accessed February 2006).
4. A.W. Allen, *Laser Focus World* **33** (March 1997) p. S15.
5. G.S. Nolas, J. Sharp, and H.J. Goldsmid, *Thermoelectrics: Basic Principles and New Materials Developments* (Springer, New York, 2001).
6. T.J. Seebeck, *Abh. K. Akad. Wiss.* (Berlin, 1823) p. 265.
7. D.T. Morelli, in *Encyclopedia of Applied Physics*, Vol. 21 (1997) p. 339.
8. P.M. Chaiken, in *Organic Superconductors,* edited by V.Z. Kresin and W.A. Little (Plenum Press, New York, 1990) p. 101.
9. A.F. Ioffe, *Semiconductor Thermoelements and Thermoelectric Cooling* (Infosearch, London, 1957).
10. J.C. Peltier, *Ann. Chem.* **LVI** (1834) p. 371.
11. H.J. Goldsmid, *Electronic Refrigeration* (Pion Limited, London, 1986).
12. D.M. Rowe, ed., *CRC Handbook of Thermoelectrics* (CRC Press, Boca Raton, FL, 1995).
13. P.L. Rossiter, *The Electrical Resistivity of Metals & Alloys* (Cambridge Press, New York, 1987); F.J. Blatt, *Physics of Electronic Conduction in Solids* (McGraw-Hill, New York, 1968); L. Solymar and D. Walsh, *Electrical Properties of Materials*, 6th Ed. (Oxford Press, New York, 1998).
14. G.A. Slack, in *CRC Handbook of Thermoelectrics*, ed. by D.M. Rowe (CRC Press, Boca Raton, FL, 1995) p. 407.
15. G.D. Mahan and J.O. Sofo, *Proc. Natl. Acad. Sci. USA* **93** (1996) p. 7436.
16. G.D. Mahan, B. Sales, and J. Sharp, *Phys. Today* **50** (3) (1997) p. 42.
17. G.A. Slack, in *Solid State Physics*, Vol. 34, edited by F. Seitz, D. Turnbull, and H. Ehrenreich (Academic Press, New York, 1979) p. 1.
18. R.R. Heikes and R.W. Ure Jr., *Thermoelectricity: Science and Engineering* (Wiley Interscience, New York, 1961) p. 405.
19. C. Wood, *Rep. Prog. Phys.* **51** (1988) p. 459.
20. M.G. Kanatzidis, S.D. Mahanti, and T.P. Hogan, eds., *Chemistry, Physics and Materials Science of Thermoelectric Materials: Beyond Bismuth Telluride* (Plenum, New York, 2003) p. 35.
21. D.Y. Chung, T. Hogan, P. Brazis, M. Rocci-Lane, C. Kannewurf, M. Bastea, C. Uher, and M.G. Kanatzidis, *Science* **287** (2000) p. 1024.
22. R.T. Littleton IV, T.M. Tritt, M. Korzenski, D. Ketchum, and J.W. Kolis, *Phys. Rev. B. Rap. Commun.* **64** 121104 (2001).
23. K.F. Hsu, S. Loo, F. Gao, W. Chen, J.S. Dyck, C. Uher, T. Hogan, E.K. Polychroniadis, and M. Kanatzidis, *Science* **303** (2004) p. 8181.
24. Q. Shen, L. Chen, T. Goto, T. Hirai, J. Yang, G.P. Meisner, and C. Uher, *Appl. Phys. Lett.* **79** (2001) p. 4165.
25. T. Caillat, J.P. Fleurial, and A. Borshchevsky, *J. Phys. Chem. Solids* **58** (1997) p. 1119.
26. I. Terasaki and N. Murayama, eds., *Oxide Thermoelectrics* (Research Signpost, Trivandrum, India, 2002).
27. M. Ohtaki, T. Tsubota, K. Eguchi, and H. Arai, *J. Appl. Phys.* **79** (1996) p. 1816.
28. R.J. Gambino, W.D. Grobman, and A.M. Toxen, *Appl. Phys. Lett.* **22** (1973) p. 506.
29. G.D. Mahan, in *Solid State Physics*, edited by F. Seitz, H. Ehrenreich, and F. Spaepen (Academic Press, New York, 1997) p. 51.
30. D.M. Rowe, G. Min, and V.L. Kuznetsov, *Philos. Mag. Lett.* **77** (1998) p. 105; D.M. Rowe, V.L. Kuznetsov, L.A. Kuznetsova, and G. Min, *J. Phys. D: Appl. Phys.* **35** (2002) p. 2183.
31. T. He, T.G. Calvarese, J.-Z. Chen, H.D. Rosenfeld, R.J. Small, J.J. Krajewski, and M.A. Subramanian, *Proc. 24th Int. Conf. on Thermoelectrics*, edited by T.M. Tritt (IEEE, Piscataway, NJ, 2005) p. 434.
32. L.D. Hicks and M.S. Dresselhaus, *Phys. Rev. B* **47** (1993) p. 12727.
33. R. Venkatasubramanian, E. Siivola, T. Colpitts, and B. O'Quinn, *Nature* **13** (2001) p. 597.
34. T.C. Harman, P.J. Taylor, M.P. Walsh, and B.E. LaForge, *Science* **297** (2002) p. 2229.
35. T.M. Tritt, *Science* **283** (1999) p. 804. □

Terry M. Tritt

M.A. Subramanian

Harald Böttner

Thierry Caillat

Terry M. Tritt, Guest Editor for this issue of *MRS Bulletin*, is a professor of physics at Clemson University. He received both his BA degree (1980) and his PhD degree (1985) in physics from Clemson University and then went to the Naval Research Laboratory (NRL) under a National Research Council postdoctoral fellowship. He subsequently became a staff scientist at NRL, where he remained for 11 years before joining the faculty at Clemson in 1996. His primary research expertise lies in electrical and thermal transport properties and phenomena, and especially in measurement and characterization techniques in novel materials. He has extensive expertise in thermoelectric materials and measurement science and has built an internationally known laboratory for the measurement and characterization of thermoelectric material parameters, particularly thermal conductivity. He has recently become involved in the synthesis and characterization of thermoelectric nanomaterials.

Tritt has served as lead organizer of three Materials Research Society symposia on thermoelectric materials, edited the three-volume *Recent Trends in Thermoelectric Materials Research* (Academic Press, 2000), and also recently edited a book published by Kluwer Press on thermal conductivity. He has been a member of the executive board of the International Thermoelectric Society (ITS) since 1999 and served as chair and host of the 24th International Conference on Thermoelectrics (ICT-2005) at Clemson in June 2005. He has written more than 140 journal publications and regularly gives invited presentations at national and international meetings.

Tritt can be reached at Clemson University, Department of Physics, 103 Kinard Laboratory, Clemson, SC 29634, USA; tel. 864-656-5319 and e-mail ttritt@clemson.edu.

M.A. Subramanian, Guest Editor for this issue of *MRS Bulletin*, is a research fellow at DuPont Central Research and Development. He holds BS and MS degrees in chemistry from the University of Madras in India and received his PhD degree in solid-state chemistry in 1982 from the Indian Institute of Technology in Madras, where he focused on synthesis and solid-state studies of oxides with pyrochlore and perovskite structures. He subsequently joined the Department of Chemistry at Texas A&M University as an NSF postdoctoral fellow, where he worked on designing new fast ion conductors for solid-state batteries. He joined DuPont in 1985 as a scientist and was recently appointed to research fellow. Subramanian's current interests include the design and understanding of structure–property relationships in new solid-state inorganic functional materials related to superconductivity, colossal magnetoresistive materials, high-κ and low-κ dielectrics, ferroelectrics, multiferroics, oxyfluorination, and thermoelectrics.

Subramanian is a visiting professor at the Institut de Chimie de la Matière Condensée de Bordeaux (ICMCB), University of Bordeaux, France. He serves as editor for *Solid State Sciences* and *Progress in Solid State Chemistry*, and serves or has served on the editorial boards of the *Materials Research Bulletin, Chemistry of Materials,* and the *Journal of Materials Chemistry*. He was awarded the Charles Pedersen Medal by DuPont in 2004 for his outstanding scientific, technological, and business contributions to the company. He has authored more than 200 publications and holds 42 U.S. patents, with 10 applications pending.

Subramanian can be reached at DuPont Central Research and Development, Experimental Station, E328/219, Wilmington, DE 19880-0328, USA; tel. 302-695-2966 and e-mail mas.subramanian@usa.dupont.com.

Harald Böttner is deputy head of the Components and Microsystems Department of the Fraunhofer Institute for Physical Measurement Techniques in Freiburg, Germany, and is currently responsible for its thermoelectric activities. He graduated with a diploma degree in chemistry from the University of Münster in 1974 and received his PhD degree in 1977 at the same university for his thesis on diffusion and solid-state reaction in the quaternary semiconductor II–VI/IV–VI material system. He joined the Fraunhofer Institut für Silicatforschung in 1978 and accepted his present appointment in 1980. He developed IV–VI infrared semiconductor lasers in parallel with activities in thermoelectrics until 1995, when he became responsible for the development of semiconductor gas sensors and thermoelectric materials until 2003. Böttner's current research activities focus on thin-film and nanoscale thermoelectrics and microelectronics-related device technology. He is the author or co-author of more than 100 publications, holds more than 10 patents, and is a member of the board of the International Thermoelectric Society.

Böttner can be reached at Fraunhofer IPM, Research Field Thermoelectrics, Heidenhofstrasse 8, 79110 Freiburg, Germany; tel. 49-761-8857121 and e-mail harald.boettner@ipm.fraunhofer.de.

Thierry Caillat is a senior member of technical staff with the Jet Propulsion Laboratory at the California Institute of Technology. He received his PhD degree in materials science from the National Polytechnique Institute of Lorraine, France, in 1991. He then received a National Research Council fellowship to study new materials for thermoelectric applications at JPL. He joined the permanent staff at JPL in 1994. Caillat's primary research interests have focused on the identification and development of new thermoelectric materials and devices. In the last ten years, he has played a key role in identifying several families of promising compounds for thermoelectric applications, including skutterudites and β-Zn_4Sb_3–based materials. More recently, he has been involved in the development of advanced thermoelectric power-generation devices for both

space and terrestrial applications.

Caillat has authored or co-authored more than 100 publications, given more than 40 invited presentations, and served on numerous national and international organization committees and panels. He was also a board member of the International Thermoelectric Society from 1996 to 2005.

Caillat can be reached at the California Institute of Technology, Jet Propulsion Laboratory, Mail Stop 277/207, 4800 Oak Grove Drive, Pasadena, CA 91109, USA; tel. 818-354-0407 and e-mail thierry. caillat@jpl.nasa.gov.

Gang Chen is a professor of mechanical engineering at the Massachusetts Institute of Technology. He received his BS (1984) and MS (1987) degrees from the Power Engineering Department at Huazhong University of Science and Technology, China, in 1984 and 1987, respectively, and his PhD degree in mechanical engineering from the University of California, Berkeley, in 1993. He was an assistant professor at Duke University from 1993 to 1997 and an associate professor at the University of California, Los Angeles, from 1997 to 2001. His research interests center on microelectronics thermal management and nanoscale transport phenomena, particularly nanoscale heat transfer, and their applications in energy storage and conversion.

Chen is a recipient of a K.C. Wong Education Foundation fellowship, an NSF Young Investigator Award, and a John Simon Guggenheim

Gang Chen

Foundation fellowship. He serves on the editorial boards of *Annual Review of Heat Transfer*, the *Journal of Computational and Theoretical Nanoscience*, the *Journal of Nanomaterials*, and *Microscale Thermophysical Engineering*. He also serves as the chair of the Advisory Board of the ASME Nanotechnology Institute and on the advisory boards of several organizations.

Chen can be reached at the Massachusetts Institute of Technology, Department of Mechanical Engineering, Room 3-158, 77 Massachusetts Avenue, Cambridge, MA 02139-4307, USA; tel. 617-253-0006 and e-mail gchen2@ mit.edu.

Ryoji Funahashi has been a senior researcher at the National Institute of Advanced Industrial Science and Technology in Japan since 1992. He received his BS (1989) and MS (1992) degrees in physical chemistry and his PhD degree (1998) in crystalline material science from Nagoya University. His research interests include novel synthetic techniques for high-performance superconducting oxide materials and, recently, the exploration of new thermoelectric oxide materials.
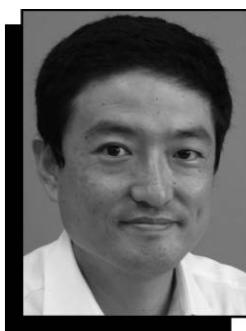
Ryoji Funahashi

Funahashi is a recipient of the Thermoelectric Conference of Japan's Best Paper Award, the *Japan Journal of Applied Physics* Paper Award, and a NEDO Industrial Technology Research and Development Project grant. He has authored or co-authored more than 150 papers, conference proceedings, invited talks, and reviews. He is also a board member of the International Thermoelectric Society and the Thermoelectric Society of Japan.

Funahashi can be reached at AIST, UBIQEN, Molecular Materials and Devices, 1-8-31 Midorigaoka, Ikeda, Osaka 563-8577, Japan; tel. 81-727-51-9485 and e-mail funahashi-r@aist.go.jp.

Xiaohua Ji is a postdoctoral researcher in the Department of Physics and Astronomy at Clemson University. In 2005, she received her PhD degree in materials physics and chemistry from Zhejiang University in China under the guidance of Xinbing Zhao. For her graduate work, she developed solvothermal and hydrothermal methods for synthesizing nanostructured thermoelectric materials. She received the Best Scientific Paper Award at the
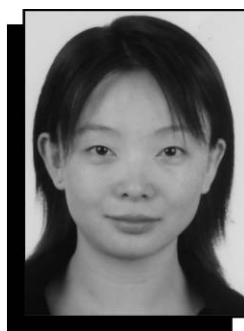
Xiaohua Ji

2004 ICT meeting in Adelaide, Australia. Under the guidance of Terry M. Tritt at Clemson, her current research involves the synthesis and characterization of nanostructured thermoelectric materials and nanocomposite bulk thermoelectric materials.

Ji can be reached at Clemson University, Department of Physics and Astronomy, Clemson, SC 29634, USA; tel. 864-656-4596 and e-mail xiaohji@clemson.edu.

Mercouri Kanatzidis is a University Distinguished Professor of Chemistry at Michigan State University, where he has served on the faculty since 1987. He received his BS degree from Aristotle University in Greece, followed by a PhD degree in chemistry from the University of Iowa in 1984. He was then a postdoctoral research associate at Northwestern University from 1985 to 1987. He has generated seminal work in metal chalcogenide chemistry through the development of novel synthetic approaches aimed at new materials discovery. His research interests include novel chalcogenides, thermoelectric materials, and the design of framework solids, intermetallic phases, and organic–inorganic nanocomposites.

Mercouri Kanatzidis

Kanatzidis is a recipient of the Presidential Young Investigator Award, the ACS Morley Medal, the ACS Exxon Solid State Chemistry Award, and the Humboldt Prize. He has been a Guggenheim fellow as well as a visiting professor at the University of Nantes, the University of Münster, and the University of Munich. The bulk of his work is described in more than 450 research publications. He holds six patents and is editor in chief of the *Journal of Solid State Chemistry*.

Kanatzidis can be reached at Michigan State University, Department of Chemistry, 406 Chemistry Building, East Lansing, MI 48824-1322, USA; tel. 517-355-9715 and e-mail kanatzid@cem.msu.edu.

Kunihito Koumoto is a professor in the Graduate School of Engineering at Nagoya University, Japan. He received BS, MS, and PhD degrees in applied chemistry from the University of Tokyo in 1974, 1976, and 1979, respectively. He served as an assistant professor and associate professor at the University of Tokyo before joining Nagoya University as a full professor in 1992. His research focuses on thermoelectric materials

Thermoelectric Materials, Phenomena, and Applications: A Bird's Eye View

Kunihito Koumoto

George S. Nolas

Joseph Poon

Apparao M. Rao

and bio-inspired processing of inorganic materials.

Koumoto received the Richard M. Fulrath Award in 1993 and the Academic Achievement Award of the Ceramic Society of Japan in 2000. He became a fellow of the American Ceramic Society and received the Chinese Ceramic Society Award in 2005. He also served the International Thermoelectric Society as president from 2003 to 2005 and is the author or co-author of more than 320 scientific papers and 38 books.

Koumoto can be reached at Nagoya University, Graduate School of Engineering, Furo-cho, Chikusa-ku, Nagoya, 464-8603, Japan; tel. 81-52-789-3327 and e-mail koumoto@apchem.nagoya-u.ac.jp.

George S. Nolas is an associate professor of physics at the University of South Florida, where he has been since 2001. He received his PhD degree from Stevens Institute of Technology in 1994 and conducted pioneering studies on the synthesis and thermal properties of filled skutterudites as a postdoctoral associate with Glen Slack at Rensselaer Polytechnic Institute. Before accepting his current position,

he spent five years as a physicist and senior member of the technical staff at Marlow Industries Inc., a thermoelectrics manufacturer in Dallas, Texas. His research interests are in the synthesis and structure–property relationships of new materials, and his current research focuses on new materials for power conversion and alternative energy applications, including thermoelectrics, photovoltaics, and hydrogen storage.

Nolas is author of *Thermoelectrics: Basic Principles and New Materials Developments*, published by Springer with co-authors Jeffrey Sharp and Julian Goldsmid. He holds three patents, with another two pending, on new materials for power-conversion applications. He has edited four Materials Research Society proceedings volumes (two as lead editor) on thermoelectric materials research, organized symposia for the American Physical Society and the American Ceramic Society, given numerous invited conference presentations and seminars, and is currently in his second term as a board member of the International Thermoelectric Society.

Nolas can be reached at the University of South Florida, Depart-

ment of Physics, PHY 114, 4202 E. Fowler Avenue, Tampa, FL 33620-5700, USA; tel. 813-974-2233 and e-mail gnolas@cas.usf.edu.

Joseph Poon is the William Barton Rogers Professor of Physics at the University of Virginia, where he joined the Physics Department in 1980. He received both his BS and PhD degrees from the California Institute of Technology and was a research associate in applied physics at Stanford University. His areas of research have included amorphous superconductors, quasicrystals, bulk amorphous metals, and thermoelectric alloys. He is a fellow of the American Physical Society and was named one of the "*Scientific American* 50" in 2004 for the creation of amorphous steel. He has published more than 200 papers.

Poon can be reached at the University of Virginia, Department of Astronomy-Physics, PO Box 400714, Jesse Beams Lab, Room 167, Charlottesville, VA 22901, USA; tel. 434-924-6792 and e-mail sjp9x@virginia.edu.

Apparao M. Rao is a professor in condensed-matter physics at Clemson University. He

obtained his PhD degree in physics from the University of Kentucky in 1989 and held a postdoctoral appointment with Mildred S. Dresselhaus at MIT until 1991. His current research focuses on understanding and controlling the synthesis of 1D nanostructured organic and inorganic materials. He has published extensively on the synthesis, characterization, and applications of carbon nanotubes.

Rao can be reached at Clemson University, Department of Physics and Astronomy, 107 Kinard Laboratory, Clemson, SC 29634-0978, USA; tel. 864-656-6758 and e-mail arao@clemson.edu.

Ichiro Terasaki is a professor in the Applied Physics Department at Waseda University in Tokyo. He received his BE, ME, and PhD degrees in applied physics from the University of Tokyo in 1986, 1988, and 1992, respectively. He began his research career as a research associate at the University of Tokyo, moving on to become chief researcher at the International Superconductivity Technology Center. He became an associate professor at Waseda in 1997 and accepted his current position as a full professor in 2004. His research in-

terests include experimental studies in condensed-matter physics, especially charge transport properties of transition-metal oxides, organic conductors, and intermetallic compounds.

Terasaki is the recipient of the Sir Martin Wood Prize and ICT's Best Scientific Paper Award. He has published more than 150 papers, conference proceedings, invited talks, books, and reviews.

Terasaki can be reached at Waseda University, Department of Applied Physics, 3-4-1 Okubo, Shinjuku-ku, Tokyo 169-8555, Japan; tel. 81-3-5286-3854 and e-mail terra@waseda.jp.

Rama Venkatasubramanian is director of the Center for Thermoelectric Research at RTI International in North Carolina and the founder and chief technology officer of Nextreme Thermal Solutions Inc., a company spun off from RTI to commercialize its unique thin-film superlattice thermoelectric technology. He earned his PhD degree in electrical engineering from Rensselaer Polytechnic Institute and is a National Talent Scholar and a graduate of the Indian Institute of Technology in Madras. His research interests include photovoltaics, heteroepitaxy of novel materials, photonic materials, the study of nanoscale thermal physics, thermal management in high-performance electronics, and direct thermal-to-electric conversion devices. He is well known for pioneering thermoelectric superlattice materials and devices. Venkatasubramanian's

Ichiro Terasaki

Rama Venkatasubramanian

Jihui Yang

work on superlattices has been recognized as a significant breakthrough in thermoelectrics using nanoscale engineered materials. This technology has won an R&D 100 Award (2002) and the Technology of the Year Award (2005) from the Council for Entrepreneurial Development in North Carolina.
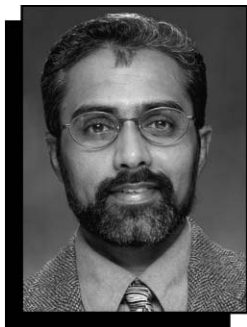
Venkatasubramanian is a recipient of the Allen B. Dumont Prize from Rensselaer, RTI's Margaret Knox Excellence Award in Research in 2002, and the IEEE Eastern North Carolina Inventor of the Year in 2003. He has several patents issued in thermoelectrics, has authored more than 100 refereed publications,

and has contributed to two book chapters.

Venkatasubramanian can be reached at RTI International, Center for Thermoelectric Research, PO Box 12194, Research Triangle Park, NC 27709-2194, USA; tel. 919-541-6889 and e-mail rama@rti.org.

Jihui Yang is a staff research scientist in the

Materials and Processes Laboratory at General Motors Research and Development Center. He received a BS degree in physics from Fudan University of China in 1989, an MS degree in physics from the University of Oregon in 1991, an MS degree in radiological physics from Wayne State University in 1994, and a PhD degree in physics from the University of Michigan in 2000. His research interests include low-temperature transport properties of intermetallic compounds and semiconductors, magnetism, thermoelectric materials, and the development of thermoelectric technology for automotive applications.

Yang has published several book chapters

and more than 30 papers. He was the recipient of the GM DEGS fellowship in 1997 and the Kent M. Terwilliger Prize for Best Doctoral Thesis from the Physics Department of the University of Michigan in 2001. He has served on various committees for APS and the Materials Research Society and organized several symposia for MRS and ACerS. He was also elected to the board of directors of the International Thermoelectric Society in 2005.

Yang can be reached at General Motors Research and Development Center, Mail Code 480-106-224, 30500 Mound Road, Warren, MI 48090, USA; tel. 586-986-9789 and e-mail jihui.yang@gm.com. □

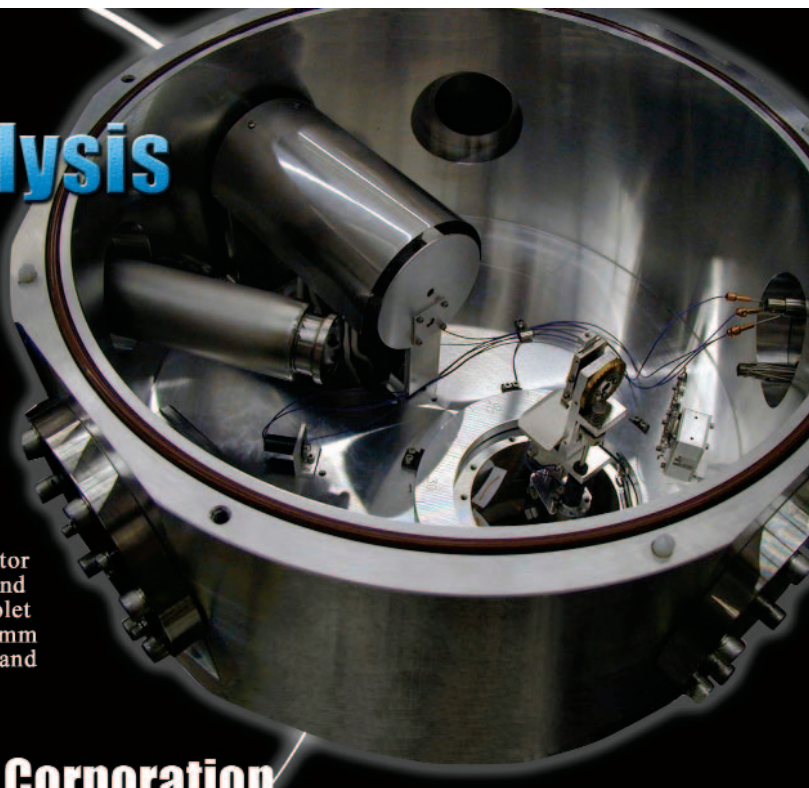*For more information, see http://www.mrs.org/bulletin_ads*

Recent Developments in Bulk Thermoelectric Materials

George S. Nolas, Joe Poon, and Mercouri Kanatzidis

Abstract

Good thermoelectric materials possess low thermal conductivity while maximizing electric carrier transport. This article looks at various classes of materials to understand their behavior and determine methods to modify or "tune" them to optimize their thermoelectric properties. Whether it is the use of "rattlers" in cage structures such as skutterudites, or mixed-lattice atoms such as the complex half-Heusler alloys, the ability to manipulate the thermal conductivity of a material is essential in optimizing its properties for thermoelectric applications.

Keywords: *alloy, compound, thermal conductivity, thermoelectricity.*

Introduction

As the search for promising bulk thermoelectric materials intensifies, certain material systems stand out as possessing the highest potential for achieving thermoelectric figures of merit well above unity. These materials possess relatively good electrical properties while maintaining very low thermal conductivities. In some cases, enhancements in the electrical properties have been realized. These results have attracted great attention, and many research laboratories worldwide are now working on one or more of these material systems in order to achieve further improvements in their thermoelectric properties. We discuss some of the bulk thermoelectric materials of primary interest in this article.

Skutterudites

The physical properties of skutterudites depend sensitively on their compositions. This compositional dependence not only provides a means to investigate the structure–property relationships in this material system but also allows the optimization of transport properties for thermoelectric (TE) applications. The diversity of potential compositional variants allows for rich variation in physical properties and is one of the key reasons this material system continues to be investigated by many research groups. One approach for optimizing these materials is void-filling.

The skutterudite-type ($CoAs_3$-type) structure is a cubic structure with the space group composed of eight corner-shared TX_6 (T = Co, Rh, Ir; X = P, As, Sb) octahedra. As depicted in Figure 1, the linked octahedra produce a void, or vacant site, at the center of the $(TX_6)_8$ cluster, occupying a body-centered position in the cubic lattice. This is a large void that can accommodate relatively large metal atoms, resulting in the formation of filled skutterudites. Many different elements have been introduced into the voids of skutterudites, including lanthanide, actinide, alkaline-earth, alkali, thallium, and Group IV elements.[1–3] The composition can be written as $\square_2X_8Y_{24}$ (typically X = Co, Rh, or Ir; Y = P, As, or Sb), with the symbol $\square$ illustrating the two voids per cubic unit cell.

The concept of introducing "guest" atoms into these voids to act as strong phonon-scattering centers, thus greatly reducing the lattice thermal conductivity of these compounds, has resulted in improvements in the TE properties of skutterudites.[1,2] The smaller and heavier the ion in the voids, the larger the disorder that is produced and thus the larger the reduction in the lattice thermal conductivity. Skutterudite antimonides possess the largest voids and are therefore of particular interest for TE applications. Results from Sales et al.[4] and Fleurial et al.[5] show high *ZT* values (the common figure of merit for comparing different TE materials) at elevated temperatures in $LaFe_3CoSb_{12}$ and $CeFe_3CoSb_{12}$ for both *p*-type and *n*-type specimens. *ZT* values approaching 1.4 above 900°C for these materials have been reported,[5] indicating their successful optimization for TE power-conversion applications.

It should be noted, however, that a small concentration of void-fillers results in a large reduction in thermal conductivity. Five percent of La[6] or Ce,[7] for example, in the voids of $CoSb_3$ results in a thermal-conductivity reduction of ~50%, as compared with $CoSb_3$. In certain cases, higher power factors have also been obtained with partial filling, as compared with more fully filled, charge-compensated compositions. The aim in investigating partially filled skutterudites is realizing an optimum electron concentration while re-
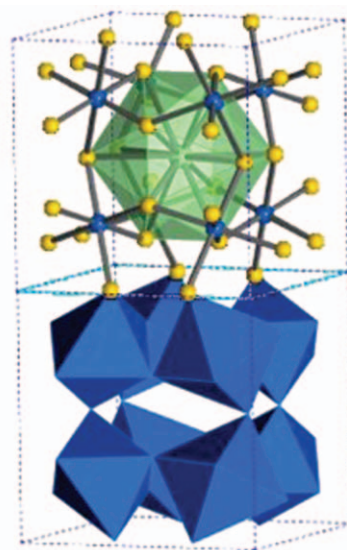

Figure 1. Schematic illustration of a skutterudite crystal, where the guest atom is inside a 12-coordinated "cage" (green) surrounded by yellow pnicogen (family of Bi, Sb, As, P, or N) atoms. The metal sites are depicted in blue. The octahedral environment surrounding the metal sites is shown in the lower portion of the figure, also in blue.

ducing the thermal conductivity, thereby maximizing ZT. This is possible, since partially filled, uncompensated skutterudites obey a rigid-band model, with the void fillers being the electron donors. Thus, improved TE properties in partially filled skutterudites are achievable, owing to the combination of a low thermal conductivity with higher power factors as compared with those of nearly fully filled skutterudites. Figure 2 in the introductory article by Tritt and Subramanian in this issue shows one example[8] ($Yb_{0.19}Co_4Sb_{12}$) of how partial filling can result in higher ZT values than full filling. $Ba_{0.24}Co_4Sb_{12}$ has also demonstrated $ZT > 1$ above 800 K.[9] Although these results are encouraging, and of technological interest for waste-heat recovery, still higher ZT values can be achieved by further optimization. Most recently, for example, a small amount of Ni doping for Co in Ba[10] and Ca[11] partially filled skutterudites has resulted in higher ZT values than the ZT values of $Ba_xCo_4Sb_{12}$[9] and $Ca_xCo_4Sb_{12}$.[12]

The success of Slack and Tsoukala's[13] "rattling-atom" approach to skutterudite research has lead to $ZT > 1$ in a bulk TE material. The research into skutterudite compounds has also led to a greater understanding of thermal transport processes, revealed novel phonon-scattering mechanisms, and resulted in efforts to explore other materials with similar properties to obtain low thermal conductivities while maintaining high power factors. In fact, the field is now focusing on low-thermal-conductivity compounds as a major component in high-ZT thermoelectric materials, as we will see in several examples to follow.

Clathrates

Clathrates are a class of novel materials that can be thought of as periodic solids in which tetrahedrally bonded atoms (typically Ge, Si, or Sn) form a framework of cages that enclose relatively large metal atoms. Clathrates have demonstrated interesting properties that are rare in condensed-matter physics. One of the more interesting of these properties for TE applications is a very low "glass-like" thermal conductivity in Type I clathrates.[14] The Type I structure (Figure 2) can be represented by the general formula $X_2Y_6E_{46}$, where X and Y are guest atoms encapsulated in two different polyhedra, while E represents the elements Si, Ge, or Sn.

There have been little data reported on the high-temperature TE potential of these materials, and even less on the optimization of the TE properties of these materials for power-conversion applications. Blake et al.[15] used density functional calculations to theoretically investigate the transport properties of Type I clathrates. Their findings showed room-temperature ZT values of up to 0.5 for optimized $Sr_8Ga_{16}Ge_{30}$ and $Ba_8In_{16}Sn_{30}$ Type I clathrates, while $ZT = 1.7$ at 800 K was predicted for optimized compositions. Kuznetsov et al.[16] were first to measure the Seebeck coefficient and resistivity above room temperature for the Type I clathrates. Estimating the high-temperature thermal conductivity from published results of low-temperature thermal transport in Type I clathrates resulted in $ZT = 0.7$ at 700 K for $Ba_8Ga_{16}Ge_{30}$ and $ZT = 0.87$ at 870 K for $Ba_8Ga_{16}Si_{30}$.

Recently, research was initiated toward optimizing the TE properties of Type I clathrates above room temperature.[17] Power factors approaching 1 W m^{-1} K^{-1} for Ge clathrates were obtained at 650 K. Together with the low thermal conductivity achieved in these materials, these data indicate the potential for high ZT values at elevated temperatures. As outlined earlier, attempts at optimizing the TE properties of these interesting materials have only recently begun. Future studies, however, should also focus on other clathrate structure types—Type VIII clathrates, for example. In n-type clathrates, optimization has reached $ZT = 0.4$ at room temperature,[18] with theoretical predictions for p-type clathrates to be $ZT = 1.2$ at 400 K.[19]

The Type II clathrate structure (Figure 3) is particularly interesting, as it allows for partial filling of the polyhedra, in contrast to the totally filled Type I structure. Thus, the electrical properties of Type II clathrates can be more readily "tuned,"
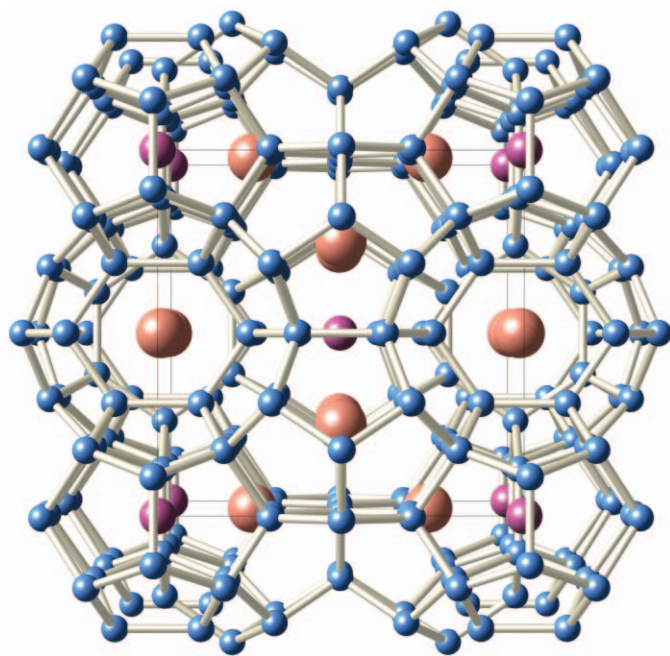

Figure 2. Crystal structure of the Type I clathrate. Framework atoms are shown in blue, guest atoms inside the tetrakaidecahedra are orange, and guest atoms inside the pentagonal dodecahedra are purple.
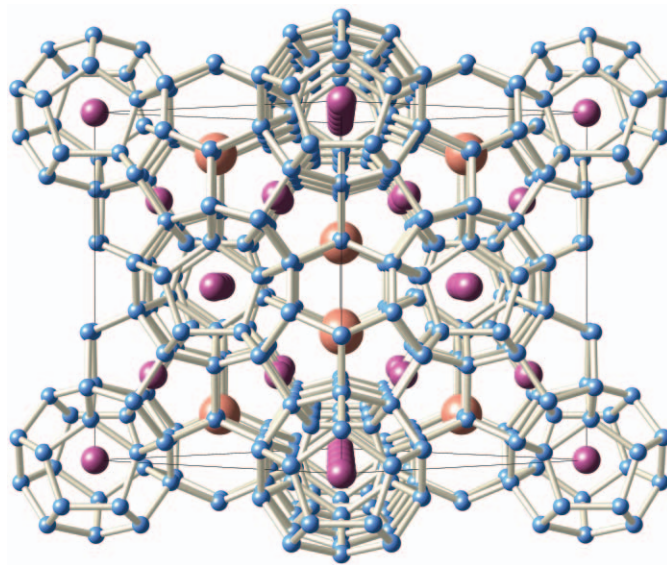

Figure 3. Crystal structure of the Type II clathrate. Framework atoms are shown in blue, guest atoms inside the tetrakaidecahedra are orange, and guest atoms inside the pentagonal dodecahedra are purple.

allowing for better control of the doping level.[17] In compounds with the Type II structure, the interstitial "guest" atoms that reside inside the polyhedra simultaneously act as electrical dopants and phonon-scattering centers. These properties allow an investigation into the interrelationship between the guest atoms and their atomic cages and how this relationship affects their TE properties.

Half-Heusler Alloys

Half-Heusler (HH) intermetallic alloys have recently received increasing attention as potential TE materials for high-temperature applications. HH phases have the MgAgAs (space group $F\bar{4}3m$),[20] or "half-stuffed GaAs," crystal structure, consisting of three interpenetrating fcc sublattices. Their chemical formula is XYZ, where X, Y, and Z can be selected from many different elemental groups.[21] Figure 4 shows the unit cell of TiNiSn, in which Ti and Sn occupy a NaCl lattice and Ni occupies an fcc sublattice. HH phases are semiconductors[21–24] when the valence count per formula unit is 8 (e.g., LiMgP has a bandgap of 2.4 eV) or 18 (e.g., TiNiSn has a bandgap of 0.3 eV). Some HH alloys are half-metallic ferromagnets and heavy-fermion metals.[22,25] The narrow bands give rise to a large effective mass that in turn leads to a large thermopower.[26] Because of the large thermopower and spin-polarized band structure, HH alloys have been investigated as thermoelectric and spintronic materials.[21,25–28]

The chemistries of the three sublattices can be tuned independently. For example, in TiNiSn, doping the Sn site provides the charge carriers, while doping the Ti and Ni sites causes mass fluctuations that can lead to the reduction of thermal conductivity. Many of the refractory metal[26,27,29,30] and lanthanide metal[28] thermoelectric HH alloys exhibit large room-temperature Seebeck coefficients of ~100 μV K^{-1} and moderate electrical resistivities of ~1–10 μΩ m. The alloys reported are attractive as high-temperature TE materials, because they are relatively easily synthesized as 100% dense samples. In particular, the refractory-based alloys exhibit high melting points of 1100–1300°C as well as chemical stability and essentially zero sublimation at temperatures near 1000°C.

The effectiveness of doping in achieving improved TE properties has been demonstrated in several HH alloys.[26–32] Sb-doped TiNiSn alloys exhibit power factors as high as 4.6 W m^{-1} K^{-1} at 650 K (380°C).[29] Despite the large power factor values, there exists the challenge of reducing the relatively high thermal conductivity ($\kappa \geq$ 10 W m^{-1} K^{-1}) that is evident in the HH al-

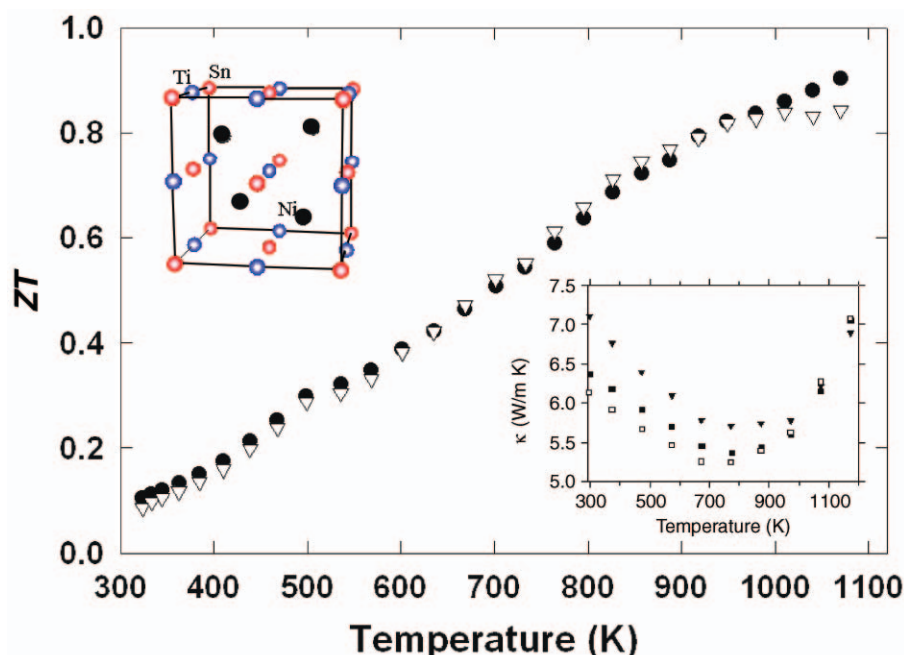Figure 4. Figure of merit ZT versus T for $Hf_{0.75}Zr_{0.25}NiSn_{0.975}Sb_{0.025}$ obtained from measured ($\triangledown$) and extrapolated ($\bullet$) thermal conductivities. (inset, upper left) Unit cell of TiNiSn half-Heusler phase. (inset, lower right) Thermal conductivities obtained from laser-flash thermal diffusivity and specific heat, with data points starting at 300 K: $Hf_{0.75}Zr_{0.25}NiSn_{0.975}Sb_{0.025}$ ($\blacktriangledown$), $Hf_{0.6}Zr_{0.25}Ti_{0.15}NiSn_{0.975}Sb_{0.025}$ ($\blacksquare$), and $Hf_{0.75}Zr_{0.25}Ni_{0.9}Pd_{0.1}Sn_{0.975}Sb_{0.025}$ ($\square$).

loys. The effect of disorder induced by differences in mass and atomic size is evident in the reduction of κ.[26–32]

Notable progress was made when Shen et al. reported a maximum $ZT \approx 0.7$ at 800 K in n-type Sb-doped ZrNiSn alloys partially substituted with the heavier Pd atoms in the Ni sublattice.[31] More recently, Sakurada and Shutoh reported maximum ZT values near 1.4 at 700 K in n-type $(Zr_{0.5}Hf_{0.5})_{0.5}Ti_{0.5}NiSn_{1-y}Sb$.[32] Despite failed attempts[33] to reproduce the results of Sakurada and Shutoh, their report has already generated considerable interest in HH alloys, as evidenced by the number of papers on HH alloys presented by researchers at the 2005 International Conference on Thermoelectrics.

Meanwhile, recent approaches have provided new impetus for evaluating the ZT of thermally stable, multicomponent HH alloys measured up to 1100 K. Indeed, the latest research has raised the prospect of achieving a ZT value near 1. In recent studies[33] performed jointly by two groups (University of Virginia and Clemson University), the HH compositions were doped with Sb contents (up to 4%), which is significantly higher than previously reported. This is because it is recognized that higher dopant content can partly mitigate the compensated behavior characterized by a

rollover in the Seebeck coefficient α observed in n-type alloys at high temperatures. It is believed that the shift of $\alpha(T)$ can lead to a larger power factor and therefore higher ZT. The idea has been verified in some (Ti,Zr,Hf)NiSn quinary alloys when indeed it was found that at higher Sb doping content, the maximum in $\alpha^2\sigma T$, where σ is the electrical conductivity, is shifted to a higher temperature. In addition to doping the Sn sites with Sb, the refractory-metal sublattices are simultaneously and randomly occupied by Hf, Zr, and Ti, providing additional tuning for optimizing the power factor as well as fluctuations in the atomic mass and interatomic force for reducing the lattice thermal conductivity.[34]

Using the laser-flash method, $\kappa(T)$ for three complex alloys have been measured up to 1160 K by Tritt. The results are shown in the lower-right inset in Figure 4. ZT for the quinary HH composition $Hf_{0.75}Zr_{0.25}NiSn_{0.975}Sb_{0.025}$ is also shown in Figure 4. It is noted that the ZT values of HH alloys are already comparable with those of state-of-the-art SiGe alloys near 800°C.

While the prospect exists of achieving even higher ZT values in complex, thermally stable, n-type HH alloys, p-type HH alloys such as MM'X (M = Ti, Zr, and Hf;

M′ = Co, Ni, and Pt; X = Sb and Sn, for example) should also be investigated. Indeed, TiCoSb exhibits a high Seebeck coefficient of ~400 μV K^{-1} at 300 K. Furthermore, one can exploit grain-boundary scattering effects[35] through grain-size refinement. A bottom-up approach has also been used to construct bulk nanostructured samples that result in a lower lattice thermal conductivity.[36]

β-Zn₄Sb₃ Alloys

A p-type intermetallic compound most suitable for use as a high-ZT material at moderate temperatures is one of the three modifications of the Zn_4Sb_3 phase, namely, β-Zn_4Sb_3 (the other two modifications are the α and γ phases).[37] The β phase has the hexagonal rhombohedric crystal structure (space group $R\bar{3}C$, unit cell dimensions $a = 12.231$ Å and $c = 12.428$ Å) and is stable between 263 K and 765 K. The highest ZT value reported for β-Zn_4Sb_3 is 1.4 at 400°C.[38] Apparently, β-Zn_4Sb_3 starts to decompose into ZnSb and Zn phases above 400°C. Single-phase, polycrystalline samples were made by melting and homogenizing Zn and Sb in sealed quartz ampoules. The obtained ingots were ground into powders. The alloy powders were then hot-pressed to form crack-free samples. In other reports, direct synthesis methods involving hot pressing or spark plasma sintering were also reported.[39–41]

Both single-crystal and polycrystalline samples have been investigated. The power factor in Zn_4Sb_3 is rather low (~0.87 W m^{-1} K^{-1} at 400°C) for a high-ZT material. For comparison, HH alloys have power factors of 3–5 W m^{-1} K^{-1} at 400°C. What makes β-Zn_4Sb_3 a remarkable TE material is its "phonon-glass" behavior, characterized by an unusually low thermal conductivity of ~0.9 W m^{-1} K^{-1} at 300 K.[42] The already low thermal conductivity in Zn_4Sb_3 can be further reduced by doping the Zn and Sn sites.[42,43] However, the doping concentrations are found to be quite limited; only a few percent of In or Sn can be added to substitute Sb without resulting in a two-phase material. Even in the case of substitution with the isostructural compound Cd_4Sb_3, the solid-solution range of (Zn,Cd)$_4$Sb$_3$ is limited to only 6 mol% Cd_4Sb_3 at 400°C.[39] However, no improvement in ZT above the highest recorded value of ~1.4 at 400°C has been reported for the doped samples.

The detailed crystal structure of β-Zn_4Sb_3 has been determined by employing both single-crystal and powder x-ray diffraction methods coupled with maximum entropy analysis.[42,44] The study has enabled the identification of valence states of Sb atoms that fully occupy the nonequivalent Sb(1) and Sb(2) sites as Sb^{3-} and Sb$_2^{4-}$ dimers, as well as the valence states of Zn atoms that occupy 90% of the Zn(1) sites as Zn^{2+}. Overall, β-Zn_4Sb_3 is a valence compound belonging to a similar class of compound semiconductors such as Bi_2Te_3 and PbTe. The study has also uncovered three different interstitial sites for Zn atoms in addition to the main Zn(1) sites that are only 90% occupied. Refinement of the structure based on this discovery of interstitial sites reveals a composition of $Zn_{12.8}Sb_{10}$. The mass density and composition of the new crystal structure are reported to be in agreement with measurements. The Zn interstitials exhibit large thermal displacements. The glass-like interstitials are largely responsible for the phonon damping that suppresses the lattice thermal conductivity. There is apparently also Sb disorder along the c-axis that can contribute to the glass-like thermal conductivity. Electronic structure and transport calculations using the crystal structure obtained have identified the compound as a p-type semiconductor,[44] in agreement with experimental findings of the doping trend. It was demonstrated that the Zn interstitial atoms play a dual role as electron donors and thermopower enhancers. First-principles calculations of electronic structure and thermoelectric properties have also been performed.[45] The band structure results reveal the covalent tendency of the compound, consistent with the good carrier mobility measured. The high Seebeck coefficient can be attributed to the strong energy-dependence of the Fermi surface topology near band-filling. Recently, study of the low-temperature phase of β known as α-Zn_4Sb_3 (composition $Zn_{13}Sb_{10}$) reveals an electronic structure similar to that of the β phase with a bandgap of ~0.3 eV.[46] Further detailed investigation of the structural and transport property changes across the α ↔ β transition will shed light on the nature of order–disorder transition in this complex crystal system.

Chalcogenides

Chalcogenide compounds comprise a large class of materials that are predominantly semiconductors. Most of the compounds are environmentally stable and can have high melting points. They combine a set of properties that make them suitable for practical thermoelectric applications. Because of the versatility in the choice of element and chalcogen and the suitable electronegativity of the chalcogen elements, which varies little from sulfur to tellurium, it is possible to obtain semiconductors with energy gaps appropriate for TE applications over a wide range of temperature (typically 100–1400 K). Chalcogenide materials have had a prominent position in the field of thermoelectricity going back to its early stages. For example, the cornerstone of today's TE cooling has been the compound Bi_2Te_3 and its solid solutions $Bi_{2-x}Sb_xTe_3$ and $Bi_2Te_{3-x}Se_x$.[47] Another chalcogenide of importance is PbTe, which has a maximum $ZT \sim 0.8$ at ~500°C; it has been suitable for power generation at intermediate temperatures. The germanium-based TAGS (Te-Ag-Ge-Sb) is more efficient than PbTe but has found little use, due to its high sublimation rate and low-temperature phase transition.[48]

The past decade has seen a strong resurgence of interest in achieving superior TE performance, and these "old" chalcogenides now have found new forms that have led to more than incremental increases in ZT.[49–51] Recent reports indicate that nanostructured thin-film superlattices of Bi_2Te_3 and Sb_2Te_3 have $ZT \sim 2.4$ at room temperature,[50] whereas $PbSe_{0.98}Te_{0.02}$/PbTe quantum dot superlattices grown by molecular-beam epitaxy have $ZT \sim 1.6$.[50] These thin-film $PbSe_{0.98}Te_{0.02}$/PbTe systems feature nanodots of PbSe embedded in a PbTe material. At ~550 K, these samples were reported to exhibit $ZT \sim 2.5$. The primary reason for the high ZT values appears to be a very marked depression of the thermal conductivity, presumably by the strong phonon scattering imposed by the nanodots of PbSe.

One approach to searching for new thermoelectrics is to build exotic new structures from scratch through solid-state exploratory synthesis. This has afforded the promising compounds $BaBiTe_3$[52] and $K_2Bi_8Q_{13}$ (Q = Se,[53,54] S[55]). These possess highly anisotropic structures, low symmetry, and large unit cells, with "loosely" bound electropositive cations in channels formed by extended Bi/Q frameworks, resulting in a low lattice thermal conductivity.

CsBi₄Te₆

One noteworthy tellurium compound is $CsBi_4Te_6$, which is in fact mixed-valent in Bi and can be viewed as containing Bi^{2+} ions that form Bi–Bi bonds. This compound features a strongly anisotropic structure with one of the directions being prominent in terms of its charge transport properties. It possesses a lamellar structure with slabs of (Bi$_4$Te$_6$)$^{1-}$ alternating with layers of Cs$^+$ ions (Figure 5a). $CsBi_4Te_6$ is very responsive to the type and level of doping agent used. Low doping levels significantly affect the charge transport properties of $CsBi_4Te_6$. Appropriate p-type doping of $CsBi_4Te_6$ with SbI$_3$ or Sb gives rise to a high ZT_{max} of 0.8 at 225 K,
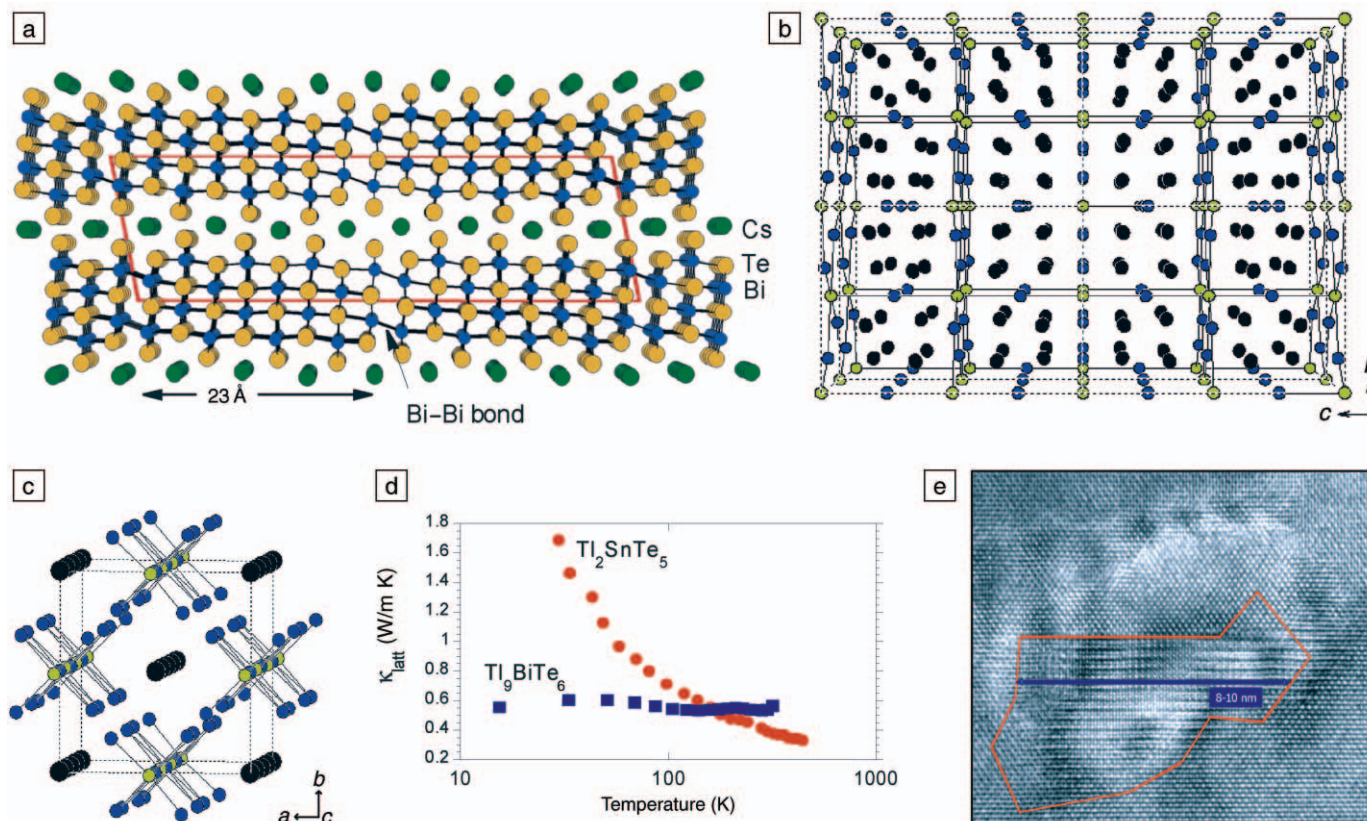
Figure 5. (a) Structure of $CsBi_4Te_6$. Yellow circles are Te atoms, blue circles are Bi atoms, and green circles are Cs atoms. (b) Structure of Tl_9BiTe_6. Yellow circles are Bi atoms, blue are Te atoms, and black are Tl atoms. (c) Structure of Tl_2SnTe_5. Black circles are Tl atoms, blue are Te atoms, and yellow are Sn atoms. (d) Thermal conductivity of Tl_9BiTe_6 and Tl_2SnTe_5. (e) High-resolution transmission electron microscopy image of a typical nanoscale inhomogeneity (indicated by the red outline) found in $Ag_{1-x}Pb_{18}SbTe_{20}$.

which is among the highest values ever reported below room temperature.[56] At this temperature, $CsBi_4Te_6$ is the best-performing TE material and raises new hope for extending the use of TE materials to lower temperatures than ever before. Different dopants can allow the ZT_{max} to be shifted to even lower temperatures, in the neighborhood of 180 K.[57] Band calculations suggest that $CsBi_4Te_6$ has very advantageous electronic structural features for a promising TE material, characterized by a great deal of anisotropic effective mass. The electrical conductivity and thermopower are directly attributed to the elaborate electronic structure of a material near the Fermi level. The presence of Bi–Bi bonds in the structure is responsible for the material having a very narrow energy gap, nearly half that of Bi_2Te_3. The narrower bandgap is related to the fact that the ZT maximum in $CsBi_4Te_6$ is achieved at lower temperatures than in Bi_2Te_3.

Tl_9BiTe_6 and Tl_2SnTe_5

In the last decade, it has been more fully appreciated that thallium chalcogenides tend to possess very low thermal conductivities. Tl_9BiTe_6 and Tl_2SnTe_5 are two such noteworthy phases. Tl_9BiTe_6 belongs to a large group of ternary compounds which can be derived from the isostructural Tl_5Te_3 (Figure 5b).[58] Tl_9BiTe_6 can be optimized to exhibit $ZT \sim 1.2$ at 500 K, mainly due to its extremely low lattice thermal conductivity of ~ 0.39 W m^{-1} K^{-1} at 300 K. This value is nearly the same as the one reported for the $PbSe_{0.98}Te_{0.02}/PbTe$ quantum dot superlattices grown by molecular-beam epitaxy.

The Tl_2SnTe_5 is a tetragonal phase, with chains of $(SnTe_5)^{2-}$ running parallel to each other and charge-balancing Tl^+ ions situated in between (Figure 5c). The Tl^+ ions are in an eightfold-coordinated site with relatively long Tl–Te bonds. These long bonds produce very low-frequency phonons, which is one of the main reasons that the compound has a very low thermal conductivity (0.5 W m^{-1} K^{-1}). This compound can be optimized to a ZT of ~ 1 at 500 K.[59]

Another interesting Tl-containing compound is Ag_9TlTe_5. It is isostructural to Ag_2Te, which has an even lower lattice thermal conductivity than Tl_2SnTe_5, as shown in Figure 5d.[60] Ag_9TlTe_5 combines extremely low thermal conductivity and relatively low electrical resistivity to give $ZT = 1.23$ at 700 K. Unfortunately, thallium-containing compounds are unlikely to be accepted for practical use, due to significant toxicity and environmental issues. Nevertheless, they are interesting from a scientific standpoint, as they could teach us a great deal about thermal conductivity and ZT optimization.

$AgPb_mSbTe_{m+2}$

Recently, the family of chalcogenide lead-based compounds, $AgPb_mSbTe_{m+2}$, or LAST-m materials ("LAST" for "lead antimony silver tellurium"), were revisited, and several suitably doped members were reported to exhibit large ZT values from ~ 1.2 (LAST-10) to ~ 1.7 (LAST-18) at 700 K.[61]

A large number of compositions can be generated by changing m. This family of compounds is compositionally complex, yet its members possess an average NaCl structure. Research work conducted on

this system in the 1950s and 1960s reported that the $AgPb_mSbTe_{m+2}$ are solid solutions of the type $(AgSbTe_2)_{1-x}(PbTe)_x$, and therefore the metal cations are randomly disordered in the NaCl structure.[62] The metals Ag, Pb, and Sb were reported as sitting on Na sites, while the chalcogen atoms occupied the Cl sites. However, recent work has shown that this is not the case.[63] Electron microscopic examination of $AgPb_{18}SbTe_{20}$ samples revealed significant compositional modulations on the 1–10-nm scale manifested in a variety of ways, including endotaxially dispersed quantum dots (see Figure 5e). This indicates that they are not solid solutions, raising important new questions as to the significance and impact of these nanostructured features on TE properties. The nanocrystals are endotaxially embedded in the matrix, with a good lattice match on all surrounding surfaces (mismatch of ~2–4%). This endotaxy occurring in these materials could be highly conducive to facile carrier transport throughout the sample.

The very high number of nanocrystal–matrix interfaces could provide a formidable barrier to phonon transmission in the bulk sample, thereby setting the foundation for a marked enhancement in *ZT* relative to that of the classical solid-solution system. The LAST materials show exceptionally low lattice thermal conductivity of ~0.45 W m^{-1} K^{-1} at 700 K (actual value depends on *m*). Experimental results indicate that the formation of the nanostructures and the TE performance of these materials are very sensitive to the synthesis conditions and small changes in chemical composition.

Summary

Investigations into materials with low thermal conductivity, and the reduction in thermal conductivity of other materials systems, are now key aspects of research into advanced thermoelectric materials. An understanding of thermal transport in new materials can provide a means to incorporate good electrical properties with low thermal conductivity and result in improved TE performance. Whether it is the use of "rattlers" in cage structures such as skutterudites or mixed-lattice atoms such as the complex half-Heusler alloys, the ability to manipulate the thermal conductivity of a material is essential in obtaining good TE materials. For example, the low thermal conductivity of chalcogenides is a key property that leads to high *ZT* values for these materials. A detailed understanding of the phonon propagation in these systems is thus desirable. Undoubtedly, additional work is needed to better

understand these materials systems. However, as proposed by Slack in the early 1990s, the phonon-glass/electron-crystal approach continues to be the most fruitful method of research in our search for higher-performance thermoelectric materials.

References
1. G.S. Nolas, D.T. Morelli, and T.M. Tritt, *Annu. Rev. Mater. Sci.* **29** (1999) p. 89 and references therein.
2. C. Uher, in *Semiconductors and Semimetals*, Vol. 69, edited by T.M. Tritt (Academic Press, New York, 2000) p. 139 and references therein.
3. B.C. Sales, in *Handbook of the Physics and Chemistry of Rare Earths*, Vol. 33 (Elsevier Science, Amsterdam, 2002) p. 1.
4. J.-P. Fleurial, A. Borshchevsky, T. Caillat, D.T. Morelli, and G.P. Meisner, in *Proc. 15th Int. Conf. Thermoelectrics* (IEEE, Piscataway, NJ, 1996) p. 91.
5. B.C. Sales, D. Mandrus, and R.K. Williams, *Science* **272** (1996) p. 1325.
6. G.S. Nolas, J.L. Cohn, G.A. Slack, and S.B. Schujman, *Appl. Phys. Lett.* **73** (1998) p. 176.
7. D.T. Morelli, G.P. Meisner, B. Chen, S. Hu, and C. Uher, *Phys. Rev B* **56** (1997) p. 7376.
8. G.S. Nolas, M. Kaeser, R. Littleton IV, and T.M. Tritt, *Appl. Phys. Lett.* **77** (2000) p. 1822.
9. J.S. Dyck, W. Chen, C. Uher, L. Chen, X. Tang, and T. Hirai, *J. Appl. Phys.* **91** (2002) p. 3698.
10. X. Tanga, Q. Zhang, L. Chen, T. Goto, and T. Hirai, *J. Appl. Phys.* **97** 093712 (2005).
11. M. Puyet, A. Dauscher, B. Lenoir, M. Dehmas, C. Stiewe, E. Müller, and J. Hejtmanek, *J. Appl. Phys.* **97** 083712 (2005).
12. M. Puyet, B. Lenoi, A. Dauscher, M. Dehmas, C. Stiewe, and E. Müller, *J. Appl. Phys.* **95** (2004) p. 4852.
13. G.A. Slack and V.G. Tsoukala, *J. Appl. Phys.* **76** (1994) p. 1665.
14. G.S. Nolas, G.A. Slack, and S.B. Schujman, in *Semiconductors and Semimetals*, Vol. 69, edited by T.M. Tritt (Academic Press, San Diego, 2001) p. 255.
15. N.P. Blake, S. Latturner, J.D. Bryan, G.D. Stucky, and H. Metiu, *J. Chem. Phys.* **115** (2001) p. 8060.
16. V.L. Kuznetsov, L.A. Kuznetsova, A.E. Kaliazin, and D.M. Rowe, *J. Appl. Phys.* **87** (2000) p. 7871.
17. G.S. Nolas, *Thermoelectrics Handbook: Macro- to Nano-Structured Materials*, edited by D.M. Rowe (CRC Press, Boca Raton, FL) in press.
18. A. Bentien, V. Pacheco, S. Paschen, Y. Grin, and F. Steglich, *Phys. Rev. B* **71** 165206 (2005).
19. G.K.H. Madsen, K. Schwarz, P. Blaha, and D.J. Singh, *Phys. Rev. B* **68** 125212 (2003).
20. W. Jeischko, *Metall. Trans. A* **1** (1970) p. 3159.
21. S.J. Poon, in *Recent Trends in Thermoelectric Materials Research II,* edited by T.M. Tritt, *Semiconductors and Semimetals*, Vol. 70, Chap. 2, treatise editors, R.K. Willardson and E.R. Weber (Academic Press, New York, 2001) p. 37.
22. J. Tobola, J. Pierre, S. Kaprzyk, R.V. Skolozdra, and M.A. Kouacou, *J. Phys. Condens. Matter* **10** (1998) p. 1013.
23. F.G. Aliev, N.B. Brandt, V.V. Moschalkov, V.V. Kozyrkov, R.V. Scolozdra, and A.I. Belogorokhov, *Phys. B: Condens. Matter* **75** (1989) p. 167.
24. S. Ogut and K.M. Rabe, *Phys. Rev. B* **51** (1995) p. 10443.
25. W.E. Pickett and J.S. Moodera, *Phys. Today* **54** (2001) p. 39.
26. C. Uher, J. Yang, S. Hu, D.T. Morelli, and G.P. Meisner, *Phys. Rev B* **59** (1999) p. 8615.
27. H. Hohl, A.P. Ramirez, C. Goldmann, G. Ernst, B. Wolfing, and E. Bucher, *J. Phys. Condens. Matter* **11** (1999) p. 1697.
28. S. Sportouch, P. Larson, M. Bastea, P. Brazis, J. Ireland, C.R. Kannenwurf, S.D. Mahanti, C. Uher, and M.G. Kanatzidis, in *Thermoelectric Materials 1998—The Next Generation Materials for Small-Scale Refrigeration and Power Generation Applications*, edited by T.M. Tritt, M.G. Kanatzidis, G.D. Mahan, and H.B. Lyon Jr. (*Mater. Res. Soc. Symp. Proc.* **545**, Warrendale, PA, 1999) p. 421.
29. S. Bhattacharya, A.L. Pope, R.T. Littleton IV, T.M. Tritt, V. Ponnambalam, Y. Xia, and S.J. Poon, *Appl. Phys. Lett.* **77** (2000) p. 2476.
30. Y. Xia, S. Bhattacharya, V. Ponnambalam, A.L. Pope, S.J. Poon, and T.M. Tritt, *J. Appl. Phys.* **88** (2000) p. 1952.
31. Q. Shen, L. Chen, T. Goto, T. Hirai, J. Yang, G.P. Meisner, and C. Uher, *Appl. Phys. Lett.* **79** (2001) p. 4165.
32. S. Sakurada and N. Shutoh, *Appl. Phys. Lett.* **86** (2005) p. 2105.
33. S.R. Culp, S.J. Poon, N. Hickman, T.M. Tritt, and J. Blumm, *Appl. Phys. Lett.* **88** 042106 (2006).
34. Y. Yang, G.P. Meisner, and L. Chen, *Appl. Phys. Lett.* **85** (2004) p. 1140.
35. J.W. Sharp, S.J. Poon, and H.J. Goldsmid, *Phys. Status Solidi A* **187** (2001) p. 507.
36. S. Bhattacharya, T.M. Tritt, Y. Xia, V. Ponnambalam, S.J. Poon, and N. Thadhani, *Appl. Phys. Lett.* **81** (2002) p. 43.
37. H.W. Mayer, I. Mikhail, and K. Schubert, *J. Less-Common Metals* **59** (1978) p. 43.
38. T. Caillat, J.-P. Fleurial, and A. Borshchevsky, *J. Phys. Chem. Solids* **58** (1997) p. 1119.
39. V.L. Kuznetsov and D.M. Rowe, *J. Alloys Compd.* **372** (2004) p. 103.
40. S.C. Ur, I.H. Kim, and P. Nash, *Mater. Lett.* **58** (2004) p. 2132.
41. K. Ueno, A. Yamamoto, T. Noguchi, T. Inoue, S. Sodeoka, H. Takazawa, C.H. Lee, and H. Obara, *J. Alloys Compd.* **385** (2004) p. 254.
42. G.J. Snyder, M. Christensen, E. Nishibori, T. Caillat, and B.B. Iversen, *Nature Mater.* **3** (2004) p. 458.
43. M. Tsutsui, L.T. Zhang, K. Ito, and M. Yamaguchi, *Intermetallics* **12** (2004) p. 809.
44. F. Cargnoni, E. Nishibori, P. Rabiller, L. Bertini, G.J. Snyder, M. Christensen, and B.B. Inversen, *Chem. Eur. J.* **20** (2004) p. 3861.
45. S.G. Kim, I.I. Mazin, and D.J. Singh, *Phys. Rev. B* **57** (1998) p. 6199.
46. J. Nylen, M. Andersson, S. Lidin, and U. Haeussermann, *J. Am. Chem. Soc.* **126** (2004) p. 16306.
47. G.S. Nolas, J. Sharp, and H.J. Goldsmid, *Thermoelectrics: Basic Principles and New Materials Developments* (Springer, New York, 2001).
48. E. Skrabeck and D.S. Trimmer, in *CRC Handbook of Thermoelectrics*, edited by

D.M. Rowe (CRC Press, Boca Raton, FL, 1995) p. 267.

49. R. Venkatasubramanian, E. Siivola, T. Colpitts, and B. O'Quinn, *Nature* **413** (2001) p. 597.

50. T.C. Harman, P.J. Taylor, M.P. Walsh, and B.E. LaForge, *Science* **297** (2002) p. 2229.

51. L.D. Hicks, T.C. Harman, and M.S. Dresselhaus, *Appl. Phys. Lett.* **63** (1993) p. 3230.

52. D.Y. Chung, S. Jobic, T. Hogan, C.R. Kannewurf, R. Brec, J. Rouxel, and M.G. Kanatzidis, *J. Amer. Chem. Soc.* **119** (1997) p. 2505.

53. T.J. McCarthy, S.P. Ngeyi, J.H. Liao, D.C. DeGroot, T. Hogan, C.R. Kannewurf, and M.G. Kanatzidis, *Chem. Mater.* **5** (1993) p. 331.

54. T. Kyratsi, J.S. Dyck, W. Chen, D.Y. Chung, C. Uher, K.M. Paraskevopoulos, and M.G. Kanatzidis, *J. Appl. Phys.* **92** (2002) p. 965.

55. M.G. Kanatzidis, T.J. McCarthy, T.A. Tanzer, L. Chen, L. Iordanidis, T. Hogan, C.R. Kannewurf, C. Uher, and B. Chen, *Chem. Mater.* **8** (1996) p. 1465.

56. D.Y. Chung, T. Hogan, P. Brazis, M. Rocci-Lane, C.R. Kannewurf, M. Bastea, C. Uher, and M.G. Kanatzidis, *Science* **287** (2000) p. 1024.

57. D.Y. Chung, T.P. Hogan, M. Rocci-Lane, P. Brazis, J.R. Ireland, C.R. Kannewurf, M. Bastea, C. Uher, and M.G. Kanatzidis, *J. Am. Chem. Soc.* **126** (2004) p. 6414.

58. B. Wolfing, C. Kloc, J. Teubner, and E. Bucher, *Phys. Rev. Lett.* **86** (2001) p. 4350.

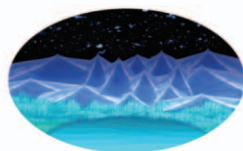59. J.W. Sharp, B.C. Sales, and D.G. Mandrus, *Appl. Phys. Lett.* **74** (1999) p. 3794.

60. K. Kurosaki, A. Kosuga, H. Muta, M. Uno, and S. Yamanaka, *Appl. Phys. Lett.* **87** 061919 (2005).

61. K.F. Hsu, S. Loo, F. Guo, W. Chen, J.S. Dyck, C. Uher, T. Hogan, E.K. Polychroniadis, and M.G. Kanatzidis, *Science* **303** (2004) p. 818.

62. S. Sportouch, M. Bastea, P. Brazis, J. Ireland, C.R. Kannewurf, C. Uher, and M.G. Kanatzidis, in *Thermoelectric Materials 1998—The Next Generation Materials for Small-Scale Refrigeration and Power Generation Applications*, edited by T.M. Tritt, M.G. Kanatzidis, G.D. Mahan, and H.B. Lyon Jr. (*Mater. Res. Soc. Symp. Proc.* **545**, Warrendale, PA, 1999) p. 123.

63. E. Quarez, K.F. Hsu, R. Pcionek, N. Frangis, E.K. Polychroniadis, and M.G. Kanatzidis, *J. Amer. Chem. Soc.* **127** (2005) p. 9177.   □

Complex Oxide Materials for Potential Thermoelectric Applications

Kunihito Koumoto, Ichiro Terasaki, and Ryoji Funahashi

Abstract

Layered CoO_2 materials are excellent candidates for potential thermoelectric applications. Their single crystals show good *p*-type thermoelectric properties at temperatures higher than 800 K in air. Recently, the mechanism of thermoelectric properties was clarified through a discussion of electronic and crystallographic structure. In order to fabricate thermoelectric modules possessing good power-generation properties, thermoelectric materials and metallic electrodes must be connected with low contact resistance and high mechanical strength. It has been found that good junctions can be formed using Ag paste including *p*- and *n*-type oxide powders. The role of spin entropy contributions to thermopower will be presented, in connection with strong electron correlation and triangular lattices.

Keywords: oxide, thermal conductivity, thermoelectricity.

Introduction

Waste heat from automobiles, factories, and similar sources offers a high-quality energy source equal to about 70% of the total primary energy, but it is difficult to reclaim because its sources are small and widely dispersed. Thermoelectric (TE) generation systems offer the only viable method of overcoming these problems by converting heat energy directly into electrical energy irrespective of source size and without the use of moving parts or the production of environmentally deleterious wastes. The requirements placed on materials needed for this task, however, are not easily satisfied. Not only must they possess a high conversion efficiency, but they must also be composed of nontoxic and abundantly available elemental materials having high chemical stability in air, even at temperatures of 800–1000 K. Oxide materials, such as those used in the present study, are particularly promising for TE applications because of their stability even at high temperatures in air.

The challenge of creating novel TE oxides has recently motivated investigations from various materials viewpoints. As it is difficult to control an electronic system and a phonon system simultaneously in a simple crystalline field, a complex crystal composed of more than two nanoblocks with different compositions and structural symmetries, the so-called hybrid crystal, is considered to be effective in controlling electron and phonon transport separately, thus enhancing the total conversion efficiency.

Layered cobalt oxides, such as Na_xCoO_2 and $Ca_3Co_4O_9$, can be regarded as consisting of complex crystalline fields.[1–4] In these oxides, CoO_2 nanosheets possessing a strongly correlated electron system serve as electronic transport layers, while sodium ion nanoblock layers or calcium cobalt oxide misfit layers serve as phonon-scattering regions to achieve low thermal conductivity.[5,6] This fact inspired us to generate high-performance TE materials from natural superlattices or hybrid crystals that are composed of the periodic arrangement of nanoblocks or nanosheets possessing different TE functions.

TE modules using oxide materials have been reported;[7,8] however, their performance is much lower than expected, considering the properties of their starting materials. This is thought to be because the contact resistance is very high at electrodes in which oxide/metal junctions are usually formed, thus severely limiting the magnitude of the output power. Moreover, cracking and exfoliation due to the great difference in thermal expansion between oxides and metals are also serious problems. Given the high temperatures (>773 K) of applications with TE oxides, conventional materials and methods for constructing electrodes cannot be used. Accordingly, the preparation of electrodes possessing good mechanical and electrical properties is considered to be one of the most important issues in realizing TE power generation. Here, we describe TE properties of *p*-type layered CoO_2 and *n*-type $Sr_{n+1}Ti_nO_{3n+1}$ materials. The fabrication of modules composed of TE oxides will be demonstrated, along with their power-generating properties.

Nanoblock Integration

Crystals, in general, can be regarded as being composed of coordination polyhedra as structural units, and they are connected with each other to form nanoblocks or nanosheets as physical property units. So if more than two kinds of unit nanoblocks, with different compositions and symmetries, are integrated into superlattices or hybrid crystals, each block can play its own role in generating a specific function, and hence, electron and phonon transport can be independently controlled (Figure 1). These functions are combined to give rise to high TE performance. Interfacial effects may be generated, leading to further performance enhancements.

p-Type Oxides: Thermoelectric Properties of the Layered Co Oxides

At present, more than ten layered Co oxides have been discovered since the discovery of the good *p*-type TE properties of Na_xCoO_2.[1] The crystal structure of Na_xCoO_2 is schematically shown in Figure 2a, in which the CdI_2-type CoO_2 layer and the Na layer alternately stack along

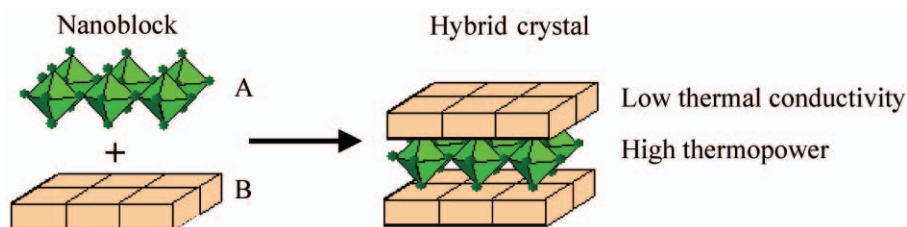# Complex Oxide Materials for Potential Thermoelectric Applications

Figure 1. Design of new functional oxides according to the concept of nanoblock integration.

the c-axis. The Na content x is varied from 0.3 to 1.0, which concomitantly changes the crystal structures indexed as the α, α', β, and γ phases.[9–11] In particular, the hydrated $x = 0.35$ sample exhibits a superconducting transition at 5 K.[12] Good TE properties are observed near $x = 0.55–0.7$ (the γ phase), which has been called $NaCo_2O_4$ after Jansen and Hoppe,[13] who first synthesized this compound in the 1970s.

Figure 2b corresponds to the Ca-based Co oxide that has been known as $Ca_3Co_4O_9$.[2] Recently, its crystal structure was precisely analyzed and found to be a misfit-layer compound composed of alternate stacks of the hexagonal CoO_2 layer of CdI_2 type and the square Ca_2CoO_3 layer of NaCl type.[3,4] Such a "hexagon-on-square" structure causes a highly distorted interface and a b-axis lattice misfit. Figure 2c shows the crystal structure of the Bi-based Co oxide $Bi_2Sr_2Co_2O_y$ that was thought to an isomorphic material to the high-temperature superconducting Cu oxide $Bi_2Sr_2CaCu_2O_8$.[14] This material is the second example of the misfit-layered oxide, consisting of the CoO_2 layer and the $Bi_2Sr_2O_4$ layer.[15,16] In this particular compound, a modulated structure is superimposed in the Bi_2O_2 plane, giving an extremely complicated structure.

Figure 3a shows the resistivity ρ of the three Co oxides along the in-plane direction. Note that the misfit oxides exhibit substantial in-plane anisotropy due to the hexagonal lattice being distorted by the square NaCl-type layer (the block layer), and only the b-axis data are shown here. The most conducting compound is Na_xCoO_2, where a low ρ of 200 $\mu\Omega$ cm at 300 K decreases in a metallic-like fashion with decreasing temperature down to 1.5 K.[1] This is as conductive as the superconducting Cu oxides, meaning that the layered Co oxide is one of the most conductive layered oxides. One thing to note is that there is no indication of localization at low temperatures, which is quite unusual in a quasi two-dimensional conductor. Furthermore, the Na layer is highly disordered by randomly distributed vacant sites, which could act as a strong scatterer for the conduction electrons. Thus, the conduction electrons in the CoO_2 layer seem to be free from the disorder in the Na layer, like the "charge confinement" in the high-temperature superconducting Cu

oxides. The other two compounds show a fairly large ρ of 1–10 mΩ cm at 300 K, with an upturn below ~50 K.[17,18] This upturn is due to a pseudogap gradually opening in the density of states at low temperatures.[19]

Figure 3b shows the Seebeck coefficient α of the three Co oxides along the in-plane direction (the b-axis data for the misfit oxides). The magnitude of α is as large as 100–150 μV K^{-1} at 300 K, comparable with that of conventional TE semiconductors. Koshibae and co-workers[20] have proposed that the low-spin-state Co^{4+} ion brings a large entropy of k_B ln 6 in the background of the low-spin state Co^{3+} ion of zero entropy. The evaluated α in the high-temperature limit is $k_B \log 6/e = 150\ \mu$V K^{-1}, which satisfactorily agrees with experiment. At low temperatures, the α values are essentially proportional to temperature, which reminds us of a mass-enhanced metal, such as a valence-fluctuation or heavy-fermion material. In fact, thermodynamic quantities such as specific heat and susceptibility are very similar to those of the valence-fluctuation material $CePd_3$.[20]

Figure 3c shows the thermal conductivity κ of the three Co oxides along the in-plane direction (the b-axis data for the misfit oxides).[5] Clearly, a more complicated block layer shows lower κ, implying that κ is predominantly determined by the

Figure 3. (a) Temperature-dependence of in-plane resistivity ρ, (b) Seebeck coefficient α, and (c) thermal conductivity κ of the three Co oxides shown in Figure 2.
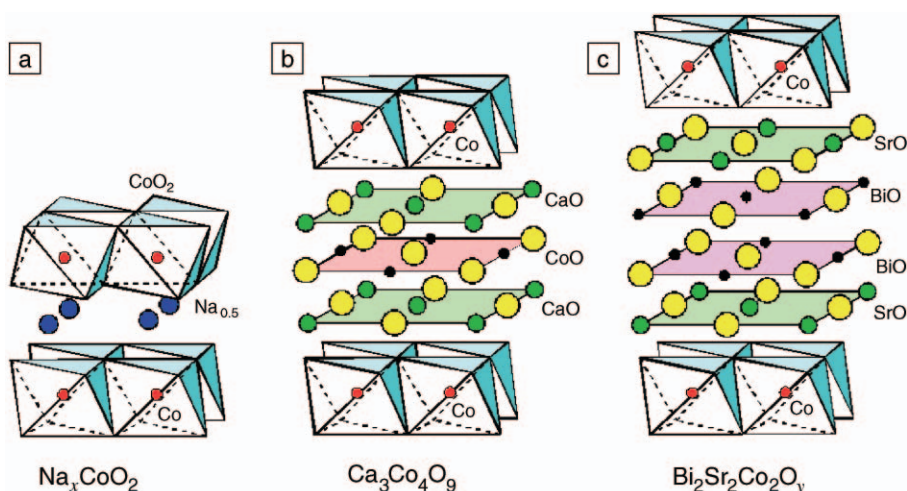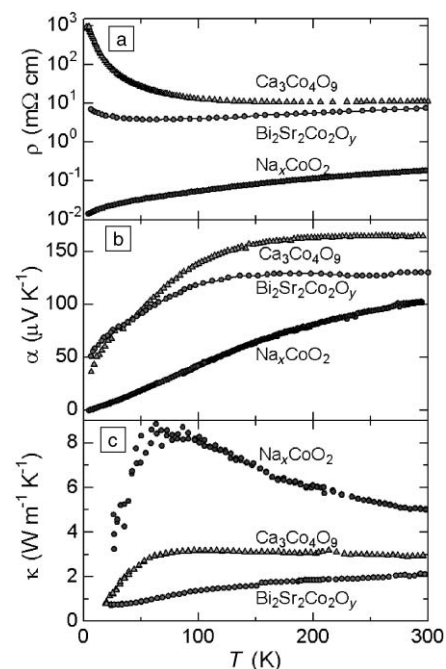

Figure 2. Schematic illustration of the crystal structure of CoO_2-based TE oxides: (a) Na_xCoO_2, (b) a Ca-based Co oxide known as $Ca_3Co_4O_9$, and (c) the Bi-based Co oxide $Bi_2Sr_2Co_2O_y$.

block layer. Thus far, high κ was expected for oxides, because oxygen is a light atom. However, this is not always true: in the layered Co oxides, the lattice thermal conductivity is determined by cations in the block layer rather than by oxygen anions.

The layered structure works quite well in two ways. The first is that the electric current and the thermal current flow in different paths in space.[5,21] This enables us to control the lattice thermal conductivity by properly choosing the insulating block layer. This is a manifestation of so-called "phonon-glass/electron-crystal" behavior,[22] and we call this type of material design "nanoblock integration." The other way is that the CdI_2-type CoO_2 block favors the low spin state of Co^{3+} and Co^{4+}, which holds the large α at high temperatures. In the case of the perovskite cobalt oxide $R_{1-x}M_xCoO_3$ (R = rare-earth, M = alkaline-earth), the high spin state of Co^{3+} seriously suppresses α.[23] These favorable conditions rarely occur in other transition-metal oxides, most of which show poor TE properties. One exception is the layered Rh oxides, where a nanoblock integration works well.[24,25]

n-Type Oxides:
Thermoelectric Performance of
Heavily Doped n-Type SrTiO₃

Strontium titanate (STO), heavily doped with donor dopants, has recently been found to show fairly good TE properties at room temperature.[26] STO has an isotropic cubic crystal structure (perovskite-type) and is known to have an electronic band structure in which the conduction band is made of the Ti $3d$ orbitals.[27] Band degeneracy N_c is 6 including the spin degeneracy with the bandgap energy of ~3.2 eV.[26] Possibly due to the d-band nature, the effective mass m^* of carrier electrons is quite large; $m^* = (1.16{\sim}10)m_0$, where m_0 is the free electron mass.[26,28]

The values for m^* estimated from the temperature-dependence of α were ~$6m_0$ and ~$7m_0$ for La-doped STO and Nb-doped STO, respectively.[29] This large effective mass gives rise to a large $\alpha > 0.1$ mV K^{-1} at 300 K and increases monotonically with increasing temperature. La- and Nb-doped (~10^{20}–10^{21} cm^{-3}) STO single crystals behave as degenerate semiconductors, and their electrical conductivity σ becomes as high as ~10^3 S cm^{-1} at 300 K. It decreases gradually with increasing temperature, which is consistent with the temperature-dependence of Hall mobility μ (~10 cm^2 V^{-1} s^{-1} at 300 K), but it decreases proportionally to $T^{-2.0}$ below ~750 K and $T^{-1.5}$ above ~750 K. The temperature-dependence of Hall mobility indicates that the carriers are scattered by polar optical phonons

below 750 K, while acoustic phonon scattering becomes predominant above ~750 K.[29] It should be noted that the power factor $\alpha^2\sigma$ of the heavily donor-doped STO reaches ~2×10^{-3} W m^{-1} K^{-2} at 300 K, which is comparable with that of conventional TE materials such as bismuth telluride. This fact strongly indicates that the electron system of STO has high potential for TE performance.

Accordingly, we have attempted to clarify the practically achievable maximum thermoelectric figure of merit ZT of STO by carefully evaluating the transport properties of the single crystal and epitaxially grown thin-film samples of good quality.[30] Figure 4 shows the temperature-dependence of ZT for La- and Nb-doped STO.[31] It can clearly be seen that the maximum $ZT = 0.37$ is obtained from 20% Nb-doped STO (Nb concentration ~4.0×10^{21} cm^{-3}) at ~1000 K. Actually, Nb doping gives rise to larger effective mass, m^*, of carrier electrons than La doping, because Nb with a larger ionic radius than Ti expands the lattice and enhances the carrier localization, while La doping leads to a smaller effective mass of electrons. The large effective mass keeps α values from greatly decreasing, even at high carrier concentration, and this fact makes Nb-doped STO a good base material for TE application.

However, the maximum ZT value of 0.37 is still too low compared with state-of-the-art materials whose ZT exceeds 1.0 or even 2.0.[32] The factor most responsible for the low ZT of STO is its high κ, ~10 W m^{-1} K^{-1} at 300 K, which cannot become lower than ~3 W m^{-1} K^{-1} at 1000 K, even though it decreases with increasing temperature.[29]
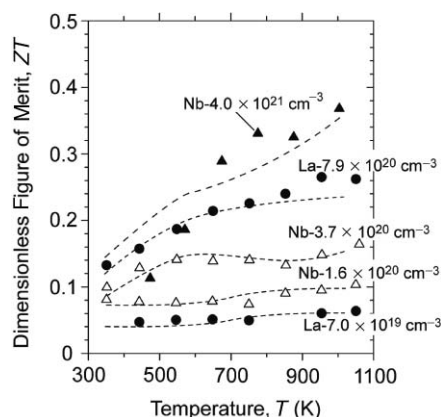

Figure 4. Dimensionless thermoelectric figure of merit ZT versus temperature for La-doped STO and Nb-doped STO; dashed curves were estimated from experimental data for lightly doped STO single crystals.[31]

Muta et al. doped STO with various rare-earth ions substituting for strontium sites and found that Dy is the most effective in reducing κ down to 3.4 W m^{-1}K^{-1} at 300 K and in increasing the figure of merit up to 3.84×10^{-4} K^{-1} at 573 K.[33] They further tried to reduce κ through substituting Ba for Sr and found that the intermediate composition gives the lowest κ of ~3.3 W m^{-1} K^{-1} at 300 K and the highest figure of merit of ~3.0×10^{-4} K^{-1} at 400–600 K.[34] However, conventional solid-solution approaches do not appear to be very effective in suppressing the thermal conduction in STO.

Natural Superlattices:
Hybrid Crystals

Based on the concept of nanoblock integration, we are interested in the Ruddlesden–Popper phases, $Sr_{n+1}Ti_nO_{3n+1}$ [$SrO(SrTiO_3)_n$, n = integer] that exist as a homologous series between $SrTiO_3$ and SrO.[35] These phases have layered perovskite structures in which SrO and $(SrTiO_3)_n$ layers are alternately stacked periodically (Figure 5).[35,36] These oxides can be regarded as natural superlattices, and therefore sublattice interfaces are expected to change the phonon behavior to suppress thermal conduction and improve the TE performance.

In our preliminary experiment, Nb-doped STO polycrystal and STO-327 polycrystal ($n = 2$, $Sr_3Ti_2O_7$) that possess similar carrier densities were employed for the measurement to compare their TE properties.[37] It is clearly seen in Table I that σ of STO-327 is slightly larger than that of STO, while α is slightly smaller. This finding is considered to be reasonable, if it is taken into consideration that the effective mass of carrier electrons in STO-327 is lower than that in STO.[38]

The κ value of STO-327 is about half that of STO. This finding firmly suggests that the formation of a hybrid crystal with
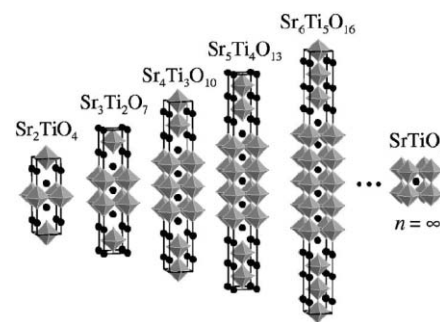

Figure 5. Crystal structures of the Ruddlesden–Popper homologous series.[36] Each octahedron consists of TiO₆. The solid black dots denote Sr ions.

Table I: Thermoelectric Properties of Polycrystals at 300 K.[36]

Polycrystal	Relative Density (%)	n (cm^{-3})	Hall Mobility, μ (cm^2 V^{-1} s^{-1})	Electrical Conductivity, σ (S cm^{-1})	Seebeck Coefficient, α (μV K^{-1})	Thermal Conductivity, κ (W m^{-1} K^{-1})	Figure of Merit, Z (K^{-1})	Thermoelectric Figure of Merit, ZT
Nb-doped STO	94	9.1×10^{20}	1.2	170	-97	7.3	2.2×10^{-5}	7×10^{-3}
STO-327	92	9.0×10^{20}	1.4	198	-86	3.7	4.0×10^{-5}	1.2×10^{-2}

a layered structure leads to enhanced scattering of phonons that are responsible for thermal conduction. As shown in Figure 6, the κ values of STO-327, STO, and SrO all decrease with increasing temperature (proportional to T^{-1}), indicating that the phonon–phonon scattering is dominant for thermal conduction in all cases.[39] A reduction in the κ value of STO-327 would have been caused by suppression of the mean free path of phonons possibly associated with the formation of sublattice interfaces. This should be further verified by a more careful experiment employing high-quality single-crystal samples.

Thermoelectric Oxide Modules
Constructing Good Oxide/Metal Junctions[41]

Bulk materials of p-type Ca$_{2.7}$Bi$_{0.3}$Co$_4$O$_9$ (Co-349) and n-type La$_{0.9}$Bi$_{0.1}$NiO$_3$ (Ni-113) were prepared using a hot-pressing technique in order to align the Co-349 grains and to densify. Both p- and n-type hot-pressed plates were cut to provide a leg element area of 3.7 mm $\times$ 4.5 mm and a leg element length of 4.7 mm. The length direction was made perpendicular to the

Figure 6. Thermal conductivity versus temperature for STO-327 [SrO(SrTiO$_3$)$_2$] compared with STO39 (SrTiO3) and SrO.[40]

hot-pressing axis for the purpose of inducing a temperature gradient.

An alumina plate 5.0 mm wide, 8.0 mm long, and 1.0 mm thick was used as a substrate. Ag paste was applied to one side of the alumina plate and solidified by heating to achieve electrical conduction. Ag paste was mixed with p-type oxide powder for connection of the p-leg and with n-type oxide powder for connection of the n-leg. The compositions of the oxide powders used were identical to those of the p- and n-legs. The same precursor powders were pulverized by ball milling to obtain a grain size smaller than 10 μm and then were mixed in varying ratios with the Ag paste (0 wt%, 1.5 wt%, 6 wt%, or 10 wt% oxide/Ag paste). After connection of the legs and substrate, the wet Ag paste was dried at 373 K and solidified by heating at 1073 K in air.

Figure 7 shows the temperature-dependence of internal resistance R_I for different versions of the unicouple constructed using the Ag paste containing various weight percentages of oxide powders. Since the difference in ρ values for each leg among the samples is <10%, the incorporation of the oxide powders is seen to be effective in reducing R_I. This is due to the reduction of contact resistance R_c between the oxide leg elements and the Ag paste. Considering the resistance of Ag on the substrate, R_c at 950 K accounts for 12.5% and 56.8% of total R_I for the unicouples

Figure 7. Temperature-dependence of internal resistance in oxide unicouples.

connected using the 6 wt% and 0 wt% oxide/Ag pastes, respectively. An increase in R_I, however, is observed when the 10 wt% oxide/Ag paste is used.

Output power P_{max} of the unicouple with 6 wt% oxide/Ag paste increases with hot-side temperature T_H and reaches 177 mW at $T_H = 1073$ K and a temperature difference ΔT between hot- and cold-side temperatures of 500 K. One of the strong points of unicouples fabricated in this manner is their high power density, which would allow a large amount of electrical power to be generated by a small, lightweight TE module. In the same oxide TE unicouple, the volume power density is 0.96 W cm^{-3} at $T_H = 1073$ K.

Fabrication and Properties of a 140-Couple Module[42]

The p-type Co-349 and n-type Ni-113 bulks were prepared by hot-pressing, as mentioned previously. The resulting hot-pressed plates were cut into p- and n-type legs with a height of 5.0 mm and a cross-sectional area of 1.3 mm $\times$ 3 mm. The legs (140 couples) were inserted alternately into the Al$_2$O$_3$ meshes for electrical contact in series. An Ag paste containing 6 wt% of the Co-349 powder was used to reduce the R_c and the differential of thermal expansion between the oxide legs and the Ag electrodes. The Ag paste was solidified by annealing at 1123 K under uniaxial pressure of 6.4 MPa for 5 h in air. The dimensions of this module are 53 mm long, 32 mm wide, and 5.0 mm thick.

The power-generating property of the module at $T_H = 1072$ K and a $\Delta T = 551$ K is shown in Figure 8a. Open-circuit voltage V_o, which corresponds to the intercept of current (I) versus voltage (V) lines, reaches 4.5 V. In the fabrication of this TE module, a critical issue is how to make electrodes that will provide low R_c between the oxide and Ag materials as well as a mechanically strong connection. In the module presented here, this concern has been overcome through the use of a Ag paste containing oxide powder to connect the legs and Ag electrodes.

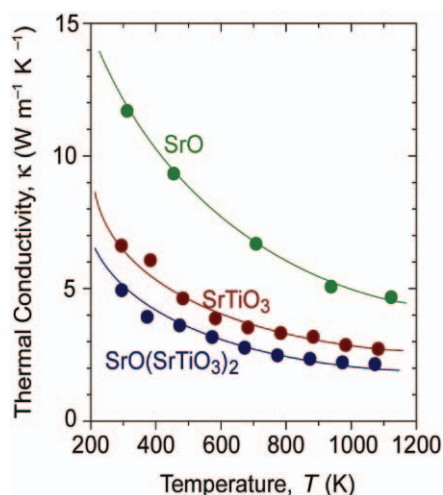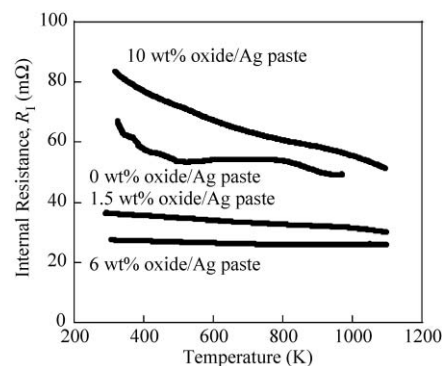A lithium-ion battery mounted in a mobile phone was charged by a 140-couple

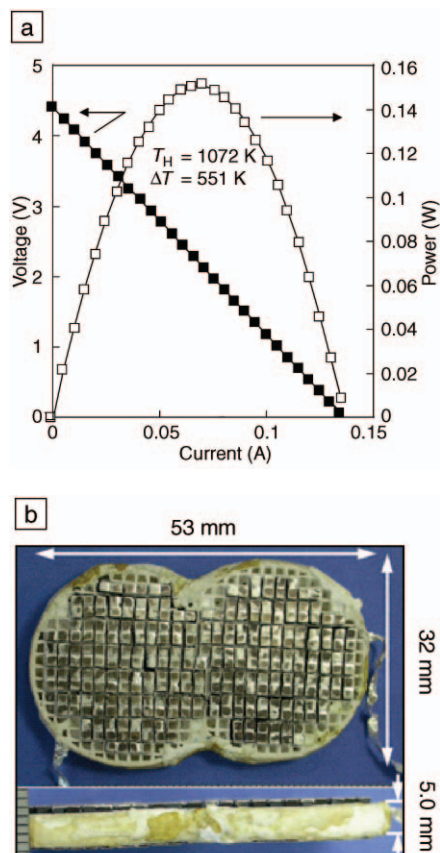$T_H = 1072$ K
$\Delta T = 551$ K

53 mm

32 mm

5.0 mm

Figure 8. (a) Power-generating property of the oxide module shown in (b).

module using a small burner and pan of water (Figure 9). This phenomenon indicates that applications of oxide modules can extend not only to generators for the recovery of high-temperature waste heat emitted by automobiles, factories, and similar sources, but also to portable generators
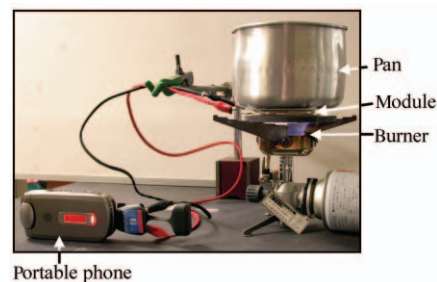
Pan

Module

Burner

Portable phone

Figure 9. Demonstration of thermoelectric charging of a portable phone.

for charging portable phones, personal computers, and other electronic devices.

Summary

It has been eight years since the first report of the thermoelectric properties of the TE oxide material Na_xCoO_2. Finally, TE modules consisting of oxide legs possessing good electrical and mechanical properties have been fabricated. Unfortunately, their conversion efficiency is lower than conventional TE modules. In order to enhance the thermoelectric properties of oxide modules, new materials with higher ZT values, especially n-type materials, are indispensable. The discovery of such oxides according to the concept of nanoblock integration is earnestly desired.

References

1. I. Terasaki, Y. Sasago, and K. Uchinokura, *Phys. Rev. B* **56** (1997) p. R12685.
2. R. Funahashi, I. Matsubara, H. Ikuta, T. Takeuchi, U. Mizutani, and S. Sodeoka, *Jpn. J. Appl. Phys. Pt. 2* **39** (2000) p. L1127.
3. A.C. Masset, C. Michel, A. Maignan, M. Hervieu, O. Toulemonde, F. Studer, B. Raveau, and J. Hejtmanek, *Phys. Rev. B* **62** (2000) p. 166.
4. Y. Miyazaki, K. Kudo, M. Akoshima, Y. Ono, Y. Koike, and T. Kajitani, *Jpn. J. Appl. Phys. Pt. 2* **39** (2000) p. L531.
5. A. Satake, H. Tanaka, T. Ohkawa, T. Fujii, and I. Terasaki, *J. Appl. Phys.* **96** (2004) p. 931.
6. M. Shikano and R. Funahashi, *Appl. Phys. Lett.* **82** (2003) p. 1851.
7. I. Matsubara, R. Funahashi, T. Takeuchi, S. Sodeoka, T. Shimizu, and K. Ueno, *Appl. Phys. Lett.* **78** (2001) p. 3627.
8. W. Shin, N. Murayama, K. Ikeda, and S. Sago, *J. Power Sources* **103** (2001) p. 80.
9. C. Fouassier, G. Matejka, J. Reau, and P.J. Hagenmuller, *J. Solid State Chem.* **6** (1973) p. 532.
10. Y. Ono, R. Ishikawa, Y. Miyazaki, Y. Ishii, Y. Morii, and T. Kajitani, *J. Solid State Chem.* **166** (2002) p. 177.
11. M. Mikami, M. Yoshimura, Y. Mori, T. Sasaki, R. Funahashi, and I. Matsubara, *Jpn. J. Appl. Phys. Part 2* **41** (2002) p. L777.
12. K. Takada, H. Sakurai, E. Takayama-Muromachi, F. Izumi, R.A. Dilanian, and T. Sasaki, *Nature* **422** (2003) p. 53.
13. M. von Jansen and R. Hoppe, *Z. Anorg. Allg. Chem.* **408** (1974) p. 104.
14. J.M. Tarascon, R. Ramesh, P. Barboux, M.S. Hedge, G.W. Hull, L.H. Greene, M. Giroud, Y. LePage, W.R. McKinnon, J.V. Waszczak, and L.F. Schneemeyer, *Solid State Commun.* **71** (1989) p. 663.
15. H. Leligny, D. Grebille, O. Pérez, A.-C. Masset, M. Hervieu, C. Michel, and B. Raveau, *C.R. Acad. Sci. Paris t.2*, Série IIc (1999) p. 409.
16. T. Yamamoto, I. Tsukada, K. Uchinokura, M. Takagi, T. Tsubone, M. Ichihara, and K. Kobayashi, *Jpn. J. Appl. Phys. Pt. 2* **39** (2000) p. L747.
17. T. Fujii, I. Terasaki, T. Watanabe, and A. Matsuda, *Jpn. J. Appl. Phys. Pt. 2* **41** (2002) p. L783.
18. I. Terasaki, *Frontiers in Magnetic Materials* (2005) p. 327.
19. T. Itoh and I. Terasaki, *Jpn. J. Appl. Phys. Pt. 1* **39** (2000) p. 6658.
20. I. Terasaki, *Proc. 18th Int. Conf. Thermoelectrics (ICT'99)* (IEEE, Piscataway, NJ, 1999) p. 569.
21. K. Takahata, Y. Iguchi, D. Tanaka, T. Itoh, and I. Terasaki, *Phys. Rev. B* **61** (2000) p. 12551.
22. G.A. Slack, *CRC Handbook of Thermoelectrics* (CRC Press, Boca Raton, FL, 1995) p. 407.
23. H. Masuda, T. Fujita, T. Miyashita, M. Soda, Y. Yasui, Y. Kobayashi, and M. Sato, *J. Phys. Soc. Jpn.* **72** (2003) p. 873.
24. S. Okada and I. Terasaki, *Jpn. J. Appl. Phys.* **44** (2005) p. 1834.
25. S. Okada, I. Terasaki, H. Okabe, and M. Matoba, *J. Phys. Soc. Jpn.* **74** (2005) p. 1525.
26. T. Okuda, K. Nakanishi, S. Miyasaka, and Y. Tokura, *Phys. Rev. B* **63** 113104 (2001).
27. L.F. Matheiss, *Phys. Rev. B* **6** (1972) p. 4718.
28. H.P.R. Frederikse, W.S. Thurber, and W.R. Hosler, *Phys. Rev.* **134** (2A) (1964) p. A442.
29. S. Ohta, T. Nomura, H. Ohta, and K. Koumoto, *J. Appl. Phys.* **97** (2005) p. 34106.
30. S. Ohta, T. Nomura, H. Ohta, M. Hirano, H. Hosono, and K. Koumoto, *Appl. Phys. Lett.* **87** (2005) p. 92108.
31. S. Ohta, T. Nomura, H. Ohta, M. Hirano, H. Hosono, and K. Koumoto, in *Extended Abstracts No. 1 of the 52nd Spring Meeting, Jpn. Soc. Appl. Phys. Related Soc.* (2005) p. 254.
32. F.J. DiSalvo, *Science* **285** (1999) p. 703.
33. H. Muta, K. Kurosaki, and S. Yamanaka, *J. Alloys Compd.* **350** (2003) p. 292.
34. H. Muta, K. Kurosaki, and S. Yamanaka, *J. Alloys Compd.* **368** (2004) p. 22.
35. S.N. Ruddlesden and P. Popper, *Acta Crystallogr.* **10** (1957) p. 38; S.N. Ruddlesden and P. Popper, *Acta Crystallogr.* **11** (1958) p. 54.
36. J.H. Haeni, C.D. Theis, D.G. Schlom, W. Tian, X.Q. Pan, H. Chang, I. Takeuchi, and X.-D. Xiang, *Appl. Phys. Lett.* **78** (2001) p. 3292.
37. K. Koumoto, S. Ohta, and H. Ohta, in *Proc. 23rd Int. Conf. Thermoelectrics* (IEEE, Piscataway, NJ, 2005).
38. W. Wunderlich, S. Ohta, H. Ohta, and K. Koumoto, in *Proc. 24th Int. Conf. Thermoelectrics* (IEEE, Piscataway, NJ, 2005) p. 237.
39. K. Kato, S. Ohta, H. Ohta, and K. Koumoto, in *Abstracts of the 43rd Symp. on Basic Science of Ceramics* (2005) p. 20.
40. H. Szelagowski, I. Arvanitidis, and S. Seetharaman, *J. Appl. Phys.* **85** (1999) p. 1.
41. R. Funahashi, S. Urata, K. Mizuno, T. Kouuchi, and M. Mikami, *Appl. Phys. Lett.* **85** (2004) p. 1036.
42. R. Funahashi, T. Mihara, M. Mikami, S. Urata, and N. Ando, in *Proc. 24th Int. Conf. Thermoelectrics* (IEEE, Piscataway, NJ, 2005) p. 292. □

Aspects of Thin-Film Superlattice Thermoelectric Materials, Devices, and Applications

Harald Böttner, Gang Chen, and Rama Venkatasubramanian

Abstract

Superlattices consist of alternating thin layers of different materials stacked periodically. The lattice mismatch and electronic potential differences at the interfaces and resulting phonon and electron interface scattering and band structure modifications can be exploited to reduce phonon heat conduction while maintaining or enhancing the electron transport. This article focuses on a range of materials used in superlattice form to improve the thermoelectric figure of merit.

Keywords: thermal conductivity, thermoelectricity.

Introduction

Ideas in using superlattices to improve the thermoelectric figure of merit (ZT) through the enhancement of electronic conductivity and reduction of phonon thermal conductivity were first discussed in a workshop by M.S. Dresselhaus, T. Harman, and R. Venkatasubramanian.[1] Subsequent publications from Dresselhaus's group on the quantum size effects on electrons drew wide attention and inspired intense research, both theoretical and experimental, on the thermoelectric properties of quantum wells and superlattices.[2] Several groups reported in recent years enhanced ZT in various superlattices such as Bi_2Te_3/Sb_2Te_3 and Bi_2Te_3/Bi_2Se_3,[3] and PbSeTe/PbTe quantum dot superlattices[4] (Figure 1). The large improvements observed in these materials systems compared with their parent materials are of great importance for both fundamental understanding and practical applications.

Superlattices are anisotropic. Different mechanisms to improve ZT along directions both parallel (in-plane) and perpendicular (cross-plane) to the film plane have been explored. Along the in-plane direction, potential mechanisms to increase ZT include quantum size effects that improve the electron performance by taking advantage of sharp features in the electron density of states,[2] and reduction of phonon thermal conductivity through interface scattering.[5] Along the cross-plane direction, one key idea is to use interfaces for reflecting phonons while transmitting electrons (phonon-blocking/electron-transmitting),[6] together with other mechanisms, such as electron energy filtering[7] and thermionic emission,[8] to improve electron performance. These mechanisms

have been explored through a few superlattice systems whose constituent materials have reasonably good thermoelectric properties to start with, V–VI materials such as Bi_2Te_3/Sb_3Te_3,[3,9] IV–VI materials such as PbTe/PbSe,[4,9] and V–V materials such as Si/Ge[10–12] and Bi/Sb,[13] with the most impressive results obtained in Bi_2Te_3 superlattices[3] and PbTe-based quantum dot superlattices.[4]

The large ZT improvements observed in these superlattices shattered the $ZT \sim 1$ ceiling that persisted until the 1990s, opening new potential applications in cooling and power generation using solid-state devices. Much research is needed in materials, understanding, and devices to further advance superlattice thermoelectric technology. In this short article, we will give a summary of the past work, emphasizing the materials aspects of superlattices, while commenting on current understanding or lack of it, and some aspects of the device research. We refer to other review articles for more in-depth discussions on these topics.[5,6,14–19]

Materials and Properties

The work on quantum well and superlattice-based thermoelectric materials mostly focused on perfect (i.e., epitaxial) layer systems. So it was not surprising that, due to the extensive worldwide experience in IV–VI epitaxy,[20,21] approaches were taken to use this material system to prove the quantum confinement as well as the acoustic phonon scattering.[4,9] As Bi_2Te_3-based materials have the highest ZT around room temperature, successful efforts were started to develop suitable epitaxial systems for the V–VI compound family.[9,22] It is worth mentioning that both IV–VI and V–VI semiconductor material families have a useful structural relationship (Figures 2a and 2b).[23] The current thin-film device technologies for IV–VI and V–VI compounds use either one or the other of these two material systems. Mixed staggered IV–V/V–VI superlattice thin-film devices are not known so far.

V–VI Superlattices

Venkatasubramanian and co-workers reported Bi_2Te_3-based superlattices grown by metallorganic chemical vapor deposition (MOCVD) on GaAs substrates.[22] The GaAs substrates were chosen for their ease of cleaning prior to epitaxial deposition and the fact that substrates with 2–4° misorientation with respect to ⟨100⟩ can be conveniently obtained. It is important to note that these trigonal-structured Bi_2Te_3 materials are grown on GaAs with fcc structure. The misorientation allows the
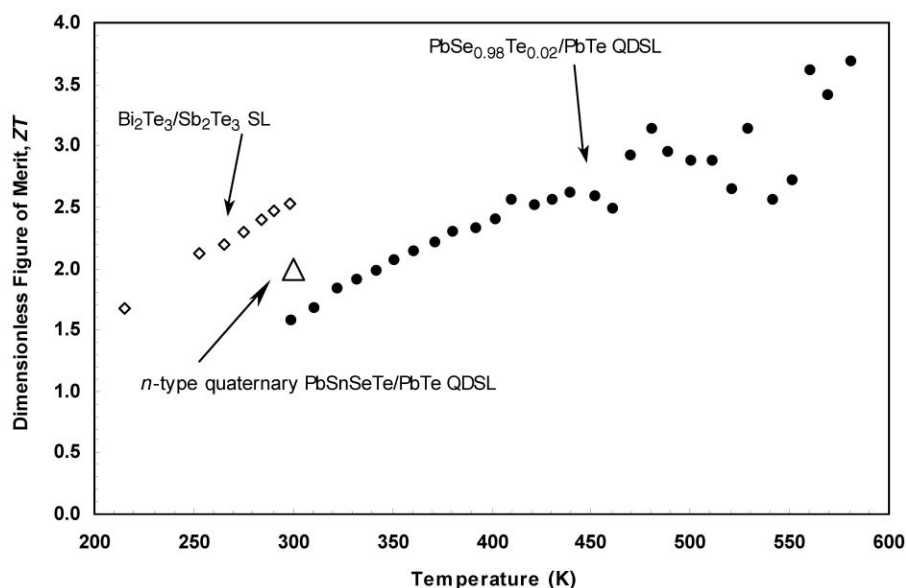
Figure 1. Thermoelectric figure of merit ZT for Bi$_2$Te$_3$/Sb$_2$Te$_3$ superlattices[3] (SL), PbSnSeTe/PbTe quantum dot superlattices (QDSL), and PbTeSe/PbTe quantum dot superlattices.[4, 45]

initiation of the epitaxial process at the kink sites on the surface, thereby allowing the growth of mismatched materials. The growth of Bi$_2$Te$_3$-based materials, with the rather weak van der Waals bonds along the growth direction, requires a low-temperature process. A low-temperature growth process leads to high-quality, abrupt superlattice interfaces with minimal interlayer mixing, and also allows the growth of highly lattice-mismatched materials systems without strain-induced three-dimensional islanding. Figure 3 shows a high-resolution transmission electron micrograph of a Bi$_2$Te$_3$/Sb$_2$Te$_3$ su-

perlattice on a GaAs substrate, delineating the two very different crystalline orientations. *In situ* ellipsometry has been used to gain further nanometer-scale control over deposition.[24]

As V–VI epitaxy is rather a scientific "virgin soil," it is not surprising that even for the single homogeneous V–VI layers of the central compound Bi$_2$Te$_3$, only minimal information regarding thin-film deposition and thermoelectric property characterization can be found. The problem of a low Te sticking coefficient is discussed in Reference 25. Different film growth methods based on MBE,[9,25–27]

MOCVD,[22] flash evaporation,[28–30] and co-evaporation[31,32] have been used to grow single layers and superlattices on various substrates. Nurnus et al.[23] used a rather high deposition temperature compared with that used in MOCVD but were still able to obtain high-quality (Bi$_2$Te$_3$)/Bi$_2$(Te,Se)$_3$ superlattices using element sources. The power factor (PF = $\alpha^2/\rho\kappa$) of 50 μW cm^{-1} K^{-2} reported in Reference 33 for Bi$_2$Te$_3$ is close to that of the best single crystals, which is 57 μW cm^{-1} K^{-2}.[34] Unfortunately, the mobility is limited to ~150 cm^2 V^{-1} s^{-1}. A critical item in maintaining the outstanding *ZT* of superlattices is their stability against cation (*p*-material) and anion (*n*-material) interdiffusion. Results reported by Nurnus et al.[23,33] strongly indicate a dependence of the superlattice stability against diffusion on perfection of the layer structure.

Recently, sputtering as a new deposition method for forming V–VI superlattices[35] was tested. Starting with alternating element layers, the corresponding superlattice thermoelectric compounds were formed by a subsequent annealing procedure. Here, at lower temperatures, the anions in the *n*-("Se/Te") alloy system or the cations in the *p*-("Bi/Sb") alloy system tend to interdiffuse while compounding the thermoelectric material. Taking into account the results by Johnson,[36] who succeeded in forming superlattices in the V–VI materials system using "modulated elemental reactants," it can be concluded that besides alternating layers, a necessary condition for the formation of superlattices is to deposit layers that are as perfectly oriented as possible in order to obtain optimum diffusion stability for reliable final devices. For the case of perfect *c*-oriented layers, the fast diffusion paths are
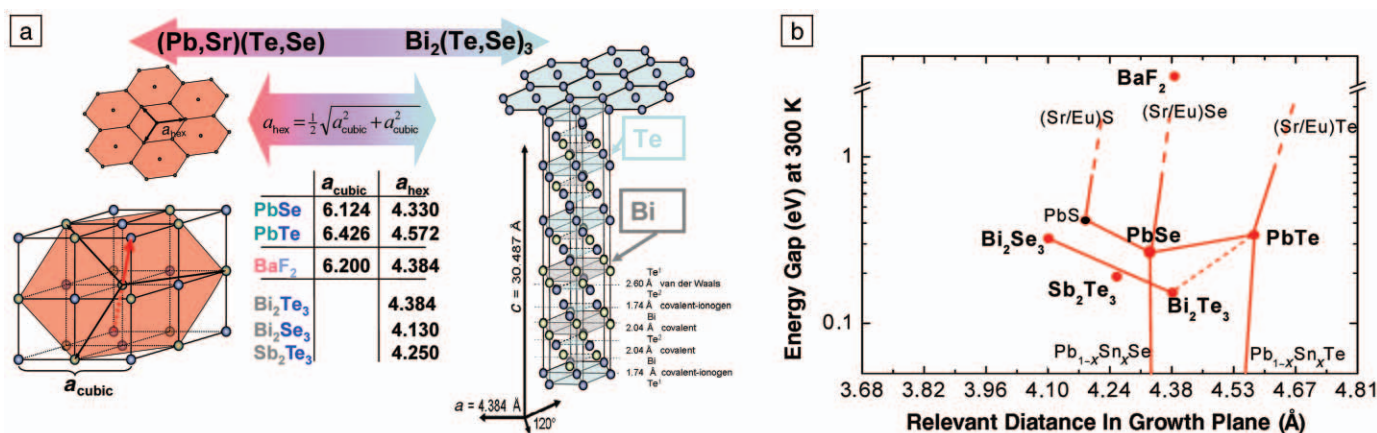

Figure 2. (a) Crystallographic data for IV–VI and V–VI compounds, highlighting the structural relationship between both material systems. (b) Epitaxial map of semiconductor materials (at room temperature) that could be suitable in combination with Bi$_2$Te$_3$, based on their relevant atomic distance with respect to the a-plane of Bi$_2$Te$_3$.
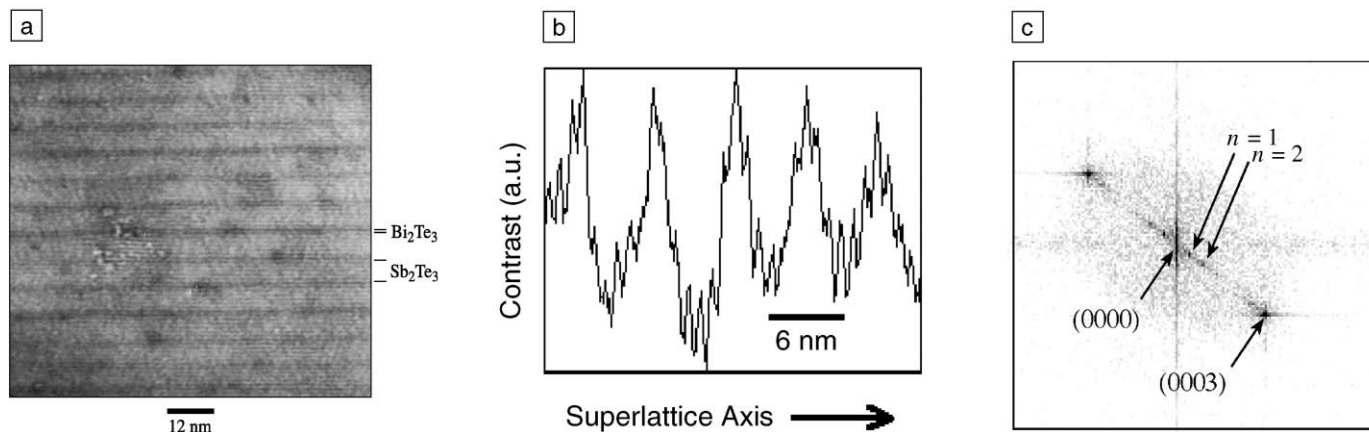
Figure 3. (a) Transmission electron micrograph of a Bi_2Te_3/Sb_2Te_3 (10 Å/50 Å) superlattice. (b) Image contrast oscillations through the superlattice. (c) Fast Fourier transform of the image in (a), showing the superlattice reflections of order n.[22]

blocked, even in the case of the non-epitaxially arranged layers, according to Johnson's work.[36] If the interdiffusion is blocked in the a-plane, superlattices will be stable until the intrinsic interdiffusion in the c-direction is activated at significantly higher temperatures. For the V–VI compounds, it is well known that the interdiffusion coefficients in the c-direction are normally smaller, by decades, than in the a-direction.[37]

The ZT values of V–VI-based superlattices can be measured in either in-plane or cross-plane directions. So far, the largest enhancement is in the cross-plane direction, with the major gain coming from the thermal conductivity reduction. Venkatasubramanian reported a cross-plane $ZT \sim$ 2.4 at room temperature for the p-type Bi_2Te_3-Sb_2Te_3 superlattices with a period of $\sim$6 nm.[4] In such superlattices, the electronic power factor is in the range of 40 μW cm^{-1} K^{-2} to 60 μW cm^{-1} K^{-2}, comparable to or higher than standard bulk p-type Bi_2Te_3 solid-solution alloys measured along the a–b axis. However, the phonon thermal conductivity (κ_p) dropped to 0.22 W/m K, about a factor of 5 lower than that of bulk alloys along a–b axis. Lambrecht et al.[38] determined an in-plane reduction of the total thermal conductivity (electrons and phonons) down to 65%, compared with homogenous Bi_2Te_3 for n-type $Bi_2Te_3/Bi_2(Se_{0.12}Te_{0.88})_3$ superlattices with a 10-nm period.

IV–VI Superlattices

IV–VI nanolayers have been successfully grown for more than a decade for IV–VI infrared lasers.[39] Because of its physical and chemical properties, the IV–VI materials system is relatively easy to handle, compared with the V–VI compounds, particularly for epitaxial growth.

Thus, a lot of literature can be found on the growth details and layer properties of IV–VI nanolayer stacks.[40,41] Here, we summarize results exclusively focused on thermoelectric applications.

The initial effort in IV–VI systems was focused on electron confinement effects. Using MBE-grown $PbTe/Eu_xPb_{1-x}Te$, Harman and co-workers showed an increased electron power factor ($\alpha^2\sigma$) inside the quantum wells along the in-plane direction,[42,43] as predicted by Hicks and Dresselhaus. However, the barriers in multiple quantum wells (MQWs) degrade the overall ZT, because they conduct heat without contributing to electron performance. Harman and co-workers further explored various IV–VI superlattices. They found that in PbTe/Te superlattices, obtained by the addition of a few nanometers of Te above the PbTe layer, ZT increased from 0.37 to 0.52 at room temperature, and this increase was associated with the formation of quantum dot structures at the interface.[44] The Harman group further discovered experimentally that quantum dot superlattices based on $PbTe/PbSe_xTe_{1-x}$ (with $x \sim$ 0.98) have an even higher ZT.[45] The quantum dot formation is due to the lattice mismatch between PbTe and PbSeTe[40] (Figure 4). PbTe-based quantum dot superlattices with a total thickness of 100–200 μm have been grown with good thermoelectric properties along the in-plane direction.[4] PbTe/PbSeTe n-type quantum dot superlattices were obtained by Bi doping, and p-type quantum dot superlattices were obtained through Na doping. The best bulk PbTe-based alloys have a room temperature ZT of $\sim$0.4. Harman et al.[4] reported n-type PbTe/PbSeTe quantum dot superlattices with $ZT = 1.6$ at room temperature, compared with $ZT \sim$ 0.4 in the

best bulk PbTe alloys, and inferred that quaternary superlattices based on PbTe/PbSnSeTe have a room temperature ZT of $\sim$2. For the ternary PbTe/PbSeTe superlattices, the factor of 4 increases come mainly from a large reduction in the thermal conductivity, while the power factor remains similar to that of the bulk, albeit at different optimum carrier concentrations. The combined electron and phonon thermal conductivity ($\kappa_e + \kappa_p$) drops from bulk values of $\sim$2.5 W/m K to 0.5 W/m K. Considering that the electronic contribution to thermal conductivity for both superlattices and bulk materials is $\sim$0.3 W/m K, a significant phonon thermal conductivity reduction is obvious.

Böttner and co-workers studied the in-plane thermoelectric properties of n- and p-doped $PbTe/PbSe_{0.20}Te_{0.80}$ systems.[9,46] Compared with corresponding bulk $PbSe_xTe_{1-x}$ material, a significant reduction in the thermal conductivity parallel to the growth direction was measured. Together with nearly unchanged power factors, an in-plane ZT enhancement of up to 40% at
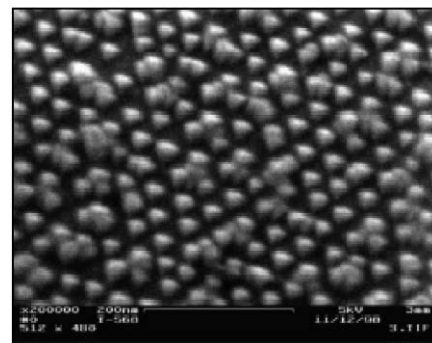

Figure 4. Quantum dot structures in the PbTe/PbSeTe system.[42]

a temperature of 500 K was estimated. Recently, Caylor et al.[47] reported their effort in growing PbTe/PbSe superlattices.

Other Superlattice Systems

Nurnus and co-workers studied IV–VI/V–VI heteroepitaxial layers to evaluate quantum confinement in V–VI layers using suitable "wide-bandgap" IV–VI alloys such as $Bi_2Te_3/Pb_{1-x}Sr_xTe$,[33,48] including results involving stability against annealing. The practical use of the concept (Figure 2) of a structural relationship between IV–VI and V–VI compounds was recently proved by Caylor et al., who deposited Bi_2Te_3 on a standard GaAs substrate as a buffer layer, followed by a IV–VI superlattice.[47] They found out, surprisingly, that superlattices in (111) and (100) orientations grow simultaneously at lower temperatures.

Other superlattice systems have been studied for their thermoelectric properties, such as Si/Ge superlattices,[10–12] Bi/Sb superlattices,[13] and skutterudite-based superlattices.[49] Si/Ge and Si/SiGe alloy superlattices have shown a large reduction in thermal conductivity compared with that of homogeneous alloys in the cross-plane direction,[10,11] while in the in-plane direction, thermal conductivity values are comparable with that of the homogeneous alloy with equivalent composition to the superlattices.[50] Despite the reduction in thermal conductivity, there are no conclusive results on the figure of merit because of difficulties in measuring the thermoelectric properties of very thin films. Reported measurements of the thermoelectric properties of Bi/Sb and skutterudite superlattices are scarce and not conclusive.[51,52]

Characterization of Thermoelectric Properties

Thermoelectric property measurements in many cases have been the bottleneck in the development and understanding of superlattice-based materials.[53] Because of anisotropy, all thermoelectric properties, including the Seebeck coefficient α, electrical conductivity σ, and thermal conductivity κ, should be measured in the same direction and, ideally, on the same sample. Along the in-plane direction, thermal conductivity is usually the most difficult parameter to measure. However, the substrate and the buffer layers can also easily overwhelm the Seebeck coefficient and electrical conductivity measurements. The need to isolate the properties of the film from those of the substrate and the buffer layer often influences the choice of the substrate and the film thickness in the growth of superlattices. In the cross-plane

direction, the 3ω method and the pump-and-probe method are often used to measure the thermal conductivity of superlattices.[54,55] However, measuring the Seebeck coefficient and the electrical conductivity in the cross-plane direction can be even more challenging. Venkatasubramanian et al.[3] adapted the transmission line model (TLM) technique used for the measurement of specific electrical contact resistivities (ρ_c) to determine the cross-plane electrical resistivities in Bi_2Te_3-based superlattices, which is feasible when ρc is smaller than the specific internal resistance of the thermoelectric film d/σ, where d is the thickness of the superlattice film.

Besides individual property measurements to determine ZT, other methods for direct ZT determination have been successful. Venkatasubramanian et al.[3] adapted the Harman method[56] to determine ZT in the cross-plane direction of Bi_2Te_3-based superlattices with a maximum thickness of the superlattice up to 5 μm. Yet the most unambiguous measurement of the enhanced ZT comes from direct measurements of the cooling effect. Harman used this method to characterize the performance of his PbTe/PbSeTe quantum dot superlattices.[4] He measured cooling based on a thermocouple with one leg made of the superlattice and the other leg made of a section of Au wire, properly matched in length. The maximum cooling measured from such a thermocouple was 43.7 K, while a similar couple made of the best bulk thermoelectric material only reached 30.8 K. To make such a couple, the total thickness of his superlattice sample was ~100 μm.

Current Understanding

Experimental results so far have shown that the thermal conductivity reduction was mainly responsible for ZT enhancement in the superlattices. Theoretical studies on the thermal conductivity have been carried out.[16,17] These models generally fall into two different camps.

The first group treats phonons as incoherent particles and considers interface scattering as the classical size effect that is analogous to the Casimir limit at low temperatures in bulk materials and Fuchs–Sonderheim treatment of electron transport.[57–59] These classical size effect models assume that interface scattering is partially specular and partially diffuse, and can explain experimental data for superlattices in the thicker period limit.

The other group of models is based on the modification of phonon modes in superlattices, considering the phonons as totally coherent.[60,61] In superlattices, the

periodicity has three major effects on the phonon spectra: (1) phonon branches fold, owing to the new periodicity in the growth direction; (2) mini-bandgaps form; and (3) the acoustic phonons in the layer with a frequency higher than that in the other layer become flat or confined because of the mismatch in the spectrum. Comparison with experimental data, however, shows that the group velocity reduction alone is insufficient to explain the magnitude of the thermal conductivity reduction perpendicular to the film plane, and it fails completely to explain the thermal conductivity reduction along the film plane.[61,62] The reason is that the lattice dynamics model assumes phase coherence of the phonons over the entire superlattice structure and does not include the possibility of diffuse interface scattering, which destroys the perfect phase coherence picture. Partially coherent phonon transport models can capture the trend of thermal conductivity variation in both the in-plane and the cross-plane directions over the entire thickness range.[63,64] Molecular dynamics simulations considering interface mixing can generate trends similar to that observed experimentally on GaAs/AlAs superlattices, which is consistent with the modeling.[65] Past models of thermal conductivity focused on III–V and IV–IV superlattices. There are no detailed models on IV–VI and V–VI superlattices. Venkatasubramanian et al.[66] observed a minimum in thermal conductivity for Bi_2Te_3-based superlattices at a periodic thickness of ~6 nm. Although similar trends can be obtained from partially coherent phonon-transport models, the minima based on such models typically occur around 3–5 monolayers (i.e., 1–2 nm).[63,64] The discrepancy could be due to the unusually large unit cell in the c-axis direction and potentially to interface mixing, which is not well included in current models, and to phonon localization.[66] The modeling conclusion that coherent states of phonons cannot reproduce experimental data has significant implications for materials synthesis, suggesting that other nanostructures can lead to similar results.[67]

While the thermal conductivity reduction has been largely responsible for the reported high ZT so far in IV–VI and V–VI superlattices, the importance of maintaining the electronic power factor cannot be overemphasized. Although in both these systems, the maximum power factors are close to those of their bulk counterparts, the optimal dopant concentrations between bulk and superlattice samples differ, at least in PbTe-based systems.[44,45] The bandgaps of the constituent

materials in the IV–VI and V–VI superlattices with high ZT are similar, suggesting that quantum size effects may not be important. However, small band-edge offsets can have an effect on the electron scattering mechanisms and shift the optimal carrier concentration. Although quantum size effects may not dominate in these materials systems, the principle of using quantum size effects to improve electron performance is sound. Minimizing interface scattering of electrons is crucial for realizing a high power factor. Better materials synthesis can potentially lead to structures that can take advantage of both increased electron performance and reduced phonon thermal conductivity.

Devices and Applications

The fabrication of superlattice-based devices can take advantage of many of the standard tools of semiconductor device manufacturing, such as photolithography, electroplating, wafer dicing, and pick-and-place systems. This allows scalability of the module fabrication, from simple modules that can pump milliwatts of heat to multiconnected module arrays. Both in-plane and cross-plane devices are under development, and each have their unique advantages, challenges, and applications.

Cross-plane superlattice-based devices typically have configurations similar to those of bulk thermoelectric modules, albeit with significantly shorter legs and smaller leg cross sections.[3,68] Such devices have extremely rapid cooling or heating characteristics, and fully functional devices can be built using 1/40,000 of the active material required for state-of-the-art bulk thermoelectric technology.

Venkatasubramanian and co-workers have developed wafer-bonding technology to fabricate Bi_2Te_3 superlattice thermoelectric devices.[68] It is clear from such device development that significant challenges exist in translating the intrinsically high ZT of the materials to the high performance of the devices. Some of the issues are related to the significant electrical and thermal parasitic resistances in a modular assembly. First, the specific electrical contact resistance ρ_c at both ends of the p-type and n-type devices must be minimized such that ρ_c is much smaller than the specific resistance d/σ of the leg. Another significant challenge is the thermal management at both the hot and the cold sides, as the heat flux through each leg can be as large as ~1000 W/cm^2. Such a high heat flux cannot be handled with usual convective cooling techniques. Heat spreading by using sparsely spaced elements or advanced thermal management methods is necessary.

Cross-plane superlattice-based devices are being considered for a variety of applications. Thermoelectric coolers have long been used for the wavelength stability of semiconductor lasers. Currently used thermoelectric coolers are based on bulk materials machined down to small sizes (~2 mm × 2 mm × 1 mm). Superlattice-based devices can better match the footprint and heat flux of semiconductor lasers with a lower profile, which is extremely important for fitting into the existing packages such as metal transistor outline cans. Superlattice thermoelectric technology is also now being actively considered for the thermal management of hot-spot and transistor off-state leakage current in advanced microprocessors.

Besides cooling applications, superlattice-based thermoelectric devices can also be used for power-conversion applications. Figure 5 shows an example of local heating and cooling that can be realized with superlattice-based devices. Early studies carried out by Venkatasubramanian and co-workers of power-conversion efficiency using single p–n couples have shown a significant correlation with the measured ZT in the "inverted" p–n couples[69] by the Harman method.

In-plane device configurations are used mainly for sensors, and most of the past work has been based on polycrystalline thermoelectric material.[70,71] Superlattices with high ZT can improve the performance of these devices. For sensor applications, thermal bypass through the substrate must be minimized by removing the substrate, transferring the superlattice film to another low-thermal-conductance substrate, or depositing the film directly on a low-thermal-conductivity substrate.[71]

One big question regarding superlattice-based thermoelectric coolers and power generators is their stability and reliability. These devices operate under high heat and current fluxes, and both thermo- and electromigration are of great concern. At this stage, only a little work has been done. Venkatasubramanian's group[72] carried out initial power-cycle testing on relatively simple superlattice couples using $Pb_{37}Sn_{63}$ bonding for flip-chip attachment. No degradation in ΔT was observed after more than 100,000 power cycles, suggesting an intrinsic reliability in the superlattice material. However, the high-temperature reliability of superlattice materials has not been studied.
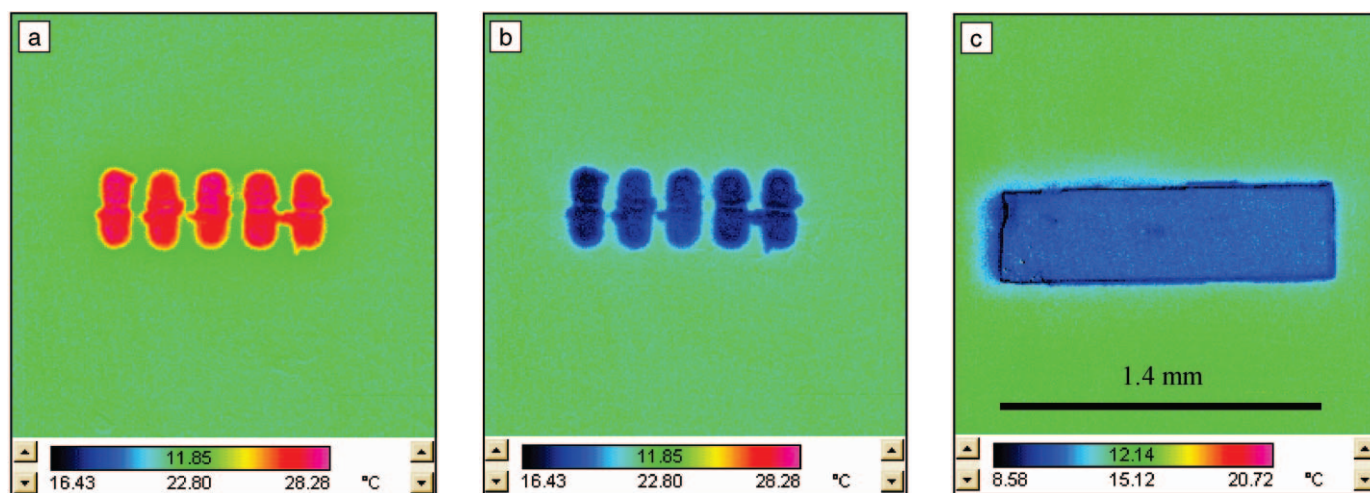

Figure 5. Infrared image of a row of five Bi_2Te_3-based thermoelectric superlattice microcoolers. (a) Discrete heating; (b) discrete cooling. (c) Combined discrete cooling devices for larger-area cooling. The scale marker in (c) applies to all three images.

Summary and Research Needs

The large figure-of-merit enhancements observed in V–VI- and IV–VI-based superlattices and quantum dot superlattices have an impact on both fundamental understanding and practical applications. For a long time, the maximum ZT for all bulk materials was limited to $ZT = 1$, and as a consequence, applications have been limited to niche areas. Progress made in superlattice-based thermoelectric materials show that $ZT = 1$ is not a theoretical limit. With the availability of high-ZT materials, many new applications will emerge. The progress made also calls for more effort in materials development, theoretical understanding, and device fabrication, concurrent with the pursuit of practical applications of these materials.

Materials-wise, research in both enhancing ZT and reducing cost is needed. Practical thermoelectric devices need both n-type and p-type materials with comparable figures of merit. So far, p-type Bi_2Te_3/Sb_2Te_3 superlattices have much higher ZT values than n-type Bi_2Te_3/Bi_2Se_3 superlattices, while PbTe/PbSeTe-based n-type and p-type quantum dot superlattices have comparable ZT values. Continuous improvements in ZT for different materials in different temperature ranges are needed. In addition to reducing the phonon thermal conductivity, the principle of increasing ZT through quantum confinement of electrons should be exploited, including the exploration of one-dimensional nanowires and nanowire superlattices.[73] Further reductions in thermal conductivity may be possible in aperiodic superlattices. Similar effects that lead to a reduction in phonon thermal conductivity may be observed in other nanostructures that are more amenable to mass production. In addition to materials development, theoretical studies are needed to further understand the electron and phonon thermoelectric transport. Particularly, quantitative tools capable of predicting thermoelectric transport properties are needed. While ZT has reached high values in superlattices, devices made of these materials have not reached the best performance of bulk thermoelectric coolers, due to difficulties in electrical contacts, heat spreading, materials matching, and fabrication. Continued progress in the device area is critical for translating the laboratory work successfully into practical applications.

Acknowledgments

References

1. *Proc. 1st Natl. Thermogenic Cooler Workshop*, edited by S.B. Horn (Center for Night Vision and Electro-Optics, Fort Belvoir, VA, 1992).
2. D. Hicks and M.S. Dresselhaus, *Phys. Rev. B* **47** (1993) p. 12727.
3. R. Venkatasubramanian, E. Siivola, T. Colpitts, and B. O'Quinn, *Nature* **413** (2001) p. 597.
4. T.C. Harman, P. Taylor, M.P. Walsh, and B.E. LaForge, *Science* **297** (2002) p. 2229.
5. G. Chen, *Semicond. Semimetals* **71** (2001) p. 203.
6. R. Venkatasubramanian, *Semicond. Semimetals* **71** (2001) p. 175.
7. B. Moyzhes and V. Nemchinsky, *Appl. Phys. Lett.* **73** (1998) p. 1895.
8. A. Shakouri and J.E. Bowers, *Appl. Phys. Lett.* **71** (1997) p. 1234.
9. H. Beyer, A. Lambrecht, E. Wagner, G. Bauer, H. Böttner, and J. Nurnus, *Physica E* **13** (2002) p. 965.
10. S.M. Lee, D.G. Cahill, and R. Venkatasubramanian, *Appl. Phys. Lett.* **70** (1997) p. 2957.
11. T. Borca-Tasciuc, W.L. Liu, T. Zeng, D.W. Song, C.D. Moore, G. Chen, K.L. Wang, M.S. Goorsky, R. Radetic, R. Gronsky, T. Koga, and M.S. Dresselhaus, *Superlattices Microstruct.* **28** (2000) p. 119.
12. G.H. Zeng, A. Shakouri, C. La Bounty, G. Robinson, E. Croke, P. Abraham, X.F. Fan, H. Reese, and J.E. Bowers, *Electron. Lett.* **35** (1999) p. 2146.
13. S. Cho, Y. Kim, S.J. Youn, A. DiVenere, G.K.L. Wong, A.J. Freeman, J.B. Ketterson, L.J. Olafsen, I. Vurgaftman, J.R. Meyer, and C.A. Hoffman, *Phys. Rev. B* **64** 235330 (2001).
14. M.S. Dresselhaus, Y.M. Lin, S.B. Cronin, O. Rabin, M.R. Black, G. Dresselhaus, and T. Koga, *Semicond. Semimetals* **71** (2001) p. 1.
15. J. Nurnus, H. Böttner, and A. Lambrecht, in *Handbook of Thermoelectrics,* edited by M. Rowe, Chapter 46 (CRC Press, Boca Raton, FL, 2005) p. 1.
16. D. Mahan, *Semicond. Semimetals* **71** (2001) p. 157.
17. M.S. Dresselhaus, G. Dresselhaus, X. Sun, Z. Zhang, S.B. Cronin, T. Koga, J.Y. Ying, and G. Chen, *Microscale Thermophys. Eng.* **3** (1999) p. 89.
18. G. Chen, M.S. Dresselhaus, J.-P. Fleurial, and T. Caillat, *Int. Mater. Rev.* **48** (2003) p. 45.
19. G. Chen and A. Shakouri, *J. Heat Transfer* **124** (2001) p. 242.
20. G. Springholz, A. Holzinger, H. Krenn, H. Clemens, G. Bauer, H. Böttner, P. Norton, and M. Maier, *J. Cryst. Growth* **113** (1991) p. 593.
21. A. Lambrecht, H. Böttner, M. Agne, R. Kurbel, A. Fach, B. Halford, U. Schiessl, and M. Tacke, *Semicond. Sci. Technol.* **8** (1993) p. 334.
22. R. Venkatasubramanian, T. Colpitts, B. O'Quinn, M. Lamvik, and N. El-Masry, *Appl. Phys. Lett.* **75** (1999) p. 1104.
23. J. Nurnus, H. Beyer, A. Lambrecht, and H. Böttner, in *Thermoelectric Materials 2000—The Next Generation Materials for Small-Scale Refrigeration and Power Generation Applications,* edited by T.M. Tritt, G.S. Nolas, G.D. Mahan, D. Mandrus, and M.G. Kanatzidis (Mater. Res. Soc. Proc. 626, Warrendale, PA, 2000) p. Z2.1.1.
24. H. Cui, I. Bhat, B. O'Quinn, and R. Venkatasubramanian, *J. Electron. Mater.* **30** (2001) p. 1376.
25. A. Mzerd, D. Sayah, G. Brun, J.C. Tedenac, and A. Boyer, *J. Mater. Sci. Lett.* **14** (1995) p. 194.
26. A. Mzerd, D. Sayah, J.C. Tedenac, and A. Boyer, *Int. J. Electron.* **77** (1993) p. 291.
27. Y.A. Boikov, V.A. Danilov, T. Claeson, and D. Erts, in *Proc. ICT'97* (IEEE, New York, 1997) p. 89.
28. A. Foucaran, A. Giani, F. Pascal-Delannoy, A. Boyer, and A. Sackda, *Mater. Sci. Eng., B* **52** (1998) p. 154.
29. F. Völklein, V. Baier, U. Dillner, and E. Kessler, *Thin Solid Films* **187** (1990) p. 253.
30. V.D. Das and P.-G. Ganesan, in *Proc. 16th Int. Conf. Thermoelectrics* (IEEE, New York, 1997) p. 147.
31. H. Zou, M. Rowe, and G. Min, in *Proc. ICT'00* (IEEE, Piscataway, NJ, 2002) p. 251.
32. L.W. Da Silva, M. Kaviany, A. DeHennis, and J.S. Dyck, in *Proc. ICT'03* (IEEE, Piscataway, NJ, 2003) p. 665.
33. J. Nurnus, H. Böttner, H. Beyer, and A. Lambrecht, in *Proc. ICT'99* (IEEE, Piscataway, NJ, 1999) p. 696.
34. J.P. Fleurial, L. Gailliard, and R. Triboulet, *J. Phys. Chem. Solids* **49** (1988) p. 1237.
35. H. Böttner, A. Schubert, H. Kölbel, A. Gavrikov, A. Mahlke, and J. Nurnus, in *Proc. ICT'04,* CD-ROM, Paper No. 009 (IEEE, Piscataway, NJ, 2004).
36. F.R. Harris, S. Standridge, C. Feik, and D.C. Johnson, *Angew. Chem. Int. Ed. Engl.* **42** (2003) p. 5295.
37. M. Chitroub, S. Scherrer, and H. Scherrer, *J. Phys. Chem. Solids* **62** (2000) p. 1693.
38. A. Lambrecht, H. Beyer, J. Nurnus, C. Künzel, and H. Böttner, in *Proc. ICT'01* (IEEE, Piscataway, NJ, 2001) p. 335.
39. A. Lambrecht, N. Herres, B. Spanger, S. Kuhn, H. Böttner, M. Tacke, and J. Evers, *J. Cryst. Growth* **108** (1991) p. 301.
40. G. Springholz, V. Holy, M. Pinczolits, and G. Bauer, *Science* **282** (1998) p. 734.
41. H. Zogg and M. Hüppi, *Appl. Phys. Lett.* **47** (1985) p. 47.
42. T.C. Harman, D.L. Spears, and M.J. Manfra, *J. Electron. Mater.* **25** (1996) p. 1121.
43. T.C. Harman, D.L. Spears, D.R. Calawa, and S.H. Groves, in *Proc. 16th Int. Conf. Thermoelectrics* (IEEE, New York, 1997) p. 416.
44. T.C. Harman, D.L. Spears, and M.P. Walsh, *J. Electron. Mater. Lett.* **28** (1999) p. L1.
45. T.C. Harman, P.J. Taylor, D.L. Spears, and M.P. Walsh, *J. Electron. Mater.* **29** (2000) p. L1.
46. H. Beyer, J. Nurnus, H. Böttner, A. Lambrecht, T. Roch, and G. Bauer, *Appl. Phys. Lett.* **80** (2002) p. 1216.
47. J.C. Caylor, K. Coonley, J. Stuart, S. Nangoy, T. Colpitts, and R. Venkatasubramanian, in

Proc. 24th Int. Conf. Thermoelectrics (IEEE, Piscataway, NJ, 2005).

48. N. Peranio, O. Eibl, and J. Nurnus, in *Proc. 23rd Int. Conf. Thermoelectrics* CD-ROM, Paper No. 1059 (IEEE, Piscataway, NJ, 2004).

49. J.C. Caylor, M.S. Dander, A.M. Stacy, J.S. Harper, R. Gronsky, and T. Sands, *J. Mater. Res.* **16** (2001) p. 2467.

50. W.L. Liu, T. Borca-Tasciuc, G. Chen, J.L. Liu, and K.L. Wang, *J. Nanosci. Nanotechnol.* **1** (2001) p. 39.

51. D.W. Song, G. Chen, S. Cho, Y. Kim, and J. Ketterson, in *Thermoelectric Materials 2000—The Next Generation Materials for Small-Scale Refrigeration and Power Generation Applications,* edited by T.M. Tritt, G.S. Nolas, G.D. Mahan, D. Mandrus, and M.G. Kanatzidis (Mater. Res. Soc. Proc. **626**, Warrendale, PA, 2000) p. Z9.1.1.

52. D.W. Song, W.L. Liu, T. Zeng, T. Borca-Tasciuc, G. Chen, C. Caylor, and T.D. Sands, *Appl. Phys. Lett.* **77** (2000) p. 3854.

53. G. Chen, B. Yang, W.L. Liu, T. Borca-Tasciuc, D. Song, D. Achimov, M.S. Dresselhaus, J.L. Liu, and K.L. Wang, *Proc. 20th Int. Conf. Thermoelectrics* (IEEE, Piscataway, NJ, 2001) p. 30.

54. S.M. Lee and D.G. Cahill, *J. Appl. Phys.* **81** (1997) p. 2590.

55. W.S. Capinski, H.J. Maris, T. Ruf, M. Cardona, K. Ploog, and D.S. Katzer, *Phys. Rev. B* **59** (1999) p. 8105.

56. T.C. Harman, *J. Appl. Phys.* **29** (1958) p. 1373.

57. C.R. Tellier and A.J. Tosser, *Size Effects in Thin Films* (Elsevier, Amsterdam, 1982).

58. G. Chen, *J. Heat Transfer* **119** (1997) p. 220.

59. G. Chen, *Phys. Rev. B.* **57** (1998) p. 14958.

60. P. Hyldgaard and G.D. Mahan, *Phys. Rev. B* **56** (1997) p. 10754.

61. S. Tamura, Y. Tanaka, and H.J. Maris, *Phys. Rev. B* **60** (1999) p. 2627.

62. B. Yang and G. Chen, *Microscale Thermophys. Eng.* **5** (2001) p. 107.

63. M.V. Simkin and G.D. Mahan, *Phys. Rev. Lett.* **84** (2000) p. 927.

64. B. Yang and G. Chen, *Phys. Rev. B* **67** 195311 (2003).

65. B.C. Daly, H.J. Maris, K. Imamura, and S. Tamura, *Phys. Rev. B* **66** 024301 (2002).

66. R. Venkatasubramanian, *Phys. Rev. B* **61** (2000) p. 3091.

67. B. Yang and G. Chen, in *Chemistry, Physics, and Materials Science for Thermoelectric*

Materials: Beyond Bismuth Telluride, edited by M.G. Kanatzidis, T.P. Hogan, and S.D. Mahanti (Kluwer Academic/Plenum, NY, 2003) p. 147.

68. R. Venkatasubramanian, E. Siivola, B. O'Quinn, K. Coonley, P. Addepalli, C. Caylor, A. Reddy, and R. Alley, *Proc. 24th Int. Conf. Thermoelectrics* (IEEE, Piscataway, NJ, 2005).

69. R. Venkatasubramanian, E. Siivola, B.C. O'Quinn, K. Coonley, P. Addepalli, M. Napier, T. Colpitts, and M. Mantini, *Proc. 2003 ACS Symp. Nanotechnol. Environ.,* ACS Symposium Series **890** (American Chemical Society, Washington, DC, 2004) p. 347.

70. F. Völklein, M. Blumers, and L. Schmitt, *Proc. 18th Int. Conf. Thermoelec.* (IEEE, Piscataway, NJ, 1999) p. 285.

71. J. Nurnus, H. Böttner, C. Künzel, U. Vetter, A. Lambrecht, J. Schumann, and F. Völklein, *Proc. 21st Int. Conf. Thermoelectrics* (IEEE, Piscataway, NJ, 2002) p. 523.

72. R. Alley, J. Canchhevaram, K. Coonley, B. O'Quinn, J. Posthill, E. Siivola, and R. Venkatasubramanian, *Proc. 24th Int. Conf. Thermoelectrics* (IEEE, Piscataway, NJ, 2005).

73. Y.-M. Lin and M.S. Dresselhaus, *Phys. Rev. B* **60** 075304 (2003).   □

Advertisers in This Issue

Properties of Nanostructured One-Dimensional and Composite Thermoelectric Materials

Apparao M. Rao, Xiaohua Ji, and Terry M. Tritt

Abstract

Over a decade ago, Dresselhaus predicted that low-dimensional systems would one day serve as a route to enhanced thermoelectric performance. In this article, recent results in the thermoelectric properties of nanowires and nanotubes are discussed. Various synthesis techniques will be presented, including chemical vapor deposition for the growth of thermoelectric nanostructures in templated alumina. Electrical transport measurements of carbon nanostructures, such as resistivity and thermopower, have revealed some very interesting thermoelectric properties. Challenges still remain concerning the measurement of individual nanostructures such as nanowires. Much work has been performed on the thermoelectric properties of carbon nanotubes, and these results will be highlighted. In addition, routes for enhanced thermoelectric materials have focused on incorporating nanostructures within the bulk materials. The role of these "hybrid composite structures" based on nanomaterials incorporated into the bulk matrix and the potential for enhanced performance are discussed.

Keywords: composite, nanostructure, thermal conductivity, thermoelectricity.

Background

The discovery and development of thermoelectric (TE) materials with a high figure of merit ($ZT \geq 1$) has proven to be a challenging task in materials science and engineering. Worldwide research efforts have culminated in somewhat of a two-pronged strategy for identifying this class of TE materials: engineered bulk materials and nanostructured materials.

In the first approach, complex crystal structures have been designed and synthesized with the aim of attaining phonon-glass/electron-crystal characteristics (low lattice thermal conductivity as in glass, with high electrical conductivity as in metals) for high ZT. Recent progress on bulk thermoelectric materials is discussed in the article by Nolas et al. in this issue.

The second approach is motivated by the presence of increased electron density of states at the Fermi level in nanostructured materials and the possibility of exploiting boundary scattering to reduce the thermal conductivity.

As indicated by its prefix, a *nano*structure has one of its crucial dimensions on the order of 1–100 nm. Various forms of nanostructures, such as nanotubes, nanowires, nanorods, nanoparticles, ultrathin films, quantum wells, and superlattices, have been prepared in the laboratory and are providing valuable insights for engineering materials with improved TE properties. In this issue, Böttner et al. provide an overview of the progress achieved in 2D nanostructured TE materials, specifically, superlattices and quantum well materials. Nanocomposites that involve the incorporation of any of the aforementioned nanostructures in the corresponding bulk material are also gaining much interest, since enhanced TE properties are expected to result from interfacial reflection and scattering of phonons in the nanocomposites. This article focuses on the bulk synthesis of 1D thermoelectric nanomaterials and their TE properties. In particular, the Seebeck coefficient will be discussed in detail for comparing different forms of nanostructured materials, since this parameter has proved to be a very powerful probe.

Carbon Nanotubes

We begin with a discussion of the TE properties of carbon nanotubes, which are the latest molecular form of carbon, discovered by S. Iijima in 1991.[1] Researchers have recently begun to synthesize other nanostructured materials, such as those based on state-of-the-art TE materials such as PbTe and Bi_2Te_3, which will be discussed later in this article. Much can be learned from the TE properties of these carbon nanotubes, and therefore, we will focus the early parts of this article on these materials.

A nanotube can be viewed as a graphene sheet rolled into a seamless cylinder with an aspect ratio (length/diameter) exceeding 1000. Carbon nanotubes are typically classified into two groups: single-walled nanotubes (SWNTs) and multiwalled nanotubes (MWNTs), which are basically a set of concentric SWNTs.[2] Nanotubes can be synthesized by one of three commonly used methods:[3] electric arc discharge, pulsed laser vaporization, and chemical vapor deposition (CVD).

In carbon nanotubes, the Seebeck coefficient α is often used to determine the sign of the dominant charge carrier[4-8] and also to probe sensitivity to gas adsorption and molecular collisions with the nanotubes.[9] Since in most metals, α is sensitive to the curvature of the band structure near the Fermi level through the Mott relation,[10]

$$\alpha_d = \frac{\pi^2 k_B T}{3e}\left(\frac{\partial \ln \sigma}{\partial \varepsilon}\right)_{\varepsilon = E_F},\qquad(1)$$

it is a good indicator of dominant carrier type. In this expression, k_B is the Boltzmann constant, T is temperature, e is the

electron charge, $\partial\ln\sigma/\partial\varepsilon$ is the energy derivative of the electrical conductivity σ, and E_F is the Fermi energy. The subscript d indicates the contribution of the diffusion thermopower to the total α.

A general comparison between $\alpha(T)$ of SWNTs and MWNTs with highly oriented pyrolytic graphite (HOPG) is quite useful. Figure 1 shows $\alpha(T)$ for four different carbon samples, which include as-prepared SWNT bundles produced by the electric arc discharge (black circles) and the pulsed laser vaporization (PLV) (blue squares) techniques, an as-prepared film of MWNTs grown by CVD (red diamonds), and HOPG (green crosses). All four samples were exposed to room air and room light for an extended period of time and are therefore considered to be sufficiently oxygen-doped. Clearly, SWNTs have a much higher room-temperature α of approximately 45 $\mu V/K$ than the MWNTs (approximately 17 $\mu V/K$). Notice that the sign of α for both the SWNTs and the MWNTs is positive, indicating p-type behavior in oxygen-doped nanotubes. The bulk graphite displays a room-temperature value of approximately -4 $\mu V/K$. This figure serves as a quick reference for $\alpha(T)$ behavior in all three of the air-exposed carbon forms.

Exposure to oxygen (or air) has been shown to have a dramatic effect on α in SWNTs[4–6] and MWNTs.[7] The sign of α in a sample of purified SWNTs switches reversibly from positive to negative in a time frame of $\sim$15–20 min as the sample is cycled between O_2 and vacuum.[4] This sign reversal in α is indicative of a change in the dominant charge carrier switching from n-type (in vacuum) to p-type (in O_2). In Figure 2a, $\alpha(T)$ data for a film of purified SWNTs in its O_2-saturated state (p-type) as well as after being completely deoxygenated (n-type) are shown.[5] Interestingly, this transformation is reversible over the entire temperature range, and field-effect transistors based on isolated semiconducting single-walled carbon nanotubes (CNTFETs) also exhibited p-type (when exposed to O_2) and n-type (annealed under vacuum) device characteristics.[11] The data in Figure 2a suggest that interaction with O_2 is responsible for the p-type character of CNTFETs in air. However, detailed studies of doping-induced FET characteristics of SWNTs conducted by the Avouris group at IBM do not seem to fully support this conclusion. In the SWNTs exposed to air or oxygen, the Fermi energy level (E_F) is extrinsically pinned near the valence-band maximum.[11] Consistent with this model, little difference in the electrical resistance R of oxygen-saturated and annealed SWNTs has been observed.[6]
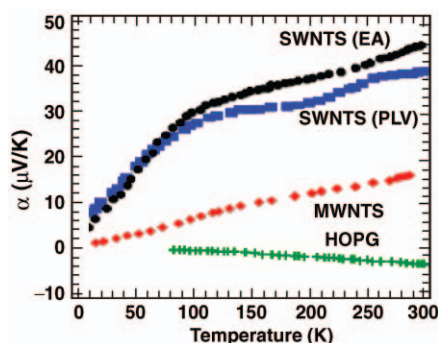

Figure 1. Seebeck coefficient α versus temperature for air-saturated single-walled nanotubes (SWNTs), multiwalled nanotubes (MWNTs), and highly oriented pyrolytic graphite (HOPG). EA and PLV refer to SWNTs prepared by electric arc and pulsed laser vaporization methods, respectively.

Alternatively, SWNTs can also be p-doped to a greater extent by immersion in concentrated nitric or sulfuric acids. $R(T)$ of such p-doped SWNTs decreases by a factor of 10 or more compared with the corresponding value in pristine SWNTs, implying that E_F is well into the semiconductor valence bands. The low-temperature $\alpha(T)$ data of these acid-treated SWNTs exhibited distinctly different behavior from oxygen-saturated and annealed SWNTs. This unusual low-temperature behavior has been attributed to phonon drag or electron–phonon scattering in 1D electronic systems.[12,13]

As in the case of acid-treated SWNTs, molecular adsorbates that engage in charge transfer with the nanotube wall are expected to significantly impact the transport of charge and heat along the wall. However, from systematic studies of α or R or bundled SWNTs, Eklund and co-workers found evidence for new scattering channels for the free carriers in metallic nanotubes. An exponential increase in the time-dependence of $\alpha(t)$ and resistance $R(t)$ of thin films of bundled SWNTs was observed, caused by physisorption of various alcohol molecules ($C_nH_{2n+1}OH$; $n = 1–4$) when a sudden change in the molecular pressure occurs.[14] The trends in the changes in α and R with adsorption of these polar molecules were explained on the basis of the interplay between the adsorption energy E_a (measured on graphitic carbons) and the molecular coverage $\sim 1/A$, where A is the projection area of a particular alcohol molecule on the nanotube surface. In another systematic study of α and R of six-membered ring hydrocarbons C_6H_{2n} ($n = 3–6$) physisorbed on SWNTs, further evidence for scattering channels in nanotubes was found.[15] Adsorption of benzene ($n = 3$) induced the largest increase in α and R. As the number of π electrons per molecule was reduced (molecules with increasing n), the impact of the molecular adsorption on α and R of the SWNT diminished (Figure 2b). These observations revealed that the magnitude of scattering scaled with the coupling of the π electrons in the adsorbed molecules to π electrons in the metallic nanotube wall. Similarly, small increases in α of SWNTs due to adsorbed H_2, He, and N_2 have also been observed and identified with the creation of additional scattering channels. At fixed gas temperature and pressure, changes in α and R of thin SWNT films were experimentally found and theoretically confirmed to scale as
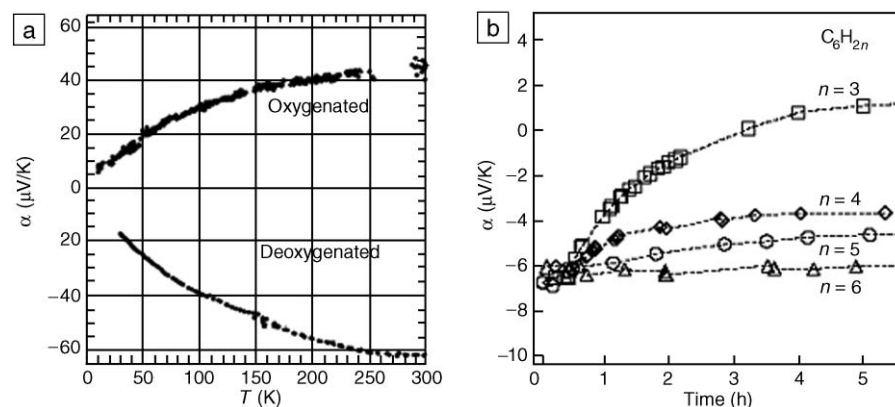

Figure 2. (a) Seebeck coefficient α versus temperature for a SWNT film exposed to O_2 and then deoxygenated.[5] (b) In situ $\alpha(t)$ during successive exposure of a degassed SWNT film to vapors of six-membered ring molecules C_6H_{2n} (n =3–6). The dashed lines in (b) are guides to the eye.[15]

$\sim M^{1/3}$, where M is the mass of the colliding gas molecules (He, Ar, Ne, Kr, Xe, CH$_4$, and N$_2$).[9]

The CNTFETs are inferior to analogous silicon devices from the standpoint of long-term device operation, since originally n-type CNTFETs acquire p-type device characteristics when exposed to air under ambient conditions. To enable carbon nanotubes to function as a basic building block in future nanoelectronic devices, it is crucial that the oxygen-induced reversal of electronic properties (discussed in Figure 2a) be arrested. One approach is to dope nanotubes with either nitrogen or boron to render them permanently n-type or p-type, respectively. Figure 3 compares $\alpha(t)$ obtained for purified pristine SWNTs (crosses) with those of as-prepared boron-doped SWNTs[8] and nitrogen-doped MWNTs.[16] The $\alpha(t)$ data of both SWNT samples were collected as they were degassed in 10^{-6} Torr vacuum at 500 K. It is clearly seen that, as adsorbed oxygen is removed from the pristine SWNT sample, $\alpha(t)$ changes sign from approximately 20 μV/K (p-type) to –20 μV/K (n-type), which is similar in behavior to data depicted in Figure 2a. However, in the case of the boron-doped SWNTs, $\alpha(t)$ remains constant at around 60 μV/K, implying a greater stability of the doped nanotubes with respect to the degassing procedure. Substituted boron in the sample would be expected to donate holes to the SWNT lattice, making it a permanently p-type material and resulting in no change in $\alpha(t)$ as the sample is degassed. Likewise, nitrogen-doped nanotubes are expected to exhibit permanent n-type characteristics, as exemplified in Figure 3.

Finally, we note other interesting TE properties in carbon nanotubes. Recent advances in mesoscopic TE measuring devices have enabled measurements of α in a single SWNT.[17] A room-temperature α = 200 μV/K, which is much larger than $\alpha \sim$ 60 μV/K measured in SWNT films, was obtained. As discussed in the introductory article to this issue by Tritt and Subramanian, "rattlers" introduced in bulk cage-like materials have the effect of reducing the thermal conductivity κ and thereby enhancing the figure of merit, $ZT = \alpha^2\sigma T/\kappa$. The rattling motion of these loosely bound atoms effectively scatters phonons, thus significantly reducing the lattice thermal conductivity of these materials. One might expect that C$_{60}$ molecules inside the hollow core of a SWNT would act like rattlers.[18] Regular SWNTs showed a room-temperature α value of 60 μV/K after air saturation, whereas the C$_{60}$@SWNTs (the @ symbol designates C$_{60}$ molecules
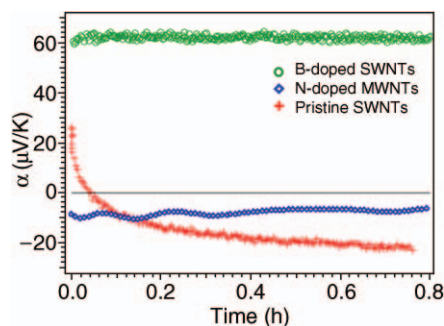

Figure 3. Seebeck coefficient α versus time in doped SWNTs and MWNTs compared with pristine SWNTs.

encapsulated inside a nanotube) saturate at 40 μV/K at 300 K.

Evidence for the existence of the Kondo effect has been reported through measurements of α in SWNTs synthesized using a variety of catalyst particles.[19] The Kondo effect arises from the interactions between a single magnetic atom, such as a transition-metal atom, and the many electrons in an otherwise nonmagnetic metal, such as a carbon nanotube. A broad peak in the $\alpha(T)$ data near 70–100 K has been associated with the Kondo effect and attributed to the presence of magnetic catalyst impurities in the SWNT films. The Kondo effect is completely suppressed when the magnetic impurities are converted to corresponding iodides by treating the SWNT sample with iodine.

Other Nanostructured Materials

Since the discovery of carbon nanotubes, there have been rapid advances in the synthesis and understanding of the physical properties of these interesting materials. As mentioned, the structure of a carbon nanotube is derived from the 2D nature of the graphene sheet that is essentially "rolled up" into a seamless 1D nanostructure, forming either a single-walled or a multiwalled nanotube. Recently, it has been found that other 2D electron systems, such as layered dichalcogenides (WS$_2$, MoS$_2$, and TiS$_2$), and other layered structures, including Bi$_2$Te$_3$, have been synthesized in a 1D nanostructure form. We will not make an effort to survey the vast amount of high-quality research that has been performed on the synthesis and development of 1D nanostructures, but will instead attempt to highlight a few areas that may be of importance to the development of higher-performance TE materials that may be eventually based on these nanostructures. We will try to also

highlight some of the broad synthesis techniques that are used to achieve these nanostructures.
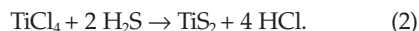
MoS$_2$ Nanotubes

As far back as 2001, nanostructures of other 2D layered compounds have been grown as 1D nanostructures.[20] Remskar et al. used a novel type of catalyzed reaction including C$_{60}$ as a growth parameter to grow subnanometer-diameter single-walled MoS$_2$ nanotubes. The SWNTs of MoS$_2$ were grown by adding C$_{60}$ (5 wt%) to MoS$_2$ powder in a transport tube as a catalyst. The reaction was run for over 20 days at 1010 K in an evacuated silica ampoule. The pressure was 10^{-3} Torr with a temperature gradient of 6 K/cm. The MoS$_2$ nanotubes grew as twisted chiral bundles. These bundles were held together by interstitial iodine, which is easily removed, thus allowing for free-standing MoS$_2$ nanotubes. These bundles contain more than 500,000 ordered nanotubes. The tubes have various lengths, up to several hundred nanometers, but are rather uniform in diameter ($\sim$0.3–0.9 nm). It is predicted that these materials should exhibit transport properties that are metallic; however, because of the narrow diameters of the tubes, energy quantization is expected to occur and yield electron-hopping perpendicular to the tube axis. However, no electrical transport measurements were reported. One would expect that large thermopower might be observed in the MoS$_2$ nanotubes, because of the sharp variation in the density of states according to the Mott formula, as discussed previously.

WS$_2$ Nanotubes

Chen et al. recently reported the synthesis of high-purity WS$_2$ nanotubes.[21] These materials were synthesized on a rather large scale by the thermal decomposition of amorphous/nano (NH$_4$)$_2$WS$_4$ in a floating hydrogen and thiophene atmosphere. The heating temperature was between 360°C and 450°C. This technique yielded large quantities of open-ended WS$_2$ nanotubes with an average length of 5 μm and diameters between 25 nm and 50 nm. They performed an extensive ball-milling procedure for about 1 h on the (NH$_4$)$_2$WS$_4$ powder, which they emphasize is a very important part of the process in order to obtain the nanotubes. They call the powders amorphous/nano because of the extensive ball-milling. They investigated various growth parameters such as temperature, flow rate, and thiophene concentration in order to obtain the optimum growth conditions for obtaining the nanotubes.

TiS₂ Nanotubes

These same authors also were able to synthesize TiS₂ nanotubes.[22] They used a low-temperature gas reaction and obtained nanotubes with an outer diameter of ~20 nm and lengths of several micrometers. The TiS₂ nanotubes were derived from the following reaction:

$$\text{TiCl}_4 + 2\,\text{H}_2\text{S} \rightarrow \text{TiS}_2 + 4\,\text{HCl}. \qquad (2)$$

The nanotubes are multiwalled and open-ended, with an outer diameter of ~20 nm, an inner diameter of ~10 nm, and fringe spacing of roughly 0.57 nm. The crystal structure for the bulk TiS₂ is shown in Figure 4. Notice that the 2D lamellar structure is very similar to the graphene sheets that result in the growth of carbon nanotubes. It is apparent that these 2D structures are very susceptible to the growth of nanostructures from the corresponding 2D parent bulk material.

So the question may be asked, why is the synthesis of materials such as these of importance to improved TE materials? The dimensionality can play a crucial role in the electronic transport processes in a material. Do the electrons interact in a 3D, 2D, or 1D manner? The dimensionality can even change a system from metallic to semiconducting behavior. Therefore, let us recall the Mott relation as described by Equation 1 but in a slightly different form. We observe that the thermopower is proportional to a derivative of the density of states (DOS) at the Fermi level, as shown in Equation 3:

$$\alpha_d \simeq \frac{1}{n(\varepsilon)}\left(\frac{\partial n}{\partial \varepsilon}\right)_{\varepsilon=E_\text{F}}. \qquad (3)$$

Here, $n(\varepsilon)$ is the density of states. Thus, as predicted by Hicks and Dresselhaus,[23] the thermopower could be enhanced in a given set of materials simply by reducing the dimensionality. Bulk TiS₂ already possesses some very interesting TE properties. It has been reported that a series of transition-metal dichalcogenides (e.g., TiS₂) exhibit very high thermopower values ($\alpha > 250\ \mu\text{V/K}$ at $T \approx 300$ K).[24] The materials are relatively large single crystals (10 mm × 5 mm × 0.1 mm) that are of nearly stoichiometric composition. These materials are grown by chemical vapor transport using I₂. The transition-metal dichalcogenides are a quasi 2D system and are considered electronically as a 2D electron gas. There should be considerable latitude for further doping in the TiS₂ system, and in addition, the samples can be intercalated with other atoms within the 2D layers, which are separated by weakly bonded van der Waals planes. When formed as nanotubes, they may be able to be intercalated within the fringe layers.

Here, again, exists the "layered structure" that appears so common among potential TE materials. It is noted in the most recent reference[22] that the carrier concentration n of the TiS₂ system is an order of magnitude larger ($n \approx 10^{21}$ carriers/cm³) than the state-of-the-art TE material Bi₂Te₃, which has an optimum carrier concentration. However, the power factor of the TiS₂ system is nearly the same as Bi₂Te₃ at $T \approx$ 300 K and remains relatively large down to as low as 50 K, thus showing some potential as a refrigeration material.

Bi₂Te₃ Nanostructures: Electrodeposition

Nanostructures of state-of-the-art TE materials such as Bi₂Te₃ have also been synthesized.[25,26] For example, Stacy and co-workers have been successful in forming Bi₂Te₃₋ₓSeₓ nanostructures using electrodeposition techniques.[27] These materials are synthesized by array fabrication methods using porous anodic alumina templates. Very good control of the sample diameter, as well as large aspect ratios, can be achieved using the alumina templates. This can be observed in Figure 5, where an array of electrodeposited Bi₂Te₃₋ₓSeₓ nanostructures is shown. A cross section is shown in Figure 5a, and a bottom view after removal of the Pt electrode is shown in Figure 5b. High-quality crystalline materials of 50 nm and 200 nm have been synthesized. The Bi₂Te₃₋ₓSeₓ crystal structure has been confirmed by x-ray diffraction, which shows that the wires are textured along the [110] direction. Stacy and co-workers have been able to achieve a relatively high density of wires, on the order of 5×10^9 cm⁻².[28] These wires had a final composite thickness of 55–70 μm and an average wire diameter of ~45 nm, which gives a wire aspect ratio of greater than 1000. Stacy et al. conclude that these arrays could be easily incorporated into devices if the properties prove superior to those of existing bulk Bi₂Te₃ materials.

Bi₂Te₃ Nanostructures: Hydrothermal Techniques

Zhao et al. and his group at Zhejiang University have also been quite successful in forming nanostructures of Bi₂Te₃ and its alloys using hydrothermal techniques.[29–32] These authors contend that the figure of merit of TE materials could be significantly improved if the materials are nanostructured, since the thermal conductivity may be decreased more significantly than the electric conductivity, in addition to a potential enhancement of the thermopower.

In their work, novel solution chemical routes such as solvothermal synthesis,[33,34] hydrothermal synthesis, low-temperature aqueous[35] chemical synthesis, and even ultrasonic chemical synthesis[36] have been developed to prepare Bi₂Te₃-based nanopowders. Various morphologies of nanoBi₂Te₃, including nanotubes and nanocapsules, have been obtained, and rare-earth elements (REs) have also been alloyed in Bi₂Te₃-based compounds.[37] Bulk TE materials and nanocomposites have been prepared by vacuum hot pressing. The TE transport properties of hot-pressed samples have been measured.

The most important result of Zhao et al.'s solution-chemical-synthesized nano-Bi₂Te₃ work is the first report of Bi₂Te₃ compounds with hollow shell nanostructures.[29,30,38] The nanotubes, hydrothermally synthesized at 150°C, have diameters of 25–100 nm and lengths of up to several micrometers. It was found that the tube walls are spiral and tilted, with the (003) plane of the Bi₂Te₃ rhombohedral lattice at an angle of about 20° to the tube axis, as shown in Figure 6. Irregular hollow nanocapsules synthesized by a low-temperature aqueous chemical method are ~10–50 nm in size, with some short, nanotube-like nanocapsules ~100–200 nm in diameter and 300–1500 nm in length.
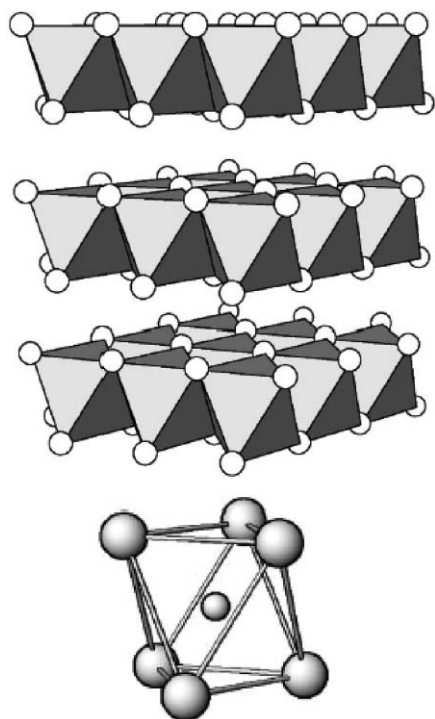

Figure 4. Crystal structure of the dichalcogenide TiS₂, also showing the TiS₆ octahedral unit that builds up the layered dichalcogenide structure.
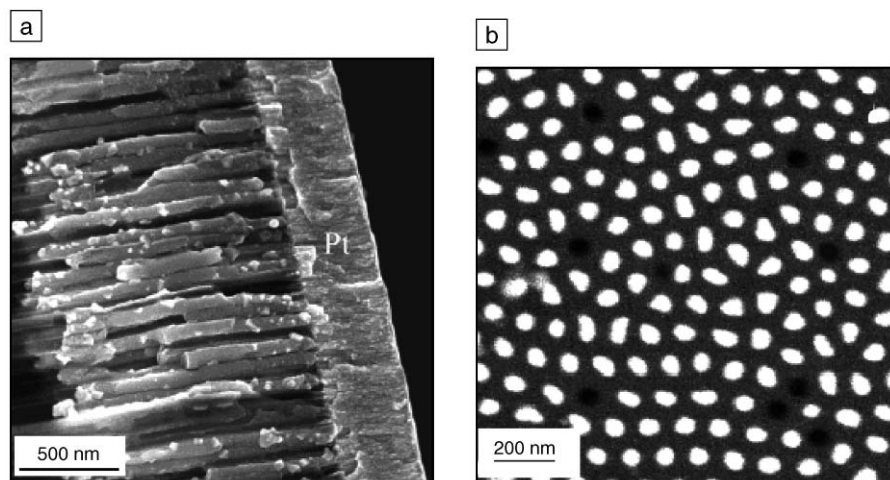
Figure 5. Scanning electron micrographs of $Bi_2Te_{3-x}Se_x$, showing an array of ~50-nm-diameter templated nanowires: (a) cross section; (b) bottom view after removal of Pt electrode. Taken from Figure 6 in Reference 25.

Another important result of the Zhao et al.'s work is the preparation of advanced Bi_2Te_3-based nanocomposites with high TE properties.[30,31] They first proposed the concept of "coessential" nanocomposites, which means that nanostructures of a specified material coexist in a matrix of the same material, for example, using commercial Bi_2Te_3-based alloys as the matrix and Bi_2Te_3 nanotubes as the additive. The objective is to reduce the thermal conductivity of a TE material without deteriorating its electric properties. A very low thermal conductivity of ~0.8 W m^{-1} K^{-1} has been obtained for the hot-pressed bulk nanocomposites. The highest dimensionless figure of merit reaches 1.25 at about 420 K, which is also one of the highest values ever reported for bulk Bi_2Te_3-based TE materials (Figure 7).

Carefully designed experiments have been performed to study the nucleation and growth of Bi_2Te_3 nanocrystals during hydrothermal synthesis.[29,32] Various nucle-

ation mechanisms, including a molecule growth model, a continuous nucleation model, and a nucleus saturation model, have been proposed for the different synthesis conditions. It was experimentally found that lateral growth, including surface-nucleation lateral growth, spiral lateral growth, and mis-layered lateral growth, dominates the Bi_2Te_3 crystal growth during hydrothermal synthesis because of the anisotropic lattice structure.

PbTe and Skutterudite Nanostructures

Recently, nanostructures of other TE materials have been fabricated. For example, nanostructures of PbSe[39] and also of $CoSb_3$ skutterudites have been accomplished.[40,41] The PbSe materials were initially grown as sphere-like structures, which after additional reaction time were grown in a wire-like structure with a typical width of 60–150 nm and length of 1–5 µm. Recently, the group at Clemson has used a CVD technique to synthesize PbTe nanoparticles.[42] Their CVD technique resulted in a high yield of cubic PbTe nanoparticles of sizes ranging between 50 nm and more than 200 nm. The $CoSb_3$ skutterudites were grown via solvothermal methods that were able to give a very high yield; grams of $CoSb_3$ could be collected from several growths. Xie and co-workers used a solvo-thermal method employing $CoCl_2$ and $SbCl_3$ as precursors. This required a two-step process
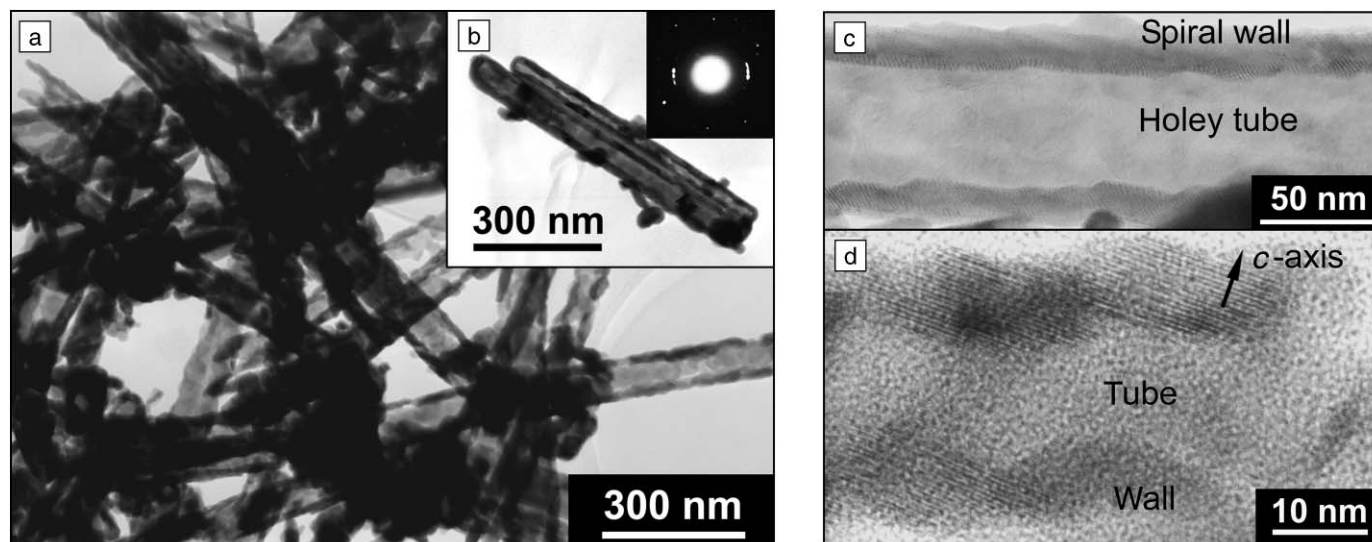

Figure 6. Transmission electron microscopy (TEM) and high-resolution TEM (HRTEM) images of Bi_2Te_3 nanotubes synthesized via hydrothermal methods in a closed system at 150°C. (a) TEM image of a cluster of hydrothermally synthesized Bi_2Te_3 nanotubes. (b) TEM image of three parallel nanotubes; the inset in (b) shows an electronic diffraction image of these three nanotubes. (c) HRTEM image of a Bi_2Te_3 nanotube, showing that the tube wall is spiral and tilted. (d) HRTEM image of another smaller Bi_2Te_3 nanotube with inclined c-axis and (003) planes with reference to the tube axis. Taken from Reference 29.
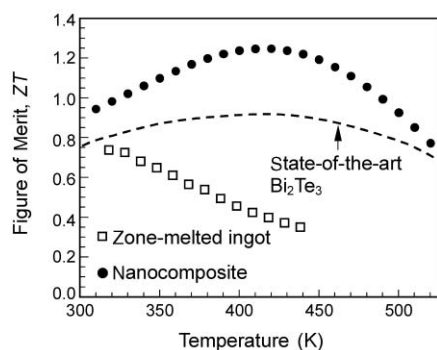
Figure 7. Thermoelectric figure of merit ZT of the Bi₂Te₃ nanocomposite, shown with those of the zone-melted sample. Adapted from Reference 43.

that resulted in large quantities of $CoSb_3$ nanoparticles of less than 30 nm in size. The XCo_4Sb_{12} system (where X is a rare-earth filler atom for the rattling motion) is much more interesting in relation to thermoelectrics since this system has already shown very favorable TE properties in bulk materials. Initially, the goal of this work was the synthesis of nanoparticles of $CoSb_3$.

One may not need to have filled skutterudite nanowires. It is possible that the filled skutterudite matrix materials, along with the incorporation of nanostructures of $CoSb_3$ as phonon scattering centers, may be enough to effectively minimize the lattice thermal conductivity κ_L in these skutterudite materials.

Concluding Remarks

The low-dimensional materials discussed in this article offer new ways to manipulate the electron and phonon properties of a given material. The key idea is to use quantum size effects to increase the electron density of states at the Fermi level and in this way to optimize the power factor. Even when the quantum size effects are not dominant, it is possible to utilize classical size effects to alter the transport processes, for example, the exploitation of boundaries to scatter phonons more effectively than electrons. However, it may be that the incorporation of these nanostructured materials into a bulk matrix of similar materials may serve to reduce the lattice thermal conductivity via nanoscale phonon scattering centers and thus improve the overall ZT in the composite. Therefore, once grown as nanostructures, these materials may be incorporated into other bulk structures to enhance the properties of the original parent materials. They could exhibit enhanced electronic properties for thermoelectric applications, or they may just act as nanostructured phonon scattering centers. Thus, the birth of hybrid or composite bulk thermoelectric materials, where a bulk TE matrix can be incorporated with TE nanostructures and densified into a new bulk composite material, may be the new direction of research in thermoelectrics.

References

1. S. Iijima, *Nature* **354** (1991) p. 56.
2. M. Dresselhaus, G. Dresselhaus, and Ph. Avouris, eds., *Carbon Nanotubes: Synthesis, Structure, Properties, and Applications* (Springer-Verlag, Berlin, 2001).
3. M. Meyyappan, ed., *Carbon Nanotubes: Science and Applications* (CRC Press, Boca Raton, FL, 2005).
4. P.G. Collins, K. Bradley, M. Ishigami, and A. Zettl, *Science* **287** (2000) p. 1801.
5. K. Bradley, S.-H. Jhi, P.G. Collins, J. Hone, M.L. Cohen, S.G. Louie, and A. Zettl, *Phys. Rev. Lett.* **85** (20) (2000) p. 4361.
6. G.U. Sumanasekera, C.K.W. Adu, S. Fang, and P.C. Eklund, *Phys. Rev. Lett.* **85** (5) (2000) p. 1096.
7. T. Savage, B. Sadanadan, J. Gaillard, T.M. Tritt, Y.-P. Sun, Y. Wu, S. Nayak, R. Car, N. Marzari, P.M. Ajayan, and A.M. Rao, *J. Cond. Matter.* **15** (2003) p. 1915; M. Grujicic, S. Nayak, T. Tritt, and A.M. Rao, *Appl. Surf. Sci.* **214** (2003) p. 289.
8. K. McGuire, N. Gothard, P.L. Gai, M.S. Dresselhaus, G. Sumanasekera, and A.M. Rao, *Carbon* **43** (2005) p. 219.
9. H.E. Romero, K. Bolton, A. Rosen, and P.C. Eklund, *Science* **307** (2005) p. 89.
10. F.J. Blatt, P.A. Schroeder, C.L. Foiles, and D. Greig, *Thermoelectric Power of Metals* (Plenum Press, New York, 1976).
11. P. Avouris, *Acc. Chem. Res.* **35** (2002) p. 1026.
12. V.W. Scarola and G.D. Mahan, *Phys. Rev. B* **66** 205405 (2002).
13. J. Vavro, M.C. Llaguno, J.E. Fischer, S. Ramesh, R.K. Saini, L.M. Ericson, V.A. Davis, R.H. Hauge, M. Pasquali, and R.E. Smalley, *Phys. Rev. Lett.* **90** 065503 (2003).
14. H.E. Romero, G.U. Sumanasekera, S. Kishore, and P.C. Eklund, *J. Phys. Condens. Matter* **16** (2004) p. 1939.
15. G.U. Sumanasekera, B.K. Pradhan, H.E. Romero, K.W. Adu, and P.C. Eklund, *Phys. Rev. Lett.* **89** 166801 (2002).
16. B. Sadanadan, T. Savage, J. Gaillard, S. Bhattacharya, T. Tritt, A. Cassell, Z. Pan, Z.L. Wang, and A.M. Rao, *J. Nanosci. Nanotech. (Special Issue)* **3** (2003) p. 99.
17. J.P. Small, L. Shi, and P. Kim, *Phys. Rev. Lett.* **91** 256801 (2003).
18. J. Vavro, M.C. Llaguno, B.C. Satishkumar, D.E. Luzzi, and J.E. Fischer, *Appl. Phys. Lett.* **80** (8) (2002) p. 1450.
19. L. Grigorian, G.U. Sumanasekera, A.L. Loper, S.L. Fang, J.L. Allen, and P.C. Eklund, *Phys. Rev. B* **60** (1999) p. R11309.
20. M. Remskar, A. Mrzel, Z. Skraba, A. Jesih, M. Ceh, J. Demsar, P. Stadelmann, F. Levy, and D. Mihailovic, *Science* **292** (2001) p. 479 and references therein.
21. J. Chen, S.-L. Li, F. Gao, and Z.-L. Tao, *Chem. Mater.* **15** (2003) p. 1012.
22. J. Chen, S.-L. Li, Z.-L. Tao, and F. Gao, *Chem. Commun.* (2003) p. 980.
23. L.D. Hicks and M.S. Dresselhaus, *Phys. Rev. B* **47** (1993) p. 12727.
24. H. Imai, Y. Shimakawa, and Y. Kubo, *Phys. Rev. B* **64** 241104-R (2001) and references therein.
25. P. Magri, C. Boulanger, J.M. Lecuire, *J. Mater. Chem.* **6** (1996) p. 773.
26. J.P. Fleurial, A. Borschevsky, M.A. Ryan, W. Phillips, E. Kolawa, T. Kacisch, and R. Ewell, in *Proc. 16th ICT* (IEEE, Piscataway, NJ, 1997) p. 641.
27. M. Martin-Gonzalez, G.J. Snyder, A.L. Prieto, R. Gronsky, T. Sands, and A.M. Stacy, *Nano Lett.* **3** (2003) p. 973 and references therein.
28. M.S. Sander, A.L. Prieto, R. Gronsky, T. Sands, and A.M. Stacy, *Adv. Mater.* **14** (2002) p. 665.
29. X.H. Ji, X.B. Zhao, Y.H. Zhang, T. Sun, H.L. Ni, and B.H. Lu, in *Proc. 23rd ICT* (IEEE, Piscataway, NJ, 2004).
30. X.B. Zhao, X.H. Ji, Y.H. Zhang, T.J. Zhu, J.P. Tu, and X.B. Zhang, *Appl. Phys. Lett.* **86** 062111 (2005).
31. X.H. Ji, X.B. Zhao, Y.H. Zhang, B.H. Lu, and H.L. Ni, *J. Alloys Compd.* **387** (2005) p. 282.
32. X.H. Ji, "Syntheses and Properties of Nanostructured Bi₂Te₃-Based Thermoelectric Materials," PhD dissertation, Zhejiang University, Hangzhou, China (2005).
33. X.B. Zhao, X.H. Ji, Y.H. Zhang, and B.H. Lu, *J. Alloys Compd.* **368** (1–2) (2004) p. 349.
34. X.H. Ji, X. Zhao, Y. Zhang, B.H. Lu, and H. Ni, in *Thermoelectric Materials 2003—Research and Applications,* edited by G.S. Nolas, J. Yang, T.P. Hogan, and D.C. Johnson (Mater. Res. Soc. Symp. Proc. **793,** Warrendale, PA, 2004) p. 21.
35. X.B Zhao, T. Sun, T.J. Zhu, and J.P. Tu, *J. Mater. Chem.* **15** (2005) p. 1621.
36. Y.Y. Zheng, T.J. Zhu, X.B. Zhao, J.P. Tu, and G.S. Cao, *Mater. Lett.* **59** (2005) p. 2886.
37. X.H. Ji, X.B. Zhao, Y.H. Zhang, B.H. Lu, and H.L. Ni, *J. Alloys Compd.* **387** (2005) p. 282; X.H. Ji, X.B. Zhao, Y.H. Zhang, B.H. Lu, and H.L. Ni, *Mater. Lett.* **59** (2005) p. 682; X.B. Zhao, Y.H. Zhang, and X.H. Ji, *Inorg. Chem. Commun.* **7** (2004) p. 386.
38. X.B. Zhao, X.H. Ji, Y.H. Zhang, G.S. Cao, and J.P. Tu, *Appl. Phys. A* **80** (2005) p. 1567.
39. A. Sashchiuk, L. Amirav, M. Bashouti, M. Krueger, U. Sivan, and E. Lifshitz, *Nano Lett.* **4** (2004) p. 159.
40. J. Xie, X.-B. Zhao, J.-L. Mi, G.-S. Cao, and J.-P. Tu, *J. Zhejiang Univ., Sci. (JZUS), Lett.* **5** (2005) p. 1504.
41. J. Xie, X.B. Zhao, G.S. Cao, M.J. Zhao, and S.F. Su, *J. Power Sources* **140** (2005) p. 350.
42. B. Zhang, J. He, and T.M. Tritt, *Appl. Phys. Lett.* **88** 043119 (2006).
43. T.M. Tritt, *Science* **283** (1999) p. 804. □

Thermoelectric Materials for Space and Automotive Power Generation

Jihui Yang and Thierry Caillat

Abstract

Historically, thermoelectric technology has only occupied niche areas, such as the radioisotope thermoelectric generators for NASA's spacecrafts, where the low cooling coefficient of performance (COP) and energy-conversion efficiency are outweighed by the application requirements. Recent materials advances and an increasing awareness of energy and environmental conservation issues have rekindled prospects for automotive and other applications of thermoelectric materials. This article reviews thermoelectric energy-conversion technology for radioisotope space power systems and several proposed applications of thermoelectric waste-heat recovery devices in the automotive industry.

Keywords: thermal conductivity, thermoelectricity.

Introduction

Of the various static energy-conversion technologies considered for radioisotope power systems for space applications, thermoelectric (TE) energy conversion has received the most interest. Radioisotope thermoelectric generators (RTGs) generate electrical power by converting the heat released from the nuclear decay of radioactive isotopes (typically plutonium-238) into electricity using a TE converter (Figure 1). RTGs have been successfully used to power a number of space missions, including the Apollo lunar missions; the Viking Mars landers; Pioneer 10 and 11; and the Voyager, Ulysses, Galileo, and Cassini outer-planet spacecrafts. These generators have demonstrated their reliability over extended periods of time (tens of years) and are compact, rugged, radiation-resistant, and scalable. They produce no noise, vibration, or torque during operation. These properties have made RTGs suitable for autonomous missions in the extreme environment of space and on planetary surfaces. Converter units use TE materials, which, when operating over a temperature gradient, pro-

duce a voltage called the Seebeck voltage[1] (see the introductory article by Tritt and Subramanian in this issue). The system conversion efficiency for state-of-practice RTGs is about 6%.

The most widely used TE materials, in order of increasing operating temperature, are bismuth telluride (Bi_2Te_3); lead telluride (PbTe); tellurides of antimony, germanium, and silver (TAGS); lead tin telluride (PbSnTe); and silicon germanium (SiGe). All of these materials, except Bi_2Te_3, have been used in RTGs on space missions.

A wide variety of physical, thermal, and TE property requirements must be met for the design of reliable RTG converters. These properties are summarized in this article; the discussion will also include lifetime power-output degradation mechanisms in state-of-practice generators.

The number of motor vehicles on U.S. roads and the number of miles driven by those vehicles continue to grow, resulting in increased air pollution and petroleum consumption, and reliance on foreign sources of that petroleum, despite improvements in vehicle emissions control

and fuel efficiency. To counter these trends, new vehicle technologies must be introduced that can achieve better fuel economy without increasing harmful emissions.

For a vehicle powered by a typical gasoline-fueled internal-combustion engine (ICE), only about 25% of the fuel energy is used for vehicle mobility and accessory power; the remainder is lost in the form of waste heat in the exhaust and coolant, as well as friction and parasitic losses such as tire rolling resistance, wind drag, brake drag, and wheel misalignment (Figure 2).[2] Furthermore, in order to meet increasing safety requirements, improve engine performance, and reduce exhaust emissions, original equipment manufacturers (OEMs) are incorporating increased electronic content, such as stability controls; telematics for accurate satellite positioning of vehicles; collision-avoidance systems; OnStar communications systems; navigation systems; steer-by-wire systems, in which the steering column is replaced with electronic control units linked in a fault-tolerant network for enhanced safety and fuel economy; electronic braking; additional powertrain and body controllers; and sensors that can automatically optimize performance, improve fuel economy, and enhance vehicle safety. All of these additional electronic devices require more energy from the engine, or use enhanced energy-management schemes.

Unfortunately, current engine designs may not meet all of our future needs. In order to meet the ever-increasing requirements of electrical power, automotive OEMs are considering several alternatives, such as 42 V systems (versus the 14 V systems in current automobiles), hybrid vehicles, fuel cell vehicles, and auxiliary electric power units. One such alternative is the use of TE technology.

Several proposed applications of TE waste-heat recovery devices in the automotive industry are reviewed here. To assess the feasibility of these applications at the vehicle level, the effect of electrical load and weight on fuel economy for a representative midsize truck is discussed. The most challenging areas of commercialization of these technologies are identified.

Radioisotope Thermoelectric Generators
Thermoelectric Converters

The RTGs used by the U.S. space program have utilized converter TE materials made from alloys of lead telluride, TAGS, or SiGe. Figure of merit (ZT) values for state-of-practice TE power-generation materials are listed in Reference 1. The TE ef-
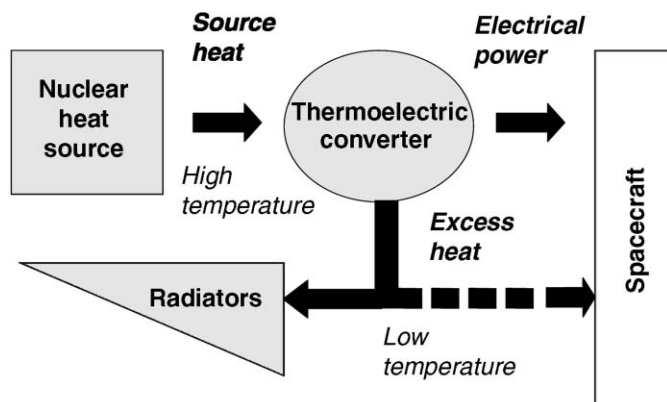
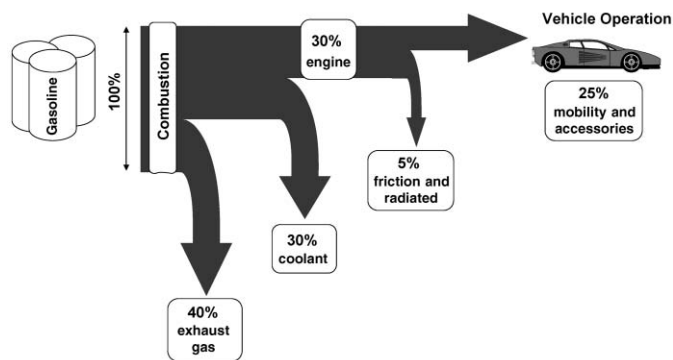Figure 1. Key components of a space-based radioisotope thermoelectric generator.

Figure 2. Typical energy path in gasoline-fueled internal-combustion engine vehicles.[2]

ficiency is proportional to ZT and the Carnot efficiency as

$$\varepsilon = \frac{T_H - T_C}{T_H} \frac{\sqrt{1 + ZT} - 1}{\sqrt{1 + ZT} + \frac{T_C}{T_H}}, \qquad (1)$$

where T_H and T_C are the hot-end and cold-end temperatures of the thermoelectric materials, respectively, and T is the average temperature. The Carnot efficiency is given by the term $(T_H - T_C)/T_H$. Equation 1 shows that increasing efficiency requires both having high ZT values and maximizing the temperature gradient across the TE materials. There is, however, no single TE material with a high average ZT between 1275 K and 300 K. Each material is best in a limited temperature range.

Earlier RTGs used TE materials that included telluride alloys, while more recent RTGs have used SiGe alloys. Telluride-based TE materials provide better performance at lower temperatures (~900 K or less), while SiGe alloys can operate up to a maximum temperature of about 1275 K. While it is important to maximize efficiency to produce more power, a better measurement of performance than efficiency for space power systems is how much power is produced per unit of mass, which is called specific power (typically expressed in W/kg). It is therefore important when designing and optimizing an RTG to optimize the heat-rejection temperature for minimizing the size and mass of the radiator used to reject the excess heat from the power converter into space (the size of the radiator varies as T_c^4).

The TE efficiency of past and current RTGs used on U.S. space missions is about 8%. The system efficiency for these RTGs is further decreased because of thermal and electrical losses that typically amount to ~10–15%, depending on the genera-

tor's cold and hot operating temperatures and design.

Past and Current Radioisotope Thermoelectric Generators

The United States began the development of RTGs in the 1950s. As previously mentioned, the earlier RTGs used telluride alloys, while the more recent RTGs have used SiGe alloys. The telluride-based generators generally required the use of a cover gas (typically a mixture of argon and helium) to minimize sublimation of the TE materials at high temperatures. SiGe materials can operate without using a cover gas in the vacuum of space. Generators using SiGe alloys must, however, be sealed with an inert cover gas on the ground to prevent oxidation of the multi-foil thermal insulation (typically molybdenum). Nearly all telluride-based generators have used pressure contact between the TE elements and the heat source. Because SiGe alloys can operate up to 1275 K, a radiation coupling between the TE elements and the heat source was used.

RTGs that used telluride-based TE materials include SNAP-3A, SNAP-9A, SNAP-19, SNAP-19B, SNAP-27, and Transit-RTG. SNAP is an acronym for "systems for nuclear auxiliary power." The Multi-Mission Radioisotope Thermoelectric Generator (MMRTG) being developed by NASA and the U.S. Department of Energy (DOE) will also used telluride-based TE materials. The beginning-of-life electric power output of MMRTG and SNAP systems ranges from 2.7 W to 125 W. A detailed list and characteristics of these generators was compiled by G. Bennet.[3] Much improvement in the design of these generators has been achieved, and while the initial RTGs had a specific power on the order of only 1.3 W/kg, the specific power for the SNAP-19 generators used

on the Pioneer and Viking missions reached 2.8 W/kg.

The MMRTG is based on the SNAP-19 RTG. The TE converter utilizes PbTe for the n-type thermoelement and TAGS/PbSnTe for the p-type segmented thermoelement. It uses eight general-purpose heat sources (GPHSs),[3] each of which delivers approximately 250 W at beginning of life. The MMRTG is designed to operate both in the vacuum of space and in the oxidizing atmosphere of Mars. The MMRTG electrical output is a function of the cold-side temperature of its TE modules and is driven by the ambient environment. The nominal power output in deep space is currently predicted to be 125 W at the beginning of the mission. This power is produced through 768 thermoelectric couples operating between 823 K and 423 K. The MMRTG measures approximately 66 cm long and has a fin-to-fin tip width of 64 cm and a specific power of 2.8 W/kg.

SiGe alloys were first used in the Multi-Hundred Watt Radioisotope Thermoelectric Generator (MHW-RTG). The MHW-RTG was designed to provide over 150 W of electric power at the beginning of mission. Because SiGe alloys are able to operate at a temperature of up to 1275 K, the generator was designed to operate the TE elements between 1275 K and 575 K with a thermoelectric efficiency of about 8%. Although a similar efficiency was achieved for the telluride-based thermoelements operating between 823 K and 483 K, operating SiGe alloys at higher temperatures allowed a significant reduction in the fin size and, in turn, an increase in the specific power to 4 W/kg for the MHW-RTG. Further improvements were introduced in the GPHS-RTG, the current standard RTG unit used in the United States. The GPHS-RTG is illustrated in Figure 3. It is designed to operate in the vacuum of space
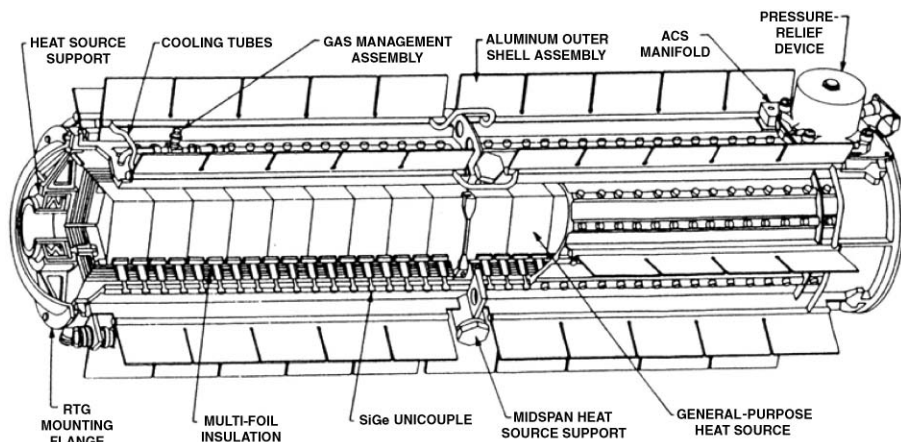
Figure 3. Configuration of a general-purpose heat source radioisotope thermoelectric generator (GPHS-RTG) using SiGe thermoelectric elements.

and uses 18 GPHS modules with a total nominal thermal power of 4500 W. The 572 SiGe unicouples are radiatively coupled around the 18 GPHS modules and connected in a series-parallel network to prevent single-point failure of the generator. The overall diameter of the RTG with fins is 42.2 cm, and it is 114 cm long. The specific power of the generator is about 5.1 W/kg, nearly four times that of the first RTGs flown. GPHS-RTGs have been used on the Galileo, Ulysses, and Cassini spacecrafts, providing years of continuous electric power.

Physical and Thermoelectric Property Requirements for Thermoelectric Materials Used in RTGs

The power-output decrease for each of the three RTGs used on the Voyager spacecrafts is 22% over 14 years, which represents a ~1.6% degradation in power output per year. Out of this 1.6%, about 0.8% is due to isotopic decay of the PuO_2 fuel. As a result of the reduced thermal input over time, the hot-junction temperature of the TE couples also decreases, resulting in a diminution of the couple conversion efficiency that accounts for about 0.47% a year of the total decrease of the generator power output. The rest of the power-output decrease, 0.33% per year, is due to (1) variations in the transport properties of the TE materials over time; (2) sublimation of the TE materials near the hot junctions of the couple, resulting in a cross-sectional reduction of the thermoelements and an increase in thermoelement resistance; (3) deposition of sublimation products, resulting in an increase in electrical and thermal losses; and (4) an increase in the interfacial con-

tact resistance of the couples. This section describes the most important potential degradation mechanisms in RTGs related to TE materials.

Sublimation

Sublimation is one of the primary degradation mechanisms for TE power-generation devices. As mentioned earlier, sublimation of the TE materials near the hot junction of the couples can result in a cross-sectional reduction of the thermoelements that can increase the resistance of the TE elements, which in turn will decrease the power output of the RTG. If substantial sublimation occurs over time, this could lead to mechanical failure of the junction between the TE material and the metallization at the couple hot junction. The sublimation rate requirement to minimize the cross-sectional reduction to an acceptable value (typically up to 5–10% reduction over 10 years) can be estimated as a function of the TE element diameter. Sublimation rates are typically expressed in $g/cm^2/h$. Figure 4 shows that, as the diameter of the thermoelements diminishes, the sublimation rate required to limit the cross-sectional reduction to within 5–10% of the nominal cross-section area rapidly decreases. The sublimation rate desired for the MMRTG and GPHS-RTG thermoelectric elements are also shown in Figure 4.

For the MMRTG, the desired sublimation rate ranges between $1 \times 10^{-6} \ g/cm^2/h$ for a 10% reduction and $6 \times 10^{-7} \ g/cm^2/h$ for a 5% reduction. As previously mentioned, a 1 atm mixture of argon and helium is maintained in the converter compartment of the generator to achieve those sublimation rates. In addition, the p-thermoelement of the MMRTG couple is

segmented, because although the TAGS material is phase-stable up to ~900 K, its sublimation rate above 673 K is above the desired value and its operation is therefore limited to 673 K in the couples. It is segmented to a top PbSnTe segment operating between 973 K and 673 K. The PbSnTe material has a much lower sublimation rate than the TAGS material in this temperature range.

The sublimation rate requirement for the SiGe alloys used in the GPHS-RTG is $6 \times 10^{-7} \ cm^2/g/h$ for a 10% reduction and $1.5 \times 10^{-7} \ cm^2/g/h$ for a 5% reduction. The desired sublimation rates for SiGe are lower than those for the TE materials used in the MMRTG couples, not only because the nominal cross section of the TE element is smaller but also because the material density is also lower. To achieve this desired rate, a Si_3N_4 coating was successfully developed, which, in conjunction with wrapping the TE elements with a quartz yarn, has been typically used on SiGe thermoelements used in RTGs.

In addition to cross-sectional reduction that can lead to substantial power output decrease and even mechanical failure of the TE couples if not controlled, sublimation products can condense within the thermal insulation between the couples and on the cold-side interconnects, potentially creating electrical and thermal shorts in the converter area of the generator. This would typically reduce the thermal efficiency and power output of the device and further justify the need for controlling the sublimation of the TE materials.

Device Considerations

Designing and fabricating mechanically stable TE power-generation devices requires, to a great extent, taking into consideration the thermal expansion and mechanical strength of the TE materials. The joins between the TE materials and the cold-side and hot-side interconnect materials are exposed to stress during fabrication, and the choice of interconnect materials is critical to achieving a mechanically stable couple. TE materials with lower coefficients of thermal expansion (CTEs) tend to be more suitable for device integration, as most refractory metals often used as interconnect materials tend to have relatively low CTEs.

Achieving long-lasting joins between the TE materials and the couple interconnects requires not only minimizing thermomechanical stresses resulting from the dissimilar nature of the joined materials, but also ensuring that chemical interactions at the joins will not increase the thermal and electrical contact resistance. The electrical contact resistance value for the
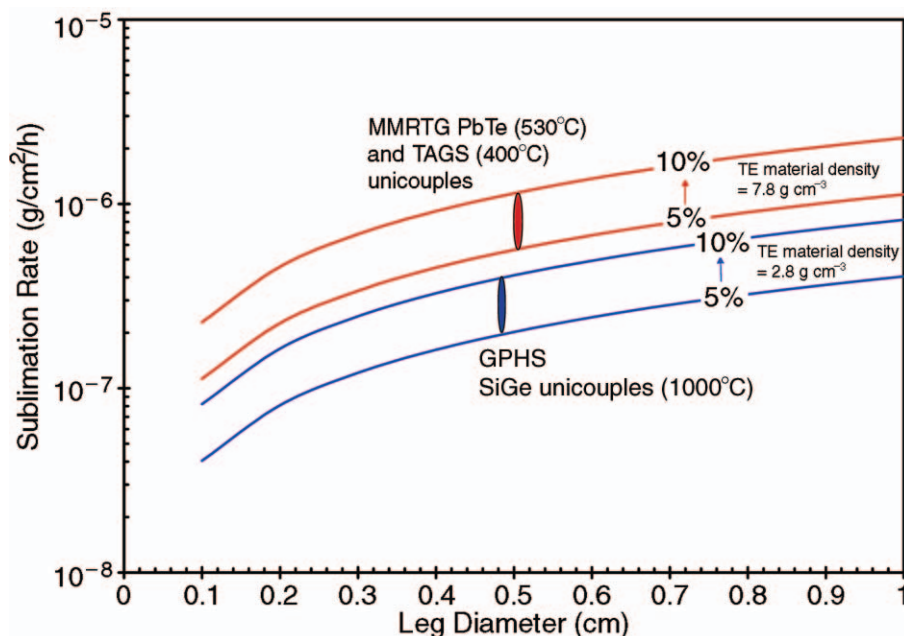
Figure 4. Calculated desired sublimation rates required to keep the cross-sectional reduction of thermoelectric (TE) elements between 5% and 10% over 10 years at the maximum operating temperature. The calculations were made for different types of thermoelectric couples and TE materials as a function of the thermoelectric element diameter and thermoelectric material density. Each TE maximum operating temperature is listed, and the filled ellipses represent the desired sublimation rate targets for the two types of thermoelectric couples. MMRTG is the Multi-Mission Radioisotope Thermoelectric Generator being developed by NASA and the U.S. Department of Energy; TAGS stands for tellurides of antimony, germanium, and silver.

joins should typically be equal to or less than 5 $\mu\Omega$ cm^2 in order to have no impact on the generator power output. Joins between the TE materials and the interconnects are typically achieved by diffusion bonding or brazing. The diffusion-bonding or brazing process should lead to some chemical reaction at the join to achieve the desired electrical contact resistance value, but this reaction should be limited over time to prevent the growth of reaction layers that may have different CTEs and could cause degradation and even mechanical failure of the bonds.

Thermoelectric Properties

The obvious requirement for a good TE material to be considered for integration into a power-generation device is to possess a high average *ZT* over the projected temperature range. This is a beginning-of-life requirement to maximize the efficiency of the generator. For practical operations and in order to predict the power output of the RTG over its lifetime, it is important to understand how the TE properties vary as a function of time and temperature.

A number of mechanisms can contribute to substantial variations in TE prop-

erties with time. In the case of SiGe alloys, the materials are saturated with dopants to achieve the highest possible *ZT* values at beginning of life. Lifetime studies of the TE properties of SiGe alloys have shown that dopants tend to precipitate from the solid solutions and form localized precipitates, resulting in a decrease in the carrier concentration of the materials.[4] The precipitation is slower at lower temperatures and has a more profound effect on the electrical resistivity than on the Seebeck coefficient and thermal conductivity. The overall effect on the *ZT* of SiGe alloys over time is relatively small.

In the case of TAGS alloys, the materials tend to undergo a phase transformation over time, especially near maximum operating temperatures.[5] This results in a change in the overall TE properties that has not been fully documented to date, although extensive life testing of the power output of PbTe/TAGS couples has been performed.

Potential Automotive Applications of Thermoelectrics

Advances in TE technology can have a significant impact on the U.S. automotive industry in terms of fuel economy

improvements by generating electricity from waste heat and enhancing air-conditioning efficiency. First, TE technology has the ability to utilize the tens of kilowatts of heat losses in vehicles[2] to generate electricity without added engine load. Second, TE technology could lead to an all-solid-state, extremely reliable, reversible automotive air-conditioning system that does not use refrigerants with greenhouse gas concerns and that can be simpler, easier to package, and more efficient to operate. TE coolers will almost certainly require more electrical power than current mechanical systems, and this should be considered. The increased reliability of batteries and selected components is generally due to being able to use TE devices to control the temperature of the battery or other device.

TE power generators could help to increase the ability of ICEs to convert fuel into useful power. By converting waste heat into electricity, engine performance, efficiency, reliability, and design flexibility could be improved significantly. TE generators could also be used to eliminate secondary loads from the engine drive train, thus reducing torque and horsepower losses from the engine. This would help reduce engine weight and direct the full power to the drive shaft, which would in turn help improve the performance and fuel economy. Furthermore, TE power generators could help improve fuel efficiency (through waste energy recovery) by supporting engine-off operation with minimum battery needs, and could increase electric power for new features. TE power generators can function for only a short period of time after the engine is turned off using available exhaust or coolant heat. A fuel burner added to the TE subsystem will use fuel, but at a much lower rate than a fully operating engine, thereby improving fuel economy without a large battery pack.

For almost a half-century between the 1940s and the early 1990s, the highest *ZT* values of all materials remained low, with *ZT* ≤ 1. Substantial federal funding since the early 1990s as well as private enterprise research and development efforts have led to significant increases in *ZT* in recent years,[6–10] reinvigorating interest in TE technology. Figure 5a shows that *ZT* ~ 3 would lead to the efficiency of a TE generator approaching 50% of the Carnot efficiency (a thermodynamic limit), and Figure 5b shows a coefficient of performance in TE coolers that outperforms those of mechanical air-conditioning units. Recent materials research breakthroughs that provide *ZT* > 1, and some as high as *ZT* ≈ 3.6,[10]
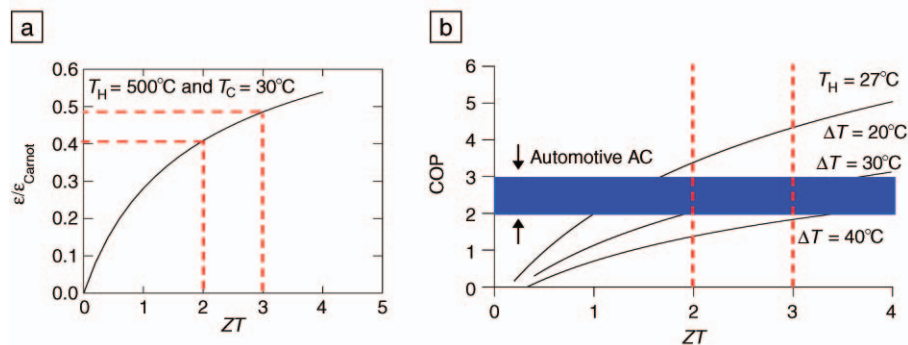
Figure 5. (a) The ratio of thermoelectric power-generation efficiency ε and the Carnot efficiency ε_{carnot} versus the figure of merit ZT for a thermoelectric power generator operating between 30°C and 500°C. (b) Coefficient of performance (COP) at room temperature as a function of ZT and temperature gradient. The COP of mechanical air-conditioning systems over a similar temperature gradient is also shown.

motivate significant interest for automotive applications of TE technology.

Efficiencies of Thermoelectric Waste-Heat Recovery Units

Because of the strong temperature-dependence of ZT for most materials, we estimate the average energy-conversion efficiency ε_{ave} of a TE waste-heat recovery unit by

$$\varepsilon_{ave} = \frac{\dfrac{T_H - T_C}{T_H} \displaystyle\int_{T_C}^{T_H} \dfrac{\sqrt{ZT + 1} - 1}{\sqrt{ZT + 1} + (T_C/T_H)} dT}{T_H - T_C}.$$

(2)

A typical vehicle exhaust gas temperature is approximately 500°C. The T_H of a TE generator at vehicle exhaust is generally lower than 500°C, because it is difficult to extract heat energy from flowing gas to the solid surface of the heat exchanger. Optimistically, we assume $T_H = 400°C$ and $T_C = 100°C$, such that the cold side of the generator is cooled by radiator coolant. The best materials for such a temperature range would be the n- and p-type filled skutterudites. Using their reported ZT values and Equation 2, ε_{ave} is approximately equal to 6.7%.[6] Based on recently developed models and test data for TE unicouples, a TE generator made of segmented unicouples with the same values of T_H and T_C and two to three different materials on each thermoelement would have $\varepsilon_{ave} = 7.5\%$,[11] which provides an additional increase in the thermal-to-electrical energy-conversion efficiency.

For a radiator TE generator, one should have $T_H \approx 100°C$ and $T_C \approx 27°C$. The materials choices in this case are the thin-film-based Bi_2Te_3/Sb_2Te_3 superlattices and $PbSe_{1-x}Te_x/PbTe$ quantum dots.[9,10] Even though these materials have the highest ZT values ever reported, a small temperature gradient for the radiator TE generator limits the Carnot efficiency (thermodynamic limit) to only 19.6%. Assuming that the ZT values for n- and p-type Bi_2Te_3/Sb_2Te_3 superlattices are identical and can be extrapolated[9] into the temperature range under consideration, $\varepsilon_{ave} \approx 6.9\%$ is estimated using Equation 2.

Methods of Improving Fuel Economy

Recently, the U.S. Department of Energy initiated several programs on automotive thermoelectric waste-heat recovery technologies. The overall objective is to achieve a 10% improvement in fuel economy. A typical vehicle electrical load, according to the Environmental Protection Agency's federal test procedures, is about 300 W. Figure 6 shows the dependence of fuel economy on electrical load at the alternator for a representative midsize truck at various weights to be in the 0–600 W load range. These results were generated by the Overdrive simulation tool internally developed by General Motors.[12] Overdrive solves systems of ordinary differential equations that approximate the rigid-body dynamics of the vehicle. The output from the simulation is a set of parameters that reflects vehicle performance, fuel economy, drive quality, and energy management.[12] These data, along with those presented in Reference 2, illustrate that if the 10% fuel economy goal is achieved, then more electrical power will be produced than is consumed by the vehicle electrical system under most driving scenarios, including EPA fuel economy and emissions test procedures.

This leads to several choices: (1) reducing electrical accessory load on the alternator using thermoelectrically generated power; (2) shifting some of the engine-driven accessories to electrical drive to raise the electrical accessory load consumption; or (3) attempting to use the excess electrical power for something other than the vehicle electrical load, such as propulsion. Examples of choice (2) include electric power steering, an electric coolant pump, an electric cooling fan, an oil pump assist, electric valve actuation and timing, and electric heating for catalytic converters. The use of electric power steering or an electric coolant pump alone, for example, could result in 2–3% or 3–5% fuel economy improvements, respectively.[13] Choice (3) is easily adaptable for hybrid vehicles. It is difficult to estimate the fuel economy gains for a TE-augmented hybrid before detailed information on packaging, electrical interface, mechanical interface, control interface, and powertrain are available. Because the excess electrical power is used directly for vehicle propulsion, this choice has the potential for the largest fuel economy gains among the three. In order to achieve the 10% fuel economy improvement goal, a combination of the three choices mentioned should be used. It should be pointed out that the fuel economy improvement technologies are not necessary additive.

It is also important to keep in mind that the addition of a TE waste-heat recovery unit would increase the overall vehicle weight and therefore reduce fuel economy. The truck represented in Figure 6 weighs 4417 lb, with an 18.8-mpg EPA
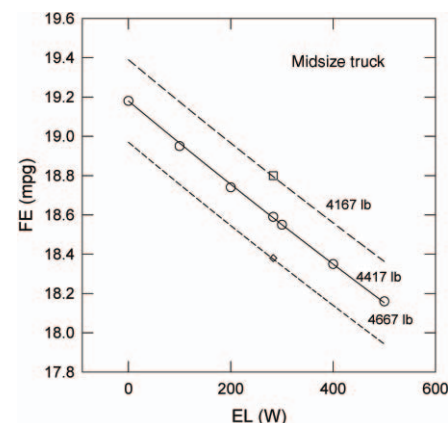

Figure 6. Dependence of fuel economy (FE) in miles per gallon (mpg) on electrical load (EL) at the alternator for a representative midsize truck at various weights. The symbols are data simulated by Overdrive, and the lines are guides for the eye.

composite rating; a 10% fuel economy improvement would mean a 1.88-mpg improvement. The mass penalty should generally not exceed 5% of the 1.88-mpg gain. Data in Figure 6 indicate an 1190 lb/Δmpg mass penalty; the total mass of a TE generator for this truck should be below ~112 lb.

Challenges for Thermoelectric Automotive Waste-Heat Recovery

Despite many new materials discoveries in the past decade, the development of large-scale automotive TE waste-heat recovery technologies remains extremely challenging. There are major challenges in the areas of materials, processes, and integration. In order to obtain higher thermal-to-electrical energy-conversion efficiency and coefficient of performance, one needs higher-ZT materials that cover a broad temperature range. The thermal stability of new materials should be addressed and evaluated. Additionally, there have been few studies on assessing TE performance at a module level using the advanced TE materials, designing optimum automotive heat exchangers, integrating TE subsystems into vehicle electrical power management, and examining fuel economy impact at a vehicle level. The great uncertainty in material, module, and subsystem costs, and in the OEM market size, is also a major factor inhibiting this technology development. Until both performance and costs are better understood, the ability to select the best thermoelectric materials for automotive waste-heat recovery remains difficult.

Conclusions

Thermoelectrics has proven to be a viable technology for space applications, as documented by the SiGe- and telluride-based couples that have accumulated millions of hours of operation in space without a single thermoelectric-related failure. Radioisotope thermoelectric generators with higher specific power would result in more on-board power for the same RTG mass, or less RTG mass for the same on-board power. This could enable the use of high-power-demand instruments or increase the mass available for the science payload.

The requirements for the choice of TE materials used in advanced couples based on new TE materials under development (and described elsewhere in this issue) are derived from the development of successful RTGs over the past 55 years. They include temperature stability and sublimation rates, thermomechanical properties, and stable thermoelectric properties as a function of time and temperature.

It is also clear that TE waste-heat recovery technology could potentially offer significant fuel economy improvements. If this is demonstrated feasibly on large-scale applications such as automobiles, a significant savings in worldwide fuel consumption can be achieved by applying the technology across the board to conventional and hybrid vehicles. However, many challenges remain for large-scale development. The key to the realization of this technology is the continued development of new materials with increased thermoelectric efficiency.

Acknowledgments

References

1. D.M. Rowe, ed., *CRC Handbook on Thermoelectrics* (CRC Press, Boca Raton, FL, 1995).
2. F. Stabler, "Automotive Applications of High Efficiency Thermoelectrics," presented at DARPA/ONR Program Review and DOE High Efficiency Thermoelectric Workshop (San Diego, CA, March 24–27, 2002).
3. G. Bennet, in *Encyclopedia of Physical Science and Technology,* Third Ed., Vol. 15 (2002) p. 537.
4. C.B. Vining, in *CRC Handbook on Thermoelectrics*, edited by D.M. Rowe (CRC Press, Boca Raton, FL, 1995) p. 329.
5. E. Skrabek, in *CRC Handbook on Thermoelectrics*, edited by D.M. Rowe (CRC Press, Boca Raton, FL, 1995) p. 267.
6. J.-P. Fleurial, A. Borschevsky, T. Caillat, D.T. Morelli, and G.P. Meisner, in *Proc. 16th Int. Conf. Thermoelectrics* (IEEE, Piscataway, NJ, 1997) p. 91.
7. T. Caillat, J.-P. Fleurial, and A. Borschevsky, *J. Phys. Chem. Solids* **58** (1997) p. 1119.
8. Q. Shen, L. Chen, T. Goto, T. Hirai, J. Yang, G.P. Meisner, and C. Uher, *Appl. Phys. Lett.* **79** (2001) p. 4165.
9. R. Venkatasubramanian, E. Siivola, T. Colpitts, and B. O'Quinn, *Nature* **413** (2001) p. 597.
10. T. Harman, "Quantum Dot Superlattice Thermoelectric Unicouples for Conversion of Waste Heat to Electrical Power" presented at the 2003 MRS Fall Meeting (Boston, MA, December 1–5, 2003).
11. T. Caillat, J.-P. Fleurial, G.J. Snyder, and A. Borschevsky, in *Proc. 21st Int. Conf. Thermoelectrics* (IEEE, Piscataway, NJ, 2001) p. 282.
12. D.G. Evans, M.E. Polom, S.G. Poulos, K.D. Van Maanen, and T.H. Zarger, SAE Technical Paper No. 2003-01-0085 (Society of Automotive Engineers, Warrendale, PA, 2003).
13. Kolbenschmidt Pierburg AG, "Thermomanagement: possible contest strategies," www.kolbenschmidt.de/pdfdoc/elektrische_kuehlmtelpumpen_e.pdf (accessed February 2006). □